UNIVERSITY OF TWENTE.

MESA+
INSTITUTE FOR NANOTECHNOLOGY

Electrochemically controlled gradients: towards directed motion of molecules

Master's thesis

Janneke Veerbeek
Chemical Engineering

Graduation committee
Prof. dr. ir. J. Huskens
S.O. Krabbenborg, M.Sc.
C. Nicosia, M.Sc.
Prof. dr. S.G. Lemay

Molecular NanoFabrication
Faculty of Science and Technology
MESA+ Institute for Nanotechnology

Enschede, July 10th 2012

Abstract

Directed motion of molecules is necessary for the controlled buildup of molecular architectures, local reactions at the nanoscale, and for fundamental understanding of processes at the molecular scale. While the synthesis of gradients has been studied extensively, almost no research has been performed on the directed motion of molecules by chemical gradients. The few studies available did not include any tunable and dynamic gradients.

Therefore, the research performed in this project aimed for the directed motion of molecules by using electrochemically controlled gradients. Supramolecular chemistry and electrochemistry were combined because of their reversibility and tunability/downscaling characteristics, respectively. Multivalent interactions were used to ensure tunability by competition or electrochemistry instead of spontaneous desorption.

At first, a covalent host surface gradient on glass was fabricated at the µm scale. Click chemistry was used to synthesize a surface gradient of coumarin units. CD molecules were reacted on top, thus forming a host surface gradient which could be visualized by fluorescence spectroscopy. Incubation with guest molecules led to a gradient in the wrong direction, which has to be further investigated.

Secondly, a non-covalent surface gradient of guest molecules was created for the first time, to our knowledge. A solution gradient of FcMeOH was produced electrochemically, that acted as a competitor for Ad_2-rhodamine on the CD printboard and resulted in a surface gradient of guest molecules at the µm scale. The direction of the gradient could be reversed by adding CD in solution. Further research is necessary to optimize the gradients, e.g. in steepness.

Thirdly, directed motion was intended to occur via a surface gradient of host molecules, or a solution gradient of a host or competitor. Motion on the synthesized host and guest gradients was not tried yet. Directed motion was tested by unequal spreading of microcontact printed lines with a host solution gradient on top. This resulted in a higher spreading rate, but no directed spreading was observed.

It is recommended to focus further research on the two successful systems, since these seem to be the most promising. Further research is needed to understand the systems completely and direct the motion of molecules by the produced gradients.

Table of contents

I Introduction

The control of motion at the molecular scale is necessary for the controlled buildup of molecular architectures, local reactions between nanoobjects in a controlled way, and for fundamental understanding of processes at the molecular scale. Since nature offers a lot of examples of directed motion, it is useful to 1) implement biological molecular motors in artificial systems, such as systems based on kinesin [1], or 2) mimic these processes to produce fully synthetic systems, such as a molecular walker [2, 3] or molecular machines [4]. In this way, biological (active) motion is translated to molecular (passive) motion. Different methods have been used to obtain directional passive motion of nanoobjects, i.e. by electrical fields [5, 6], magnetic fields [7], optical traps [8], and chemical gradients [9, 10].

Another well-studied subject in nature is the haptotaxis of cells, where cells move in the direction of higher nutrient concentration by a gradient in cellular adhesion receptors [11]. This can be translated to the use of synthetic surface gradients to direct the motion of molecules, where a gradient may be defined as a gradual change of a property [12]. Whereas haptotaxis is a well-studied subject, the research within the synthetic field is still in its infancy.

Although the synthesis of gradients has been extensively studied in recent years [12, 13], only a few studies have investigated the control of molecular motion by gradients. The directed motion by chemical gradients is even scarcer, while chemical gradients have many advantages over physical techniques. These advantages include chemical specificity, the possibility to control the duration and the speed of the movement, and the extension to 2D control by two orthogonal gradients. Examples of directed motion by chemical gradients include the directed motion of dendrimers via an aldehyde gradient [14], the directed diffusion of single molecules induced by a hydrophobicity gradient [10, 15], and the direction motion of guest molecules on an evolving gradient of uncomplexed host molecules [16]. However, none of them included a tunable gradient or a dynamic change of properties over time.

So, while the control of motion is an interesting and promising area, motion induced by chemical gradients is hardly investigated. Most chemical gradients are made at the millimeter (mm) scale or even larger. However, to control the motion of molecules, smaller gradients are necessary. Therefore, electrochemistry was used in this report to induce gradient formation, so a smaller scale could be easily achieved by downscaling the size of the electrodes and of the gaps between them. Because of the use of electrochemistry, gradient formation becomes tunable by switching on/off or changing the potential. In contrast, conventional solution gradients only stop when the solution is removed. Within the Molecular NanoFabrication (MnF) group at the University of Twente, micrometer (μm) solution gradients are being fabricated by electrochemistry and transferred to surface gradients.

To direct the motion of molecules, a tunable and dynamic gradient was desired, since it is useful to start the experiments simultaneously with the in situ analysis, for example. Therefore, the synthesis of gradients in this report is based on supramolecular chemistry, that enables flexibility due to its reversibility and precise control over binding kinetics and thermodynamics [17]. In addition, electrochemistry [18] can be used as an external stimulus to control supramolecular chemistry. This is based on ferrocene (Fc) which forms stable supramolecular complexes with β-cyclodextrin (CD) hosts while the (electrochemically) oxidized form does not [19]. The MnF group has already studied this type of supramolecular chemistry extensively, including the synthesis and characterization of host molecules on surfaces, the so-called molecular printboards [20]. These printboards consist of self-assembled monolayers (SAMs) of host molecules, in specific CD, which can bind guest molecules by multivalent supramolecular interactions.

The main aim of this research was to induce the directed motion of molecules by using electrochemically controlled gradients. This was subdivided into three minor objectives. At first, an attempt was made to create covalent surface gradients in host molecules at the µm scale (chapter 4). Secondly, non-covalent gradient formation of guest molecules on surfaces at the µm scale was attempted (chapter 5). Thirdly, an attempt was made to achieve directed motion of molecules (chapter 6). Directed motion was intended to occur via a surface gradient of host molecules, or a solution gradient of a host or competitor.

2 Theoretical background

This chapter gives an overview of the literature on the synthesis of gradients and the directed motion of nanoobjects. At first, two famous examples of directional motion based on natural systems are described. The synthesis of surface gradients is reviewed briefly, most of them on the mm scale or even larger. Subsequently, the directed motion by surface gradients is reviewed. Finally, the properties of CD printboards and in specific the interactions between CD and ferrocene-functionalized redox active guest molecules are described.

2.1 Directional motion

Many synthetic systems for directional motion are based on natural systems. Two famous examples are described below, including one natural system and one fully synthetic system.

Vogel et al. [1] have used kinesin tracks to direct the motion of microtubules powered by adenosine triphosphate (ATP). The microtubules were guided by patterning a kinesin-coated polyurethane surface with 2 µm wide and 1 µm deep channels (Figure 2.1), but climbing against a wall was also observed. The microtubules could be loaded with cargo and transport these beads across the surface. The velocity of the microtubules could be rapidly increased by exposure to UV light, since that released caged ATP. Although directional motion could be obtained by the surface topography, the initial direction of movement is still random. Asymmetric channel features could be used to limit the bidirectional motion to unidirectional motion [21], but then the direction cannot be turned around.

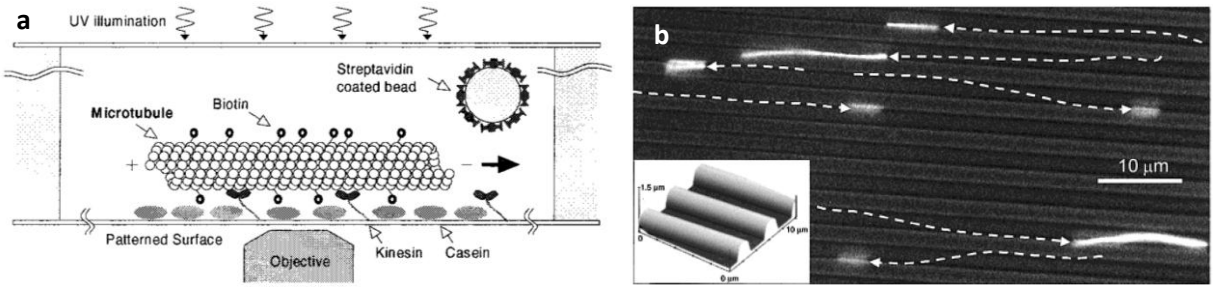

Figure 2.1. a) Schematic representation of the system to direct the motion of microtubules by a patterned surface of kinesin, and b) movement of microtubules on a kinesin-coated polyurethane surface patterned with 2 µm wide and 1 µm deep channels [1]

In order to mimic biological motor proteins, Leigh et al. [2] have produced a molecular walker. They synthesized a molecule, consisting of two legs and 21 atoms, that could walk up and down a so-called four-foothold molecular track (Figure 2.2). The interactions between the walking molecule and the different feet are labile under other conditions (acidic (condition I) or basic (condition II)), so that one end of the molecule can be temporarily fixed to one foot. This resulted in a random walking process, since the probability to move backwards or forwards is equal in every step. When one of the reactions was replaced by a kinetically controlled redox reaction, the directed motion was increased for one step (condition III). The use of covalent bonds is advantageous because their bond strength prevents complete detaching, but it is disadvantageous that the experimental conditions have to be switched for every step.

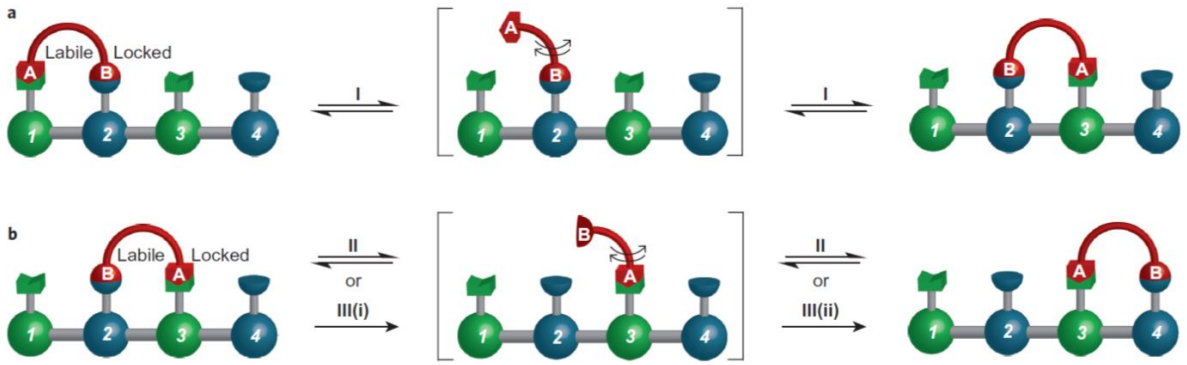

Figure 2.2. Four-foothold molecular track upon which a two-legged molecule walks up and down [2]

2.2 Surface gradients

The synthesis of patterns by using lithography techniques, for example soft lithography [22], has attracted considerable attention during the past few years. These techniques are very useful for creating surface patterns, even down to the nanoscale. However, by using these techniques, a sharp border is established between the patterned and the unpatterned areas. Many recent studies have therefore focused on the synthesis of surface gradients instead of sharp borders, where a gradient can be defined as a gradual change of a property [12]. Applications of these surface gradients include the fast screening of physicochemical phenomena, the fabrication of material structures that are normally difficult to produce, recording method for monitoring a process, or the use to drive [9] and/or direct a transport phenomenon [13].

The synthesis of surface gradients can be subdivided into bottom-up and top-down methods [13] (Figure 2.3). Bottom-up techniques include the buildup of gradients by gradually depositing different building blocks. This can be achieved by 1) spontaneous deposition methods, i.e. via diffusion or a propagating front, or 2) controlled processes, i.e. sample dipping into a solution, deposition-dependent methods or external field-assisted methods. On the other hand, top-down methods include a starting material that is modified chemically or physically, e.g. the reductive desorption of thiols by an in-plane gradient on gold. Within this process, different techniques can be combined to make a gradient geometry. Furthermore, it is also possible to create a substrate-free gradient that is subsequently transferred onto a support, for example the formation of a chemical gradient inside a microfluidic chip.

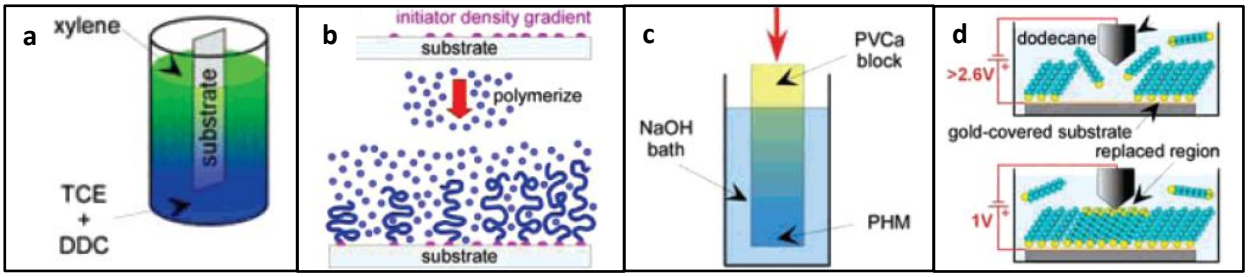

Figure 2.3. Examples of methods to create surface gradients via bottom-up techniques: a) liquid diffusion of organosilanes, and b) forming a molecular gradient of an initiator on a substrate followed by grafting-from polymerization; or via top-down methods: c) hydrolysis of poly(vinylene carbonate), and d) replacement lithography of alkanethiols [13]

The properties of surface gradients can be subdivided into different categories [13] (Figure 2.4): directionality (orthogonal, radial or directional), time dependency (static or dynamic), dimensionality (1D, 2D or 3D), functionality, type of interactions (chemical or physical) and length scale (discrete or continuous).

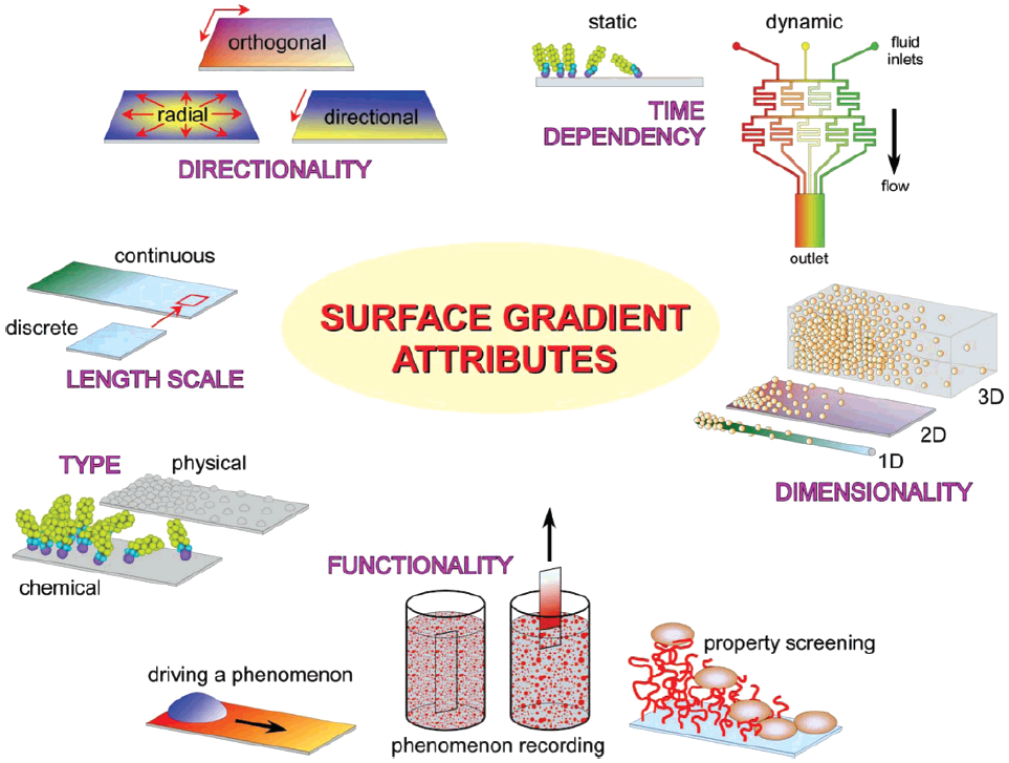

Figure 2.4. Overview of different properties surface gradients [13]

Concerning time dependency, almost all studied gradients are static, meaning that the gradient is fixed after production [13]. This can be applied to the screening of material properties, or a dynamical process such as the movement of liquids along surfaces. However, it is also possible to fabricate surface gradients whose properties change in time when varying an external stimulus (temperature, pH, external electrical field, ion concentration, etc.). These dynamic gradients can be used to drive a certain phenomenon, i.e. motion of liquids, particles, living cells or mixing liquids.

With respect to the length scale, almost all studied gradients are on the mm scale or even larger. Only a few studies have investigated the production of (sub)µm gradient patterns, which is desired to control the motion of nanoobjects. However, no literature was found about (sub)µm gradients with a dynamic change of properties in time.

Within MnF, µm solution gradients are being synthesized by using electrochemistry and are subsequently transferred to surface gradients. For example, a solution gradient of Cu^{+} was created to activate click chemistry on the surface (Figure 2.5a). In addition, a pH solution gradient was fabricated by the electrolysis of water (Figure 2.5b), which was transferred to the surface by pH-dependent imine-bond hydrolysis.

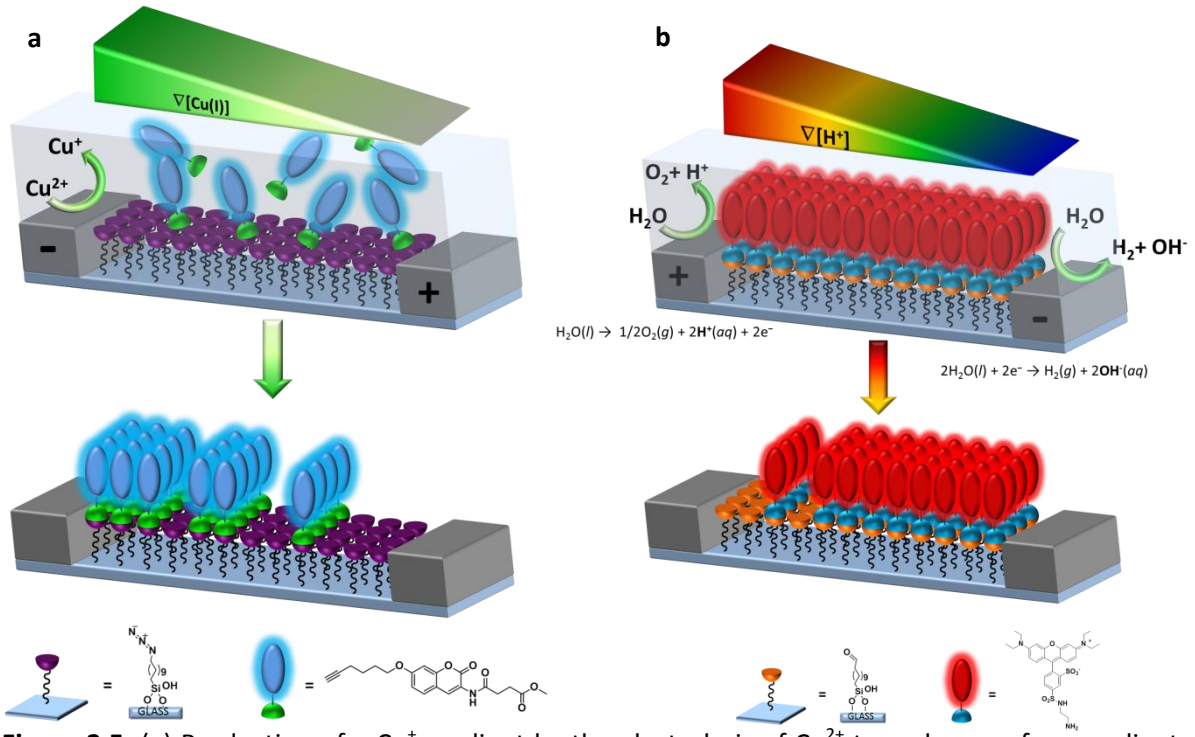

Figure 2.5. (a) Production of a Cu^{+} gradient by the electrolysis of Cu^{2+} to make a surface gradient of an alkyne dye and (b) production of a pH gradient by the electrolysis of water to make a surface gradient of an amine dye by pH-dependent imine-bond hydrolysis.

2.3 Inducing directed motion by using surface gradients

In biology, haptotaxis [15] means that cells are moving on a surface directed by an external chemical gradient, which is a well-studied area. Synthetic surface gradients have been studied extensively already [12, 13], but only a few studies have already investigated the directed motion of (nano)objects or molecules by using surface gradients. These few studies are described in this section.

At first, Chang et al. [14] reported the directed motion of dendritic macromolecules, which are labeled with a dye. They attached poly(propyleneimine) dendrimers to glass substrates by using multiple imine bonds. The movement of these dendrimers is based on the hydrolysis and reformation of the imine bonds. This movement is random without an external stimulus, but can be directed by applying an aldehyde gradient on the glass substrate instead of a homogeneous coverage with aldehyde groups. In this way, it is more likely that the dendrimer moves in one direction, since the change is higher to form imine bonds at a place where more aldehyde groups are present. The aldehyde gradient was generated by using dip coating and afterwards the dendrimers were printed onto the substrate (Figure 2.6).

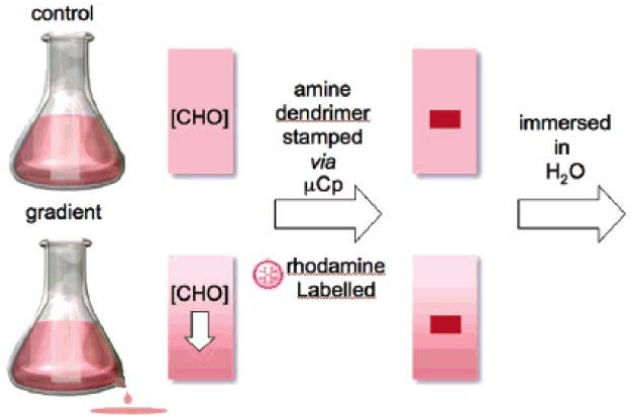

Figure 2.6. Substrate preparation by modified dip coating and printing [14]

Furthermore, Burgos et al. [15] investigated the directed diffusion of single molecules induced by surface energy gradients. They produced a surface gradient by using selective photo-oxidation, so that the surface changes from hydrophilic to hydrophobic over a few micrometers. Single poly(ethylene glycol) chains were driven towards the hydrophilic side of the surface by diffusion. The diffusion coefficient on these surfaces was more than an order of magnitude higher than on surfaces without a surface energy gradient.

Walder et al. [10] also studied directed motion by using a gradient of hydrophobicity, made by using selective photodegradation (Figure 2.7). They used 20 nm particles instead of polymer chains and only a small fraction of the surface consisted of the gradient region.

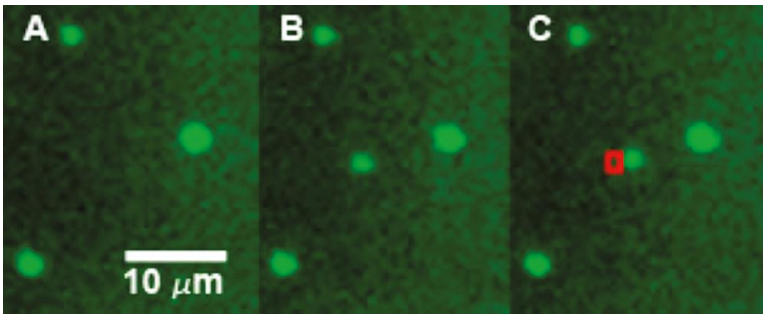

Figure 2.7. Total internal reflection fluorescence (TIRF) microscope images showing a) three adsorbed nanobeads, b) the adsorption of a new nanobead, and c) movement of the new bead towards the region with higher hydrophobicity after 8 s [10]

Within MnF, Perl et al. [16] studied the spreading of mono-, di- and trivalent guest molecules on a CD printboard. The guest molecules were printed onto the host surface. Subsequently, competition with CD in solution induced weakening of the supramolecular interactions, thus inducing movement of the guest molecules over the surface. This spreading was directional along a gradient of uncomplexed host molecules, which was steep directly after microcontact printing and became less steep over time. The spreading depended on the valency of the guest molecule and the concentration of CD in solution. Different surface diffusion mechanisms were identified, including walking, hopping and flying (Figure 2.8).

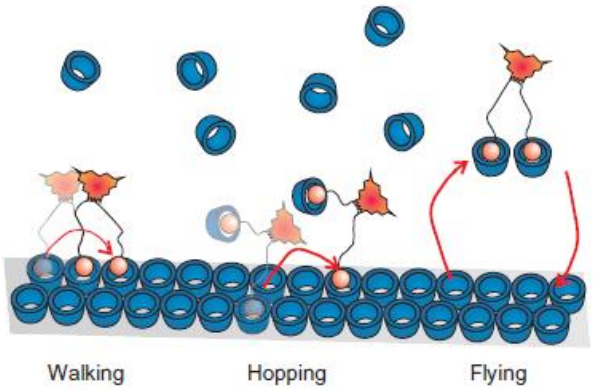

Figure 2.8. Mechanisms involved in gradient-driven motion [16]

All systems are on the µm scale, except for the research of Chang et al. [14] that acts on the mm scale. However, the gradient formation of all these systems is not tunable and included a static instead of a dynamic gradient. Only the research of Perl et al. [16] included a dynamic gradient, since the amount of vacant host molecules changed in time. Nevertheless, this system was not tunable by an external stimulus to switch the gradient and the direction of the motion, as was desired in the research of this report.

2.4 Molecular printboard of CD with ferrocene as redox active guest molecule

Supramolecular chemistry includes non-covalent binding or complexation [23], where a molecule (a 'host') binds another molecule (a 'guest') to form a 'host-guest' complex. Mostly the host is a large molecule with a central hole or cavity, while the guest can be a monatomic cation, simple inorganic anion, an ion pair or a more sophisticated neutral or charged molecule (hormone, neurotransmitter, etc.). Supramolecular interactions are often established by hydrogen bonding, ionic bonds, hydrophobic forces and van der Waals forces.

In this report, supramolecular chemistry is used because of its reversibility and precise control over binding kinetics and thermodynamics [17]. The MnF group has already studied supramolecular chemistry extensively, in particular focused on β-cyclodextrin (CD) as the host molecule. Figure 2.9 shows the structure of β-cyclodextrin, a cyclic oligosaccharide that consists of seven glucopyranoside groups [23]. The cavity inside the molecules is hydrophobic due to the hydroxyl groups, which enables the complexation of organic guests in an aqueous solution, while the outer face is hydrophilic. Water molecules inside the cavity have a relatively high energy due to their limited interactions with the hydrophobic wall. Therefore, guest complexation is promoted by expulsion of these high-energy water molecules from the cavity.

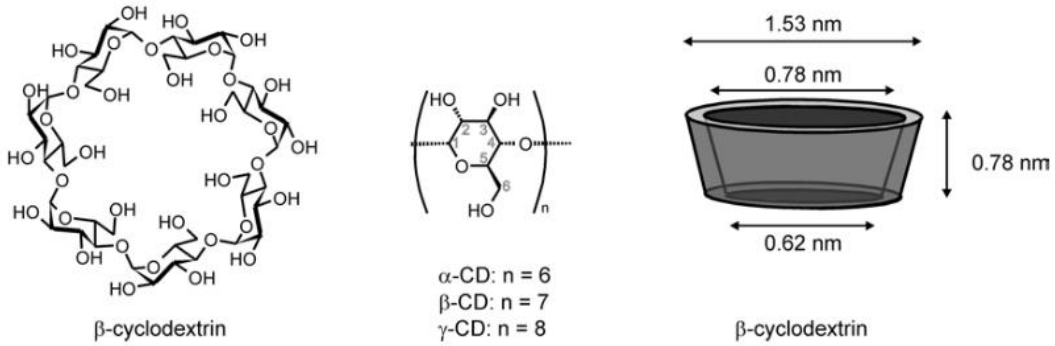

Figure 2.9. Structure and dimensions of β-cyclodextrin [24]

The CD host molecules have been applied to the synthesis of molecular printboards [17, 20], which consist of self-assembled monolayers (SAMs) of CD on glass or gold. These printboards can bind guest molecules reversibly by hydrophobic interactions, for example guests with adamantyl groups. The systems based on divalent and trivalent guests are kinetically stable when only water is present. When free CD molecules are added to the solution, a part of the guest molecules desorbs due to competition, as shown in Figure 2.10. When a guest with multivalent interactions is used, i.e. two or more groups bind to the host surface, the supramolecular interactions are stronger and less competition with CD in solution occurs [16].

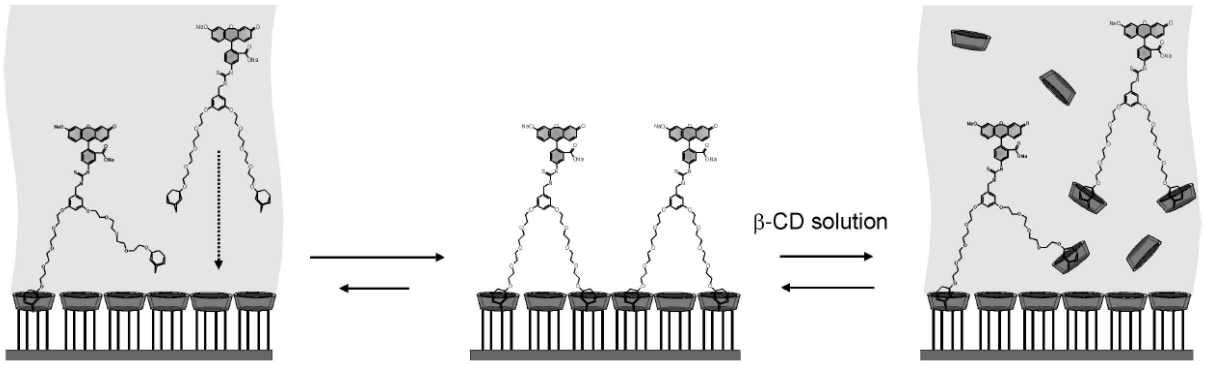

Figure 2.10. Schematic representation of the adsorption of guest molecules and their desorption by competition with CD in solution [20]

In this report, electrochemically controlled gradients were produced to obtain directed motion of molecules. Due to the use of reversible supramolecular interactions, a gradient could be produced by desorbing the guest molecule on a part of the surface only, for example. Consequently, a redox active guest was needed in most designed systems. Ferrocene-functionalized guest molecules were chosen, since ferrocene forms stable 1:1 complexes with CD, while the oxidized form, the ferrocenium ion Fc^+, forms only very weak inclusion complexes with CD and thus desorbs from the surface. Different examples of Fc-CD systems were found in literature, as described below.

Within MnF, Nijhuis [19, 25] investigated redox active dendrimers at molecular printboards, especially focusing on Fc dendrimers with multivalent interactions as guest molecules. The electrochemically controlled adsorption and desorption behavior was studied for different generations of dendrimers, including 4 up to 64 Fc functionalities with several spacers. Both SAMs of CD on gold and CD monolayers on glass were used as host surface. The dendrimers could be efficiently desorbed from the surface by using electrochemical oxidation of the Fc groups (Figure 2.11), and re-adsorption/desorption could be repeated a number of times without significant destruction of the system. After desorption, the host molecules could be reused by binding adamantyl dendrimers.

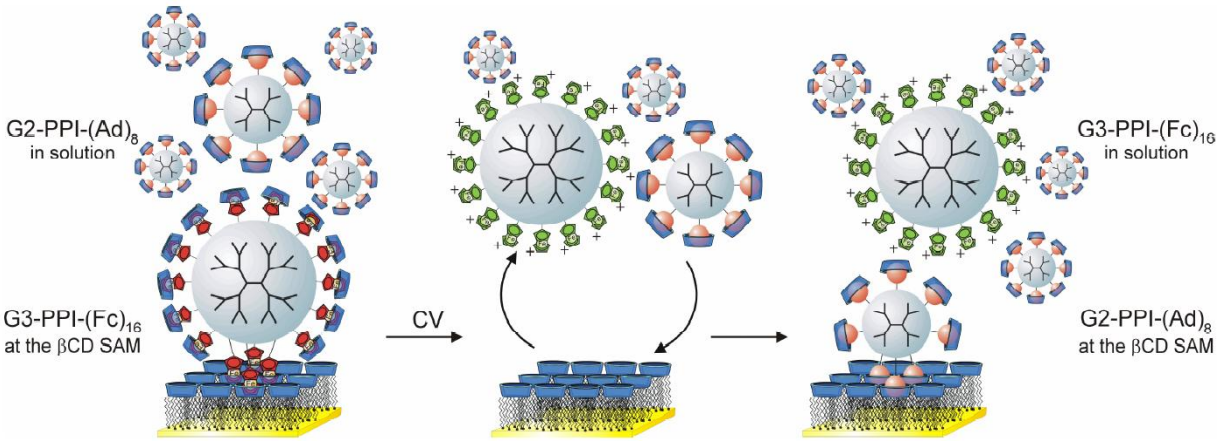

Figure 2.11. A monolayer of G3-PPI-$(Fc)_{16}$ at the CD SAM on gold efficiently blocked the binding of guest molecules from solution, e.g. G2-PPI-$(Ad)_8$. Only electrochemically induced desorption of G3-PPI-$(Fc)_{16}$ exposed the free binding sites and G2-PPI-$(Ad)_8$ can bind to the host surface [25].

Dubacheva et al. [26] also studied the adsorption/desorption behavior of ferrocene groups on a gold surface with CD SAMs, but they used ferrocene-functionalized polymers instead of dendrimers. All specifically attached polymer chains could be desorbed from the CD monolayer by applying a potential. Furthermore, Chen et al. [27] found that Fc-functionalized nanotubes formed host-guest complexes with CD SAMs, which were also tunable by electrochemistry. Ling et al. [28] used the Fc dendrimers employed by Nijhuis as a supramolecular glue to reversibly bind and unbind CD-functionalized nanoparticles.

2.5 Research strategy

In connection with the theoretical background described, a strategy was thought up for the research of this report. The designed systems were based on host-guest chemistry because of its reversibility and precise control over binding kinetics and thermodynamics [17]. Furthermore, supramolecular chemistry was chosen because the MnF group has studied this area extensively and has described an example of motion on supramolecular printboards already [16].

In order to obtain directed motion of molecules, the molecules had to ‘sense’ the gradient on the molecular scale. Therefore, gradients were produced on the µm scale and the density differences on the surface had to be as high as possible.

Electrochemistry was used to obtain small scale gradients by downscaling the size of the electrodes and of the gaps between them. Flexibility is induced since gradient formation becomes tunable by switching on/off or changing the potential. In addition, electrochemistry can be used as an external stimulus to control supramolecular chemistry, since Fc guests form stable supramolecular complexes with CD hosts while the (electrochemically) oxidized form does not [19].

3 Experimental details

3.1 Synthesis of Fc_4-rhodamine

3.1.1 Materials

The following chemicals were used as received without further purification: dichloromethane (CH_2Cl_2, Sigma-Aldrich, p.a.), *N*,*N*-diisopropylethylamine (DIPEA, Biosolve), ferrocenecarboxylic acid (FcCOOH, Acros, 97%), lissamine rhodamine B sulfonylchloride (mixture of isomers, sulforhodamine B acid chloride, Sigma), methanol (MeOH, Sigma-Aldrich, p.a.), oxalyl chloride (Acros, 98%), potassium carbonate (K_2CO_3, Acros, anhydrous), sodium bicarbonate ($NaHCO_3$, Sigma-Aldrich), sodium sulfate (Na_2SO_4, Sigma-Aldrich, anhydrous), tetrakis(acetonitrile)copper(I) hexafluorophosphate ($[Cu(CH_3CN)_4]PF_6$, Aldrich), thiophosgene ($CSCl_2$, Acros, 97%) and trifluoroacetic acid (TFA, Acros, 99% extra pure). MilliQ water was used in all experiments.

Furthermore, 11-azido-3,6,9-trioxaundecan-1-amine [29], 3,5-diethynylaniline [30, 31], *tert*-butyl (6-(bis(3-aminopropyl)amino)hexyl)carbamate [24] and tris[(1-benzyl-1*H*-1,2,3-triazol-4-yl)methyl]amine (TBTA) [32] were synthesized by others according to literature procedures.

3.1.2 Synthetic procedures

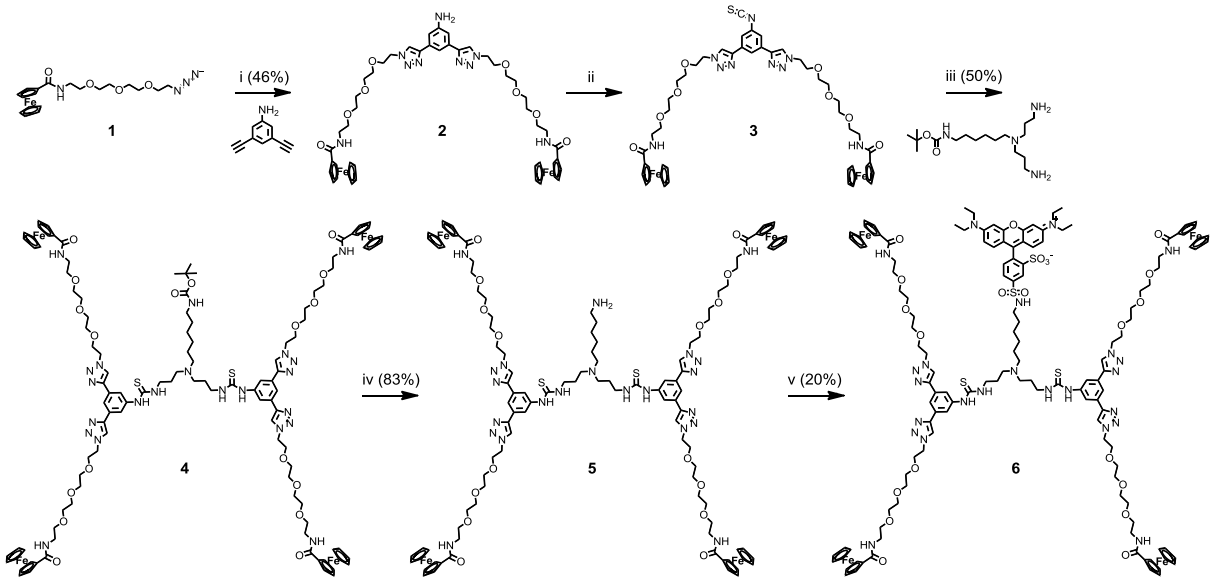

Scheme 3.1. Synthesis route towards the fluorescent ferrocene-functionalized guest molecule **6**: i. 3,5-diethynylaniline, $Cu(CH_3CN)_4PF_6$, TBTA, CH_2Cl_2/MeOH, r.t., 24 h; ii. a. saturated $NaHCO_3$, CH_2Cl_2, 0 °C, 5 min, b. $CSCl_2$, r.t., 45 min; iii. *tert*-butyl (6-(bis(3-aminopropyl)amino)hexyl)carbamate, CH_2Cl_2, r.t., o.n.; iv. TFA, CH_2Cl_2, 0 °C, 1 h; v. lissamine rhodamine B sulfonylchloride (mixture of isomers), DIPEA, CH_2Cl_2, r.t., o.n.

Synthesis of 1. The synthesis of **1** ([[[2-[2-(2-azidoethoxy)ethoxy]ethyl]amino]carbonyl]-ferrocene) was adapted from the method described by Perl [33]. At first, ferrocenylcarbonyl chloride was synthesized [34] by adding oxalyl chloride (0.42 mL, 5.0 mmol) dropwise to a stirred solution of ferrocenecarboxylic acid (0.46 g, 2.0 mmol) in dichloromethane (30 mL). The solution was stirred at room temperature for 2 h under argon. Removing the solvent in vacuo resulted in ferrocenylcarbonyl chloride as red crystals, which were used subsequently without further purification. Thereafter, a suspension of 11-azido-3,6,9-trioxaundecan-1-amine (0.44 g, 2.0 mmol), ferrocenylcarbonyl chloride (0.50 g, 2.0 mmol) and K_2CO_3 (1.4 g, 5.0 mmol) was stirred at room temperature in 30 mL CH_2Cl_2 for 15 h under argon. K_2CO_3 was removed by filtration over celite. After evaporating the solvent under

reduced pressure, the resulting red brown oil was subjected to column chromatography (SiO_2, CH_2Cl_2/MeOH = 98/2). This yielded product **1** in 72% yield (620 mg) as a dark red oil.

Synthesis of 2. A solution of 3,5-diethynylaniline (92.5 mg, 0.65 mmol) in 10 mL CH_2Cl_2 was added to **1** (620 mg, 1.4 mmol) dissolved in another 10 mL CH_2Cl_2 (ratio 1 : 2.2). Subsequently, under nitrogen a solution of $[Cu(CH_3CN)_4]PF_6$ (36.6 mg, 0.10 mmol) and TBTA (52.1 mg, 0.10 mmol) in methanol (5 mL) was added to the reaction mixture, since Cu^+ ions are necessary for the click chemistry reaction (copper-catalyzed azide-alkyne cycloaddition). The mixture was stirred at room temperature for 24 h under argon. After evaporation of the volatiles under reduced pressure, the product was purified by column chromatography (SiO_2, CH_2Cl_2/MeOH = 94/6), giving product **2** as yellow crystals (304 mg, 46%).

Synthesis of 3. To a cooled mixture (0 °C) of **2** (200 mg, 0.20 mmol) in 10 mL CH_2Cl_2 was added saturated $NaHCO_3$ (10 mL) and the biphasic mixture was stirred rigorously for 5 min. The stirring was stopped and 1.1 equivalent of thiophosgene (16.8 µL, 0.22 mmol) was added via a pipet to the organic layer. The reaction mixture was removed from the ice bath and stirring was continued for 45 min. The layers were separated and the aqueous layer was extracted with CH_2Cl_2 (2 x 10 mL), dried over Na_2SO_4 to remove water traces and filtered. The volatiles were evaporated under reduced pressure and the product was used subsequently without further purification. The yield of this product is unknown.

Synthesis of 4. Under nitrogen, *tert*-butyl (6-(bis(3-aminopropyl)amino)hexyl)carbamate (27.5 mg, 0.083 mmol) was added to a solution of **3** (208 mg, 0.083 mmol) in CH_2Cl_2 (10 mL). The solution was stirred overnight at room temperature under argon. The solvent was removed by evaporation under reduced pressure and the product was purified by preparative thin layer chromatography (Al_2O_3, CH_2Cl_2/MeOH = 97/3). This resulted in the product in 50% yield (101 mg, 0.042 mmol). The low yield is probably due to test experiments with column chromatography that did not work.

Synthesis of 5. The synthesis of **5** was adapted from the method described by A. Mulder [24]. To remove the protective *t*-Boc (tert-butyloxycarbonyl) group from **4**, TFA (1 mL, 13.5 mmol, large excess) was added to a cooled solution of **4** (101 mg, 0.042 mmol) in CH_2Cl_2 (4 mL). This solution was stirred for 1 h, after which the solvent was evaporated. Thereafter, the solution was diluted with 20 mL CH_2Cl_2. The residue was extracted with a saturated $NaHCO_3$ solution (2 x 20 mL), dried over Na_2SO_4 to remove water traces and filtered. Evaporating the solvent under reduced pressure resulted in the free amine **5** (80 mg, 0.035 mmol, 83%) which was used subsequently without further purification.

MS (MALDI-TOF): *m/z* = 2320 $[M+H]^+$ (calcd. 2319)

Synthesis of 6. The synthesis of **6** was adapted from the method described by A. Mulder [24]. The fluorescent dye lissamine rhodamine B sulfonylchloride (mixed isomers, 29.9 mg, 0.052 mmol) was added to a solution of **5** (80 mg, 0.035 mmol) and DIPEA (17.6 µL, 0.10 mmol) in CH_2Cl_2 (10 mL). The solution was stirred overnight at room temperature under argon. The solvent was evaporated under reduced pressure, and the residue was purified twice by preparative thin layer chromatography (SiO_2, CH_2Cl_2/MeOH = 92/8) to give the aimed molecule **6** as a purple solid (20 mg, 7.0 µmol, 20%).

MS (MALDI-TOF): *m/z* = 2860 $[M+H]^+$ (calcd. 2867)
MS (ESI): *m/z* = 969 $[M+3Li]^{3+}$ (calcd. 968), *m/z* = 1066 $[M+3K]^{3+}$ (calcd. 1070), *m/z* = 1219 $[\mathbf{5}+Na+K]^{2+}$ (calcd. 1219), *m/z* = 1444 $[M+2Li]^{2+}$ (calcd. 1444)

3.1.3 Characterization methods

Chromatography. Analytical thin layer chromatography (TLC) was performed on aluminum sheets precoated with silica gel 60 F_{254} (Merck) or aluminum sheets precoated with aluminum oxide 150 F_{254} neutral (Merck, 0.2 mm thickness). Column chromatography was performed using silica gel 60 (Merck, 0.040-0.063 mm, 230-240 mesh). Preparative thin layer chromatography was performed on glass plates (20 x 20 cm) precoated with silica gel 60 F_{254} (Merck, 1.0 or 2.0 mm) or glass plates precoated with alumina 150 F_{254} 1.5 mm (Merck).

NMR spectroscopy. Nuclear Magnetic Resonance (NMR) spectra were recorded at 25 °C on a Varian Unity 300 MHz spectrometer. The chemical shifts (δ) of the ^{1}H NMR spectra are given relative to the residual solvent signal of $CHCl_3$ (7.25 ppm).

Mass spectrometry. Matrix-Assisted Laser Desorption Ionization (MALDI) Time-of-Flight (TOF) mass spectra were recorded using a Perkin-Elmer/PerSeptive Biosystems Voyager-DE-RP MALDI-TOF mass spectrometer using dithranol as a matrix. ESI-TOF-MS (Electrospray Ionization) mass spectra were recorded using a LCT Mass spectrometer (Waters/Micromass) with cone 20, 40 or 60. Dichloromethane was used as solvent with a bit of methanol.

UV/Vis spectroscopy. UV/Vis spectroscopy was performed by using a PerkinElmer Lambda 850 UV/Vis spectrometer.

Fluorescence spectroscopy. Fluorescence spectroscopy spectra were recorded using a PerkinElmer LS55 Fluorescence Spectrometer. All spectra were recorded at room temperature.

3.2 Gradient formation and motion

3.2.1 Materials

The following chemicals were used as received without further purification: L-ascorbic acid (Sigma), 11-bromoundecyltrichlorosilane (ABCR, 95%), chloroform ($CHCl_3$, Fluka), copper sulfate pentahydrate ($CuSO_4.5H_2O$, Acros, >98%), curing agent (Sylgard 184, Dow Corning), *N,N*-dimethylformamide (DMF, AnalaR Normapur), dimethyl sulfoxide (Merck), ethanol (Emsure Merck, p.a.), ethylenediaminetetraacetic acid (EDTA, Fluka), ferrocenemethanol (FcMeOH, Aldrich), 1-hexadecanethiol (ABCR, 90%), iron sulfate heptahydrate ($FeSO_4.7H_2O$, Acros),), lissamine rhodamine B sulfonylchloride (Sigma), methanol (MeOH, Sigma-Aldrich, p.a.), 16-mercaptohexadecanoic acid (Aldrich), poly(dimethylsiloxane) (PDMS, Sylgard 184, Dow Corning), potassium ferricyanide ($K_3Fe(CN)_6$, Acros), potassium ferrocyanide trihydrate ($K_4Fe(CN)_6.3H_2O$, Acros), potassium hexachloroiridate(III) (K_3IrCl_6, Aldrich), potassium hydroxide (KOH, Acros, 85%), potassium sulfate (K_2SO_4, Acros), p-phenylene diisothiocyanate (DITC, Acros, 99%), sodium azide (NaN_3, Sigma-Aldrich), sodium chloride (NaCl, Sigma-Aldrich), sodium phosphate dibasic (Na_2HPO_4, Sigma), sodium phosphate monobasic (NaH_2PO_4, Sigma), sodium sulfate (Na_2SO_4, Sigma-Aldrich), toluene (Sigma-Aldrich), *N*-[3-(trimethoxysilyl)propyl]ethylenediamine (TPEDA, Aldrich, 97%) and β-cyclodextrin (Acros, 99%). MilliQ water was used in all experiments.

In addition, these compounds were synthesized by others according to literature procedures: fluorogenic coumarin **7** with alkyne and methyl-4-oxo-2-butenoate groups at the 7 and 3-position [35], two divalent adamantyl-functionalized guest molecules (Ad_2-fluorescein and Ad_2-rhodamine) [36], a trivalent adamantyl-functionalized guest molecule (Ad_3-rhodamine) [16], heptakis-thio-β-cyclodextrin (β-CD-$(SH)_7$) [37], hexa(ethylene glycol) mono(adamantyl ether) (HEG-Ad) [38], propargyl hexa(ethylene glycol) (HEG-alkyne) [39], tris[(1-benzyl-1*H*-1,2,3-triazol-4-yl)methyl]amine

(TBTA) [32], β-CD-heptamine (β-CD-$(NH_2)_7$) [40] and β-CD heptathioether (heptakis-{6-deoxy-6-[12-(thiododecyl)dodecanamido]}-β-cyclodextrin) [41].

The chemical structures of the fluorescent guest molecules synthesized by others are shown in Figure 3.1.

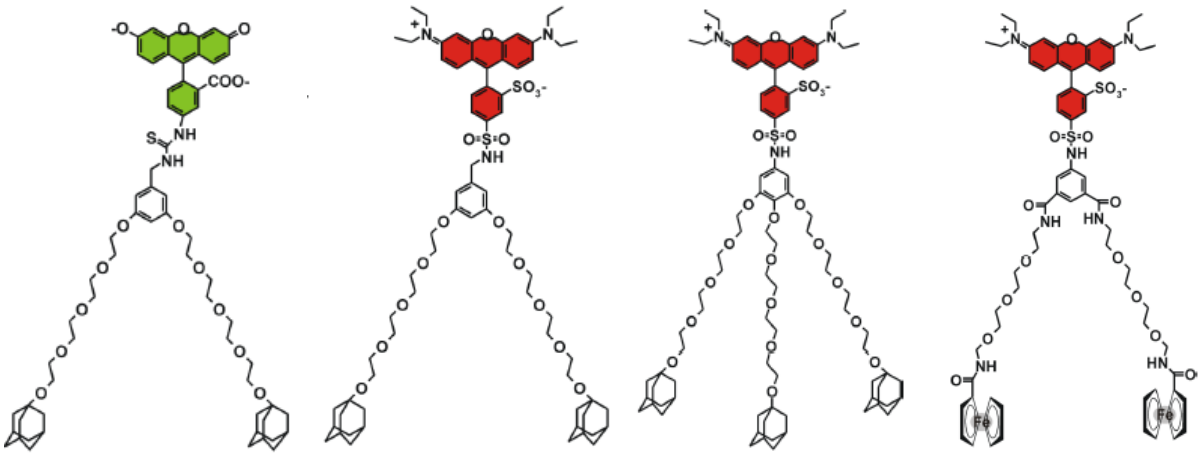

Figure 3.1. Chemical structures of the di- and trivalent fluorescent guest molecules used [16]

3.2.2 Synthetic procedures

Synthesis of azide monolayers on glass. Azide monolayers were produced in between the electrodes of an interdigitated electrode array (glass substrate with Pt electrodes, Figure 3.4), according to the procedure shown in Scheme 3.2 [35]. The substrates were rinsed with ethanol, dried with nitrogen and activated with oxygen plasma for 20 minutes (Plasma Prep II, power tuned at 40 mA) to create surface hydroxyl groups. Dry glassware was used to avoid polymerization by water during the silanization step. The samples were immersed in a solution of 0.05 mL 11-bromoundecyltrichlorosilane in 50 mL dry toluene for 60 minutes under argon. After reaction, the samples were washed three times with toluene, sonicated in toluene for 30 sec and rinsed with ethanol. After drying with nitrogen, the samples were dried in the oven at 120 °C for 5 min. For the nucleophilic substitution reaction, a saturated solution of NaN_3 in *N,N*-dimethylformamide (500 mg in 50 mL) was prepared. The substrates were exposed to this solution at 70 °C for 48 h under argon to create an azide monolayer. Thereafter, the slides were rinsed with water and dried with nitrogen. Since usage of the monolayer resulted in the expected fluorescence patterns, it is assumed that the azide monolayer is formed and no further characterization was performed.

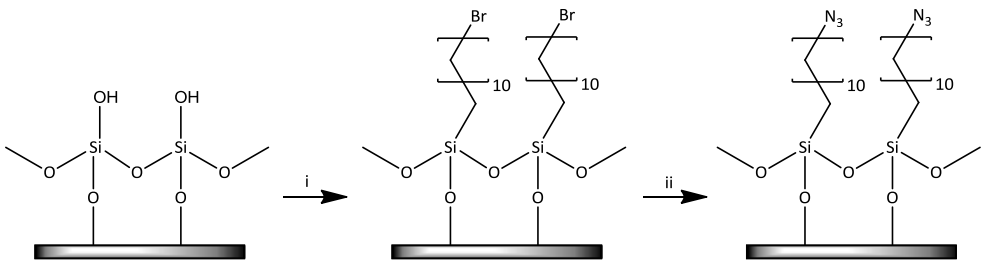

Scheme 3.2. Synthesis scheme for the preparation of azide monolayers on glass, with i. 0.05 mL 11-bromoundecyltrichlorosilane in 50 mL dry toluene, 60 min under argon; ii. saturated NaN_3 solution in DMF, 70 °C, 48 h under argon

Synthesis of a CD molecular printboard on gold. Round glass-supported gold substrates for electrochemistry (2.54 cm diameter, 20 or 200 nm Au) were obtained from Ssens bv (Enschede, the Netherlands). The substrates were cleaned by oxygen plasma for 10 min. Subsequently, the gold substrates were left in absolute ethanol for 10 min to remove the oxide layer. The substrates were immersed into a 0.01 mM CD heptathioether adsorbate solution in EtOH and $CHCl_3$ (20:30 mL) for 16 h at 60 °C under argon. The samples were rinsed sequentially with chloroform, ethanol and water to remove the excess of adsorbate. The resulting CD molecular printboard on gold is shown in Figure 3.2. The interaction between the thiol groups and gold is regarded as covalent binding [42].

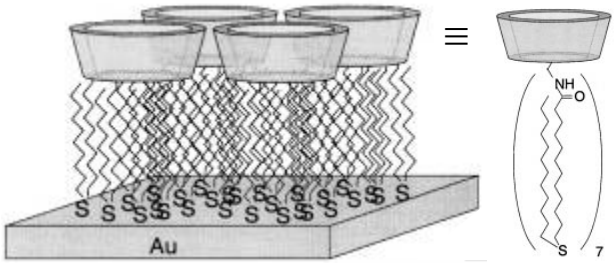

Figure 3.2. Schematic representation of CD molecular printboard on gold [41]

Impedance spectroscopy was used to determine the charge transfer resistance, which reflects the order and packing density of the CD layer. The charge-transfer resistance towards $Fe(CN)_6^{3-}/Fe(CN)_6^{4-}$ as external redox couple was about 1.1 kΩ. This value is much lower than reported before (110 kΩ [41]), which indicates a much worse packing of the heptathioether groups on the gold substrate. Due to scarcity of the heptathioether molecule within MnF, a 0.01 mM immersion solution of CD heptathioether was used instead of 0.1 mM used by de Jong et al. [41], which probably explains the large difference between the measured charge-transfer resistance values.

Dynamic contact angle measurements were performed on the CD monolayer on gold, as shown in Table 3.1. Although the advancing contact angle is higher than reported before, the values are indicative of a rather hydrophilic surface. The difference is probably due to the poor packing of CD groups on the surface, as indicated by impedance spectroscopy.

Table 3.1. Dynamic contact angle measurements for CD on gold

Sample	Dynamic contact angle	
	Advancing [°]	Receding [°]
From this report	67.2	< 20
Literature [41]	55	< 20

Synthesis of a CD molecular printboard on glass. A β-cyclodextrin printboard was synthesized in between the electrodes of an interdigitated electrode array. The procedure was adapted from Onclin et al. [20] and is shown schematically in Scheme 3.3. At first, the substrates were rinsed with ethanol, dried with nitrogen and activated with oxygen plasma for 10 minutes (power tuned at 40 mA) to create surface hydroxyl groups. After this activation step, the samples were used immediately for CD monolayer formation. To produce the amine-terminated silane monolayer, the substrates were enclosed in a vacuum desiccator with 0.1 mL TPEDA, with continuous pumping for 10 min to create a vapor phase. After overnight incubation, the samples were rinsed extensively with toluene and ethanol to remove any excess of diamine and subsequently dried in a nitrogen flow.

The diamine monolayer was converted to an isothiocyanate monolayer by exposing the samples to a 1 mM DITC solution in dry toluene at 50 °C for 2 h. An argon environment was used to avoid polymerization by air humidity. The substrates were rinsed thoroughly with toluene and ethanol, and

dried in a stream of nitrogen to get rid of the excess DITC. The CD monolayer was formed by placing the substrates in an aqueous 1 mM CD-heptamine solution for 2 h at 50 °C under argon. The samples were rinsed thoroughly with water to get rid of the excess β-cyclodextrin and finally dried in a nitrogen stream.

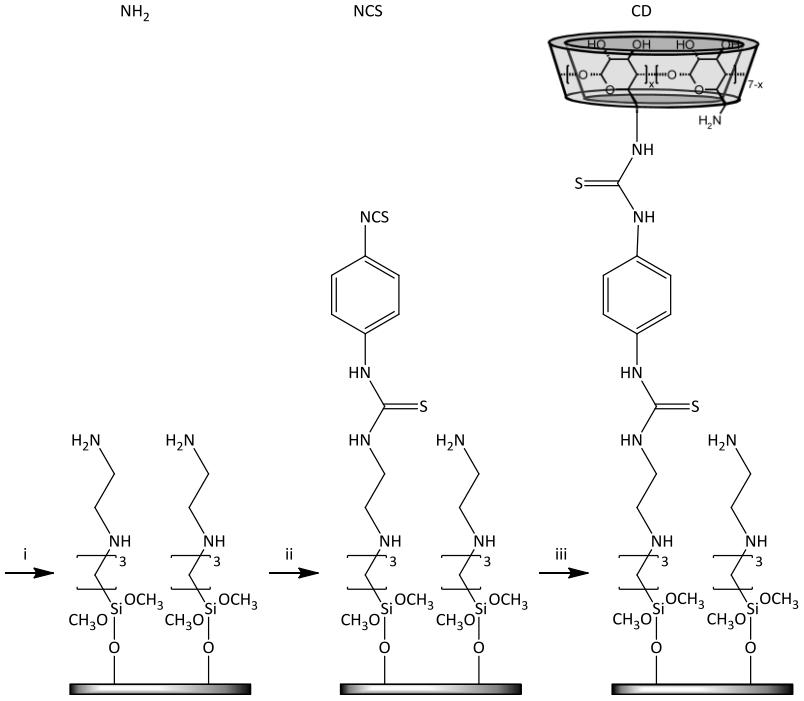

Scheme 3.3. Synthesis scheme for the preparation of CD monolayers on glass, with i. 0.1 mL TPEDA, overnight, vapor deposition; ii. 1 mM DITC in dry toluene, 50 °C, 2 h under argon; iii. 1 mM β-CD-$(NH_2)_7$ in water, 50 °C, 2 h under argon

Static contact angle measurements were performed for the different reaction steps on a glass slide, as shown in Table 3.2. As can be concluded, the trend in contact angles is comparable for the measured angles and the values from the literature, although the relative amount of increase and decrease differs. The exact values are not comparable however, since the dynamic contact angles were not measured. When CD monolayers were formed in between electrodes, no contact angle measurements could be performed.

Table 3.2. Static contact angle measurements for CD on glass

Reaction step	Measurement Static value [°]	Literature [20] Advancing [°]	Receding [°]
OH (oxygen plasma)	< 20	-	-
NH_2	44	60 ± 1	25 ± 2
SCN	54	68 ± 1	< 20
β-CD	47	49 ± 1	< 20

Incubation of guest molecules. To incubate guest molecules on CD monolayers, 100 µL was placed on top of the substrate in a silicone isolator (Electron Microscopy Sciences) to avoid leaking of the solution to the back of the electrodes. All incubation steps were performed for 10 min, unless otherwise stated.

The Fc_4-rhodamine solution consisted of 1 µM Fc_4-rhodamine in water with pH 3 and 0.5% MeOH to increase the solubility. Other solutions included Ad_2-fluorescein (>50 µM in water), Ad_2-rhodamine (5

μM in water, 0.5% MeOH), Ad_3-rhodamine (5 μM in water, 0.5% MeOH), and Fc_2-rhodamine (5 μM in water, 5% MeOH).

Host gradient formation on glass. After producing an azide monolayer in between electrodes on glass via the procedure described above, wires were soldered onto the platinum electrodes. Subsequently, a surface gradient of a coumarin unit with an alkyne functionalization (molecule **7**, Figure 3.3) was made via click chemistry. A solution of 7 (2 mM in DMSO) and a catalyst mixture (2 mM $CuSO_4.5H_2O$ and 2 mM TBTA in DMSO) were mixed equally in a bucket (50 μL each). A potential of 1.0 V was applied with a power supply for 2 min. Afterwards the samples were rinsed with ethanol, sonicated in ethanol for 30 s, and again rinsed with ethanol. To prepare a CD gradient on top of the coumarin surface gradient, the sample was incubated in 1 mM heptakis-thio-β-cyclodextrin (CD-$(SH)_7$) in DMSO/phosphate buffer (3/1, v/v) at pH 7.5 for about 20 min. The substrate was rinsed with water and dried with nitrogen. As a control step, the CD gradient was incubated with Ad_2-fluorescein, Ad_2-rhodamine, or an aqueous solution of HEG-Ad (1 mM) and Ad_2-rhodamine (1 μM).

In some experiments, propargyl hexa(ethylene glycol) (HEG-alkyne) was added via a gradient or an incubation step after CD incubation. In the gradient formation step, a solution of HEG-alkyne (2 mM in DMSO) and a catalyst mixture (2 mM $CuSO_4.5H_2O$ and 2 mM TBTA in DMSO) were mixed equally in a bucket (50 μL each). After exchanging the positive and negative electrode, a potential of 1.0 V was applied with a power supply for 2 min. In the incubation step, the sample was overnight incubated in an aqueous solution of 30 mM HEG-alkyne, 50 mM NaCl, 1 mM $CuSO_4.5H_2O$, and 40 mM ascorbic acid, in accordance with the process described in [35]. The sample was rinsed with water afterwards.

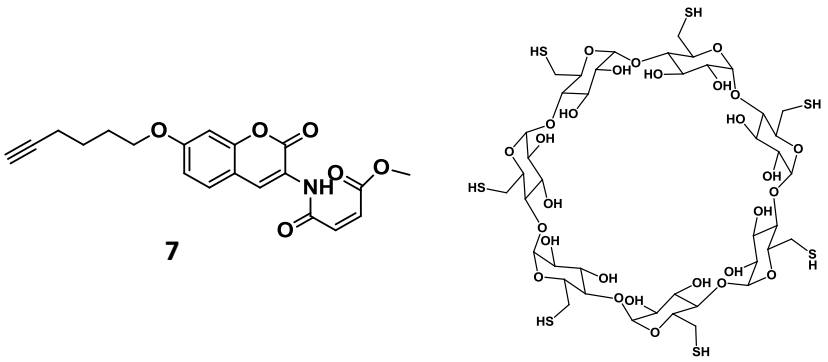

7 **CD-$(SH)_7$**

Figure 3.3. Chemical structure of a coumarin unit with an alkyne functionalization to couple to an azide monolayer, and a methyl-4-oxo-2-butenoate group to couple with a thiol group (molecule **7**); and the chemical structure of heptakis-thio-β-cyclodextrin (CD-$(SH)_7$)

Host gradient formation on gold. A self-assembled monolayer of 1-hexadecanethiol was made by immersing a gold substrate (same as for the molecular printboard) in a 5 mM solution of 1-hexadecanethiol in ethanol for 1 h under argon. Afterwards the substrate was rinsed with ethanol and dried under nitrogen. A bipotentiostat was used to apply -0.4 V and -1.8 V for 60 s on the left and right side of the gold substrate, respectively, with 0.5M KOH in methanol on top. Backfilling was established by immersion the sample in a 1 mM solution of 16-mercaptohexadecanoic acid in ethanol for 30 min, subsequent rinsing with ethanol and drying with nitrogen. The sample was characterized by contact angle measurements.

Guest gradient on glass by a sink of divalent guest molecules. A CD molecular printboard in between electrodes was incubated with Fc_2-rhodamine and rinsed with water for 1 min. An aqueous solution was placed on top with 5 μM Fc_2-rhodamine as guest, 5% MeOH to improve dissolution and 0.1 M K_2SO_4 as electrolyte. A bipotentiostat was used to apply 0.70 V and 0.0 V for 2 h to both working electrodes, respectively.

Guest gradient formation on glass with K_3IrCl_6 as mediator. A CD molecular printboard in between electrodes was incubated with Fc_4-rhodamine and rinsed with water for 1 min. A mediator solution was placed on top, consisting of 2 mM K_3IrCl_6 as reductor and 0.1 M K_2SO_4 as electrolyte. A potentiostat was used to apply a potential (0.75 V or 0.3 V) to one electrode of the interdigitated electrode array for 100 s. A separate counter electrode was used for all testing experiments.

Guest gradient on glass with FcMeOH as competitor. A CD molecular printboard in between electrodes was incubated with Ad_2-rhodamine and rinsed with water for 1 min. A solution of 1 mM FcMeOH and 0.1 M K_2SO_4 was placed on top, eventually with 0.6 mM CD. A bipotentiostat was used to apply 0.47 V and 0.0 V for 3 h to both working electrodes, respectively.

Guest gradient on gold. A CD molecular printboard on gold was incubated with Fc_2-rhodamine to perform cyclic voltammetry. Fluorescence tests were carried out after microcontact printing Fc_2-rhodamine on CD molecular printboard on gold.

Molecular motion experiments. Before spreading could be studied, lines of Ad_2-rhodamine were microcontact printed (Scheme 3.4) on a CD molecular printboard on a glass slide or in between electrodes. PDMS stamps were prepared by casting the precursor poly(dimethylsiloxane) and curing agent at 10:1 volume ratio (total 33 mL) against a silicon master. The air bubbles were removed by vacuum for 30 min. The stamps were cured overnight at 60°C. Before microcontact printing, the cut stamps were oxidized by putting them in oxygen plasma (power tuned at 40 mA) for 30 sec. Afterwards, the stamps were inked with 100 µL guest solution (5 µM Ad_2-rhodamine in water) for 2 min. The stamps were dried in a stream of nitrogen and brought into conformal contact with the substrate for 1 min. Stamps with 5 µm lines and 25 µm spacing were used. Subsequently, the printed substrate was rinsed with water for 30 sec and imaged by fluorescence microscopy. The stamps were not reused.

Spreading was induced by placing a solution with either 0.6 mM CD (motion Perl) or 0.6 mM CD with 1.0 mM FcMeOH (directed motion) on top of the patterned substrate. Fluorescence images were taken frequently (every 10 min and every 1 min, respectively) for 2 h on the same place of the sample.

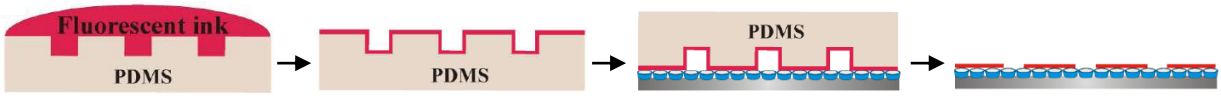

Scheme 3.4. Consecutive steps for microcontact printing of fluorescent guest molecules onto a CD monolayer [33]

3.2.3 Characterization methods

Contact angle. Static or dynamic contact angles (θ) were measured with MilliQ water (18.2 MΩ·cm) on a Krüss G10 Contact Angle Measuring Instrument equipped with a CCD camera. For static measurements, three drops were measured (six data points in total) and averaged to obtain θ. For advancing and receding contact angles, measurements were performed during the growth and shrinkage of a droplet.

Fluorescence microscopy. An Olympus inverted research microscope IX71 was used to record fluorescence microscopy images, equipped with a mercury burner U-RFL-T as light source and a digital Olympus DP70 camera for taking pictures. The fluorescence of the coumarin dye, UV excitation (325 nm ≤ λ_{ex} ≤ 375 nm) and blue emission (λ_{em} ≥ 420 nm) was filtered using a Dapi Olympus filter cube. In order to record the fluorescence of a fluorescein dye, UV excitation (460 nm ≤

$\lambda_{ex} \leq 490$ nm) and blue emission ($\lambda_{em} \geq 525$ nm) was filtered using a U-MWG Olympus filter cube. To image the fluorescence of a rhodamine dye, green excitation (510 nm $\leq \lambda_{ex} \leq$ 550 nm) and red emission ($\lambda_{em} \geq 590$) was filtered using a U-MWB Olympus filter cube. All fluorescence images were obtained at room temperature with magnification 10x and iso 800. Intensity profiles were obtained by averaging the images from at least three different places at the surface.

Electrochemistry. For gradient formation on glass, an interdigitated electrode array was used. Figure 3.4 shows the design of this array, with gaps of 100 µm and an electrode width of 50 µm. The electrodes consist of platinum on glass substrates, with a titanium adhesion layer. CD monolayers were produced in between the electrodes by using the procedure shown in Scheme 3.3.

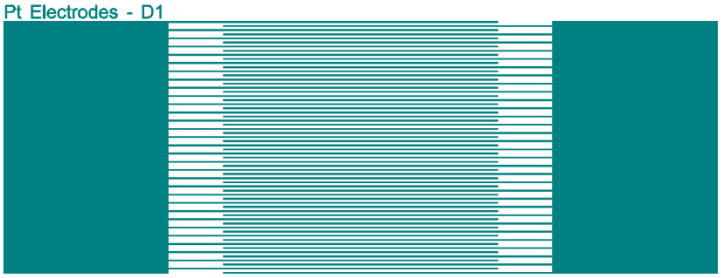

Figure 3.4. Design of the interdigitated electrode array used

In one set of experiments (section 5.4, guest gradient on glass with K_3IrCl_6) an electrochemical cell with a volume of 20 mL was used. To scale down the experiment and decrease the amount of solution needed, a Teflon cell was ordered as shown in Figure 3.5. In this case only 400 µL solution is needed and the wires are directly connected to the electrodes which avoids soldering.

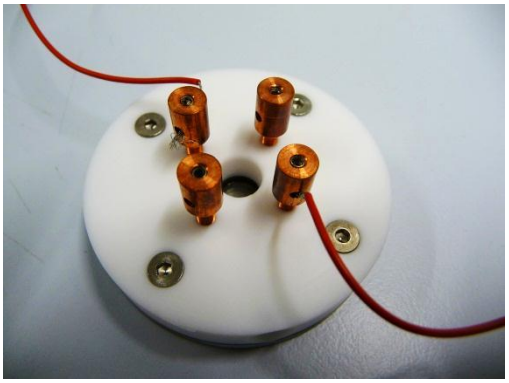

Figure 3.5. Picture of the Teflon cell used for electrochemistry

One set of experiments (section 5.4, guest gradient on glass with K_3IrCl_6) was performed with a potentiostat (Autolab PGSTAT10), where one of the electrodes from the interdigitated array was used as working electrode and the other as counter electrode. In this way, the potential at the counter electrode cannot be controlled, so the reactions at that side are unknown. Therefore, a bipotentiostat (CHI 760D Cambria Scientific) was used for the other experiments, so a controlled potential could be applied to both electrodes from the interdigitated array or the left and right side of a gold electrode. In this way, two working electrodes were present on the surface and a separate counter electrode (Pt) was used in solution. Only the formation of a host gradient on glass was performed using a power supply (Delta Elektronika, ES015-10), since this procedure was already optimized within MnF.

All potentials are given relative to a red rod reference electrode (Ag/AgCl, 0.200 V vs. SHE, saturated KCl solution, Radiometer Analytical). All solutions were bubbled with nitrogen beforehand to remove oxygen.

Cyclic voltammograms were recorded in 0.1 M K_2SO_4 in water or 0.5 M KOH in methanol by normal staircase voltammetry, at scan rates of 40 or 100 mV/s. Differential pulse voltammetry was performed in guest solutions with 0.1 M K_2SO_4 between -0.05 V and 0.8 V at an increasing potential of 2 mV. An amplitude of 40 mV and a pulse width of 0.1 s were used.

Impedance spectroscopy data were obtained in a solution with 1 mM $K_3Fe(CN)_6$, 1 mM $K_4Fe(CN)_6$ and 0.1 M Na_2SO_4 starting at 0.21 V with an amplitude of 5 mV using a frequency range from 50 kHz to 0.1 Hz. The charge transfer resistance was determined using a Nyquist plot.

4 Covalent host gradient formation

This chapter describes the host surface gradient formation by covalent binding. Before motion on these gradients could be tested, the working principle of gradient formation was tested on glass (section 4.1) and gold (section 4.2).

4.1 Host gradient on glass

Scheme 4.1 shows the formation of a CD gradient on glass using click chemistry followed by a Michael addition step. In the first step, coumarin units functionalized with an alkyne group are bound to an azide monolayer on glass via click chemistry. This Cu^{+}-catalyzed cycloaddition reaction is performed in between the electrodes of the interdigitated electrode array to make a surface gradient. Via the reduction and oxidation of Cu^{2+} and Cu^{+} respectively, a Cu^{+} gradient is formed in solution. Since the highest amount of Cu^{+} is formed at the negative electrode, at that side the highest extent of click reaction occur between azide and alkyne groups.

In the second step, the other end of the coumarin molecule is functionalized with heptakis-thio-β-cyclodextrin (CD-$(SH)_7$) via a Michael addition reaction, thus producing a CD surface gradient on top of the coumarin layer. After step 1, the fluorescence of the coumarin unit is internally quenched by photoinduced electron transfer [35]. After the Michael addition reaction, the quenching is stopped and the fluorescence is restored, because the quenching group is transformed into a non-quenching group. In this way, the formation of the CD gradient can be visualized, assuming that there are no aspecific interactions between CD-$(SH)_7$ and unreacted azide functionalities near the positive electrode. As a second control step, step 3 includes incubation with a guest, for example Ad_2-rhodamine, which should lead to a surface gradient of guest molecules.

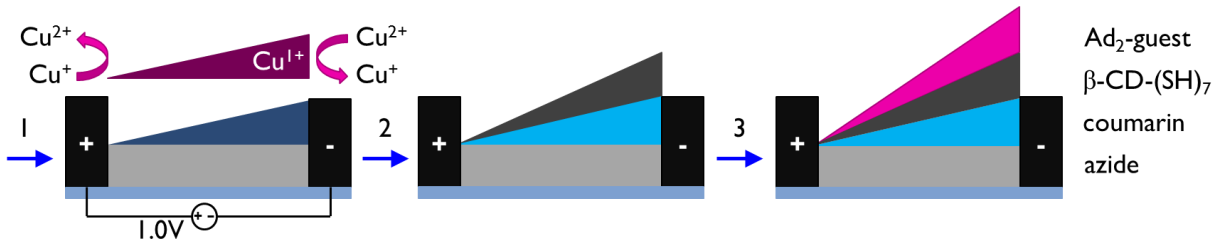

Scheme 4.1. CD gradient formation using 1) click chemistry of a coumarin molecule on an azide monolayer, 2) Michael addition via incubation of CD-$(SH)_7$, and 3) guest incubation

The fluorescence images of the three steps and their intensity profiles are shown in Figure 4.1 and Figure 4.2, respectively. The intensity profiles of the first two steps (Figure 4.2a) are as expected, but incubation of Ad_2-fluorescein resulted in a constant intensity profile instead of the desired gradient formation (Figure 4.2b). The sample was sonicated (30 s) in order to remove any physisorbed molecules. The resulting intensity profile shows a low and gradual gradient in fluorescein. However, the gradient is formed in the wrong direction, since the highest intensity should be located close to the negative electrode instead of the positive electrode.

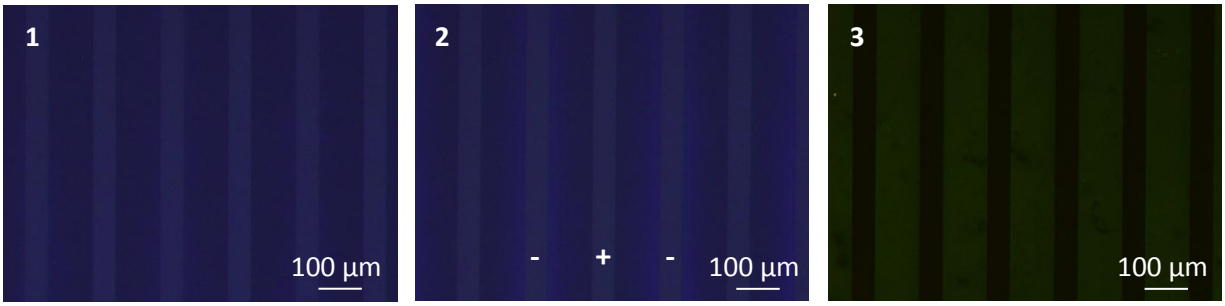

Figure 4.1. Fluorescence images of the different steps of CD gradient formation, as shown in Scheme 4.1; exposure time 1000 ms

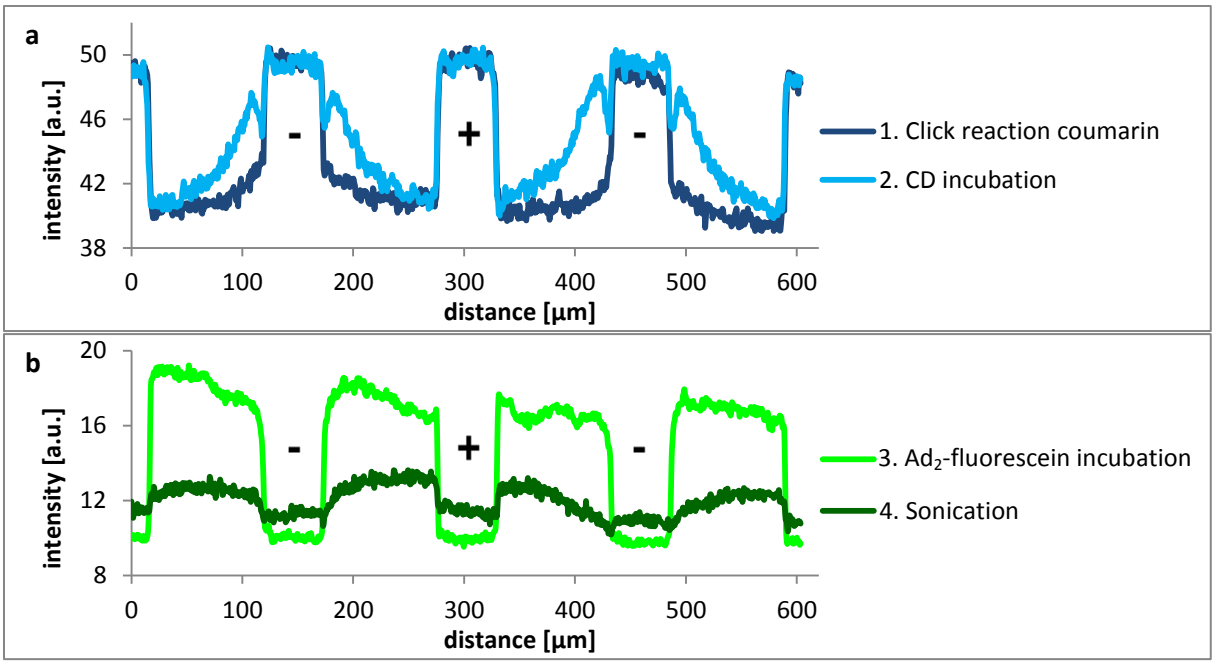

Figure 4.2. Intensity profiles of the different steps of a) CD gradient formation and b) guest incubation and sonication afterwards. The scale of both graphs differs in order to enlarge the fluorescein gradient visible after sonication.

To prevent the physisorption of guest molecules on unreacted azide functionalities, propargyl hexa(ethylene glycol) (HEG-alkyne), consisting of an alkyne group and a long hydrophilic chain, was reacted onto the free azide groups. In this way, the remaining azide groups were replaced by long hydrophilic chains, which should decrease physisorption. This concept was firstly tested by physisorption of guest molecules on a full monolayer of azide groups versus physisorption on a monolayer of HEG-alkyne (Scheme 4.2).

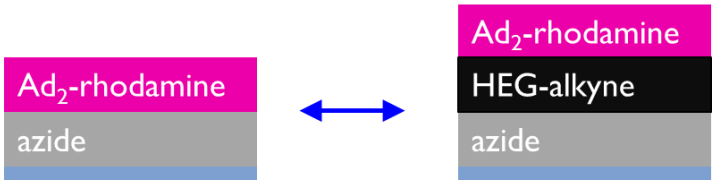

Scheme 4.2. Concept of testing the adhesion resistance of HEG-alkyne on an azide monolayer

The resulting intensity profiles are shown in Figure 4.3, where it should be noted that the exposure time of the sample with HEG-alkyne is four times higher, so the real difference between the two profiles is even larger than the graph shows. In conclusion, the HEG-alkyne layer reduced the physisorption of Ad_2-rhodamine with a factor of 14 compared to free azide groups.

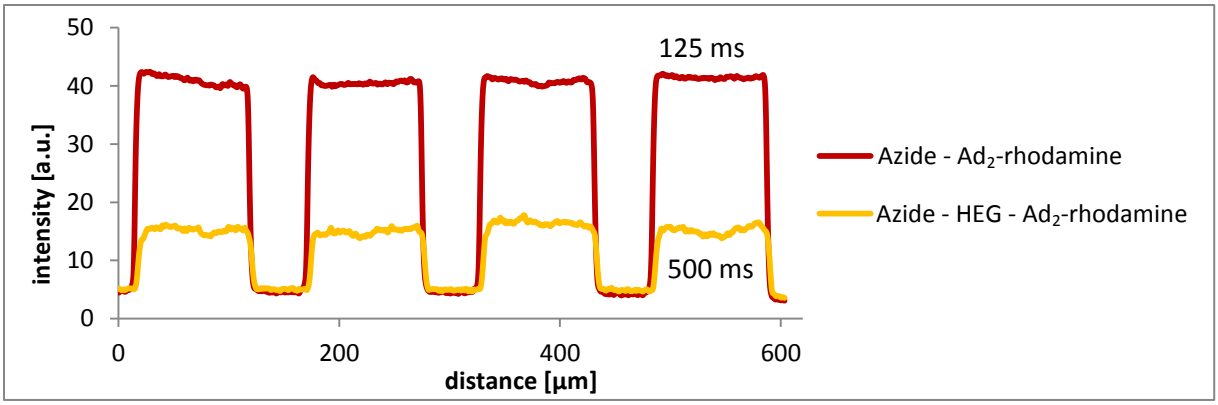

Figure 4.3. Intensity profiles of the different steps of CD gradient formation

The process as shown in Scheme 4.1 was adapted to Scheme 4.3, which includes an extra incubation step with HEG-alkyne.

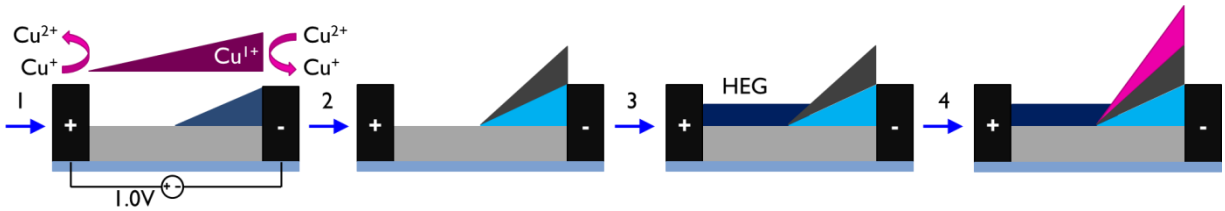

Scheme 4.3. CD gradient formation using 1) click chemistry of a coumarin molecule on an azide monolayer, 2) Michael addition of CD-$(SH)_7$, 3) HEG-alkyne incubation via click chemistry to prevent physisorption on unreacted azide moieties and 4) guest (Ad_2-rhodamine) incubation

As can be seen in Figure 4.4, the HEG incubation step does not strongly influence the intensity profile of the coumarin molecule. After the fourth step, the guest gradient is clearly visible, even without sonication, but the direction is still wrong and the intensity is still very high for the region where HEG-alkyne should prevent interactions between azide groups and Ad_2-rhodamine.

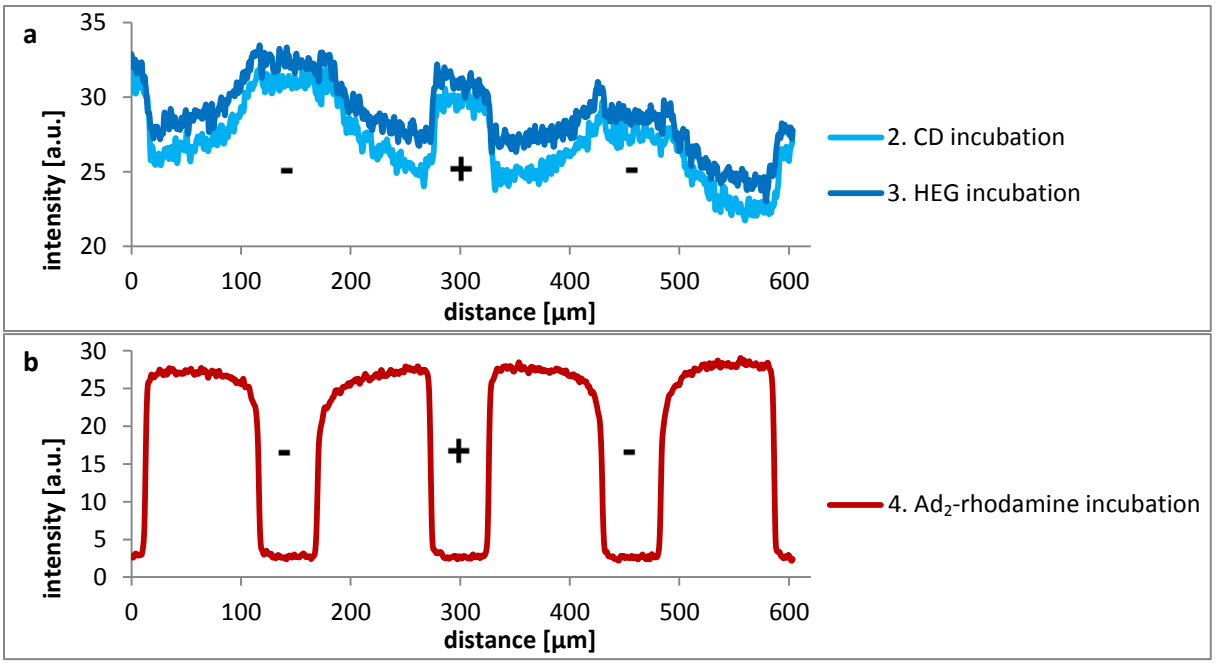

Figure 4.4. Intensity profiles of a) steps 2-3 of CD gradient formation including HEG-alkyne incubation and b) guest incubation. The scale of both graphs differs in order to enlarge the coumarin gradients.

Next, a HEG layer was introduced as a gradient instead of the incubation step by exchanging the positive and negative electrode and making a new Cu^+ solution gradient. Incubation of Ad_2-rhodamine did not result in gradient formation, also not after short (30 s) incubation in water or a 10 mM CD solution. Only incubation in a CD solution for 3.5 h decreased the intensity a little bit, but the intensity profile was still flat in between the electrodes.

It is difficult to explain the wrong direction of the guest gradient. The density of CD molecules close to the negative electrode might be low, for example due to a low density of coumarin molecules. If the CD density is too low, the Ad_2-rhodamine molecules might have monovalent interactions with CD instead of divalent and can thus be easily desorbed by rinsing. If this is true, it should be possible to backfill the empty CD molecules with Ad_2-fluorescein. However, no fluorescence of fluorescein could be observed, even though the sample was rinsed for only a few seconds to prevent immediate desorption.

To prevent physisorption of Ad_2-rhodamine and promote supramolecular interactions only, a solution of 1 mM HEG-Ad and 1 µM Ad_2-rhodamine was incubated in the fourth step. It is assumed that HEG-Ad interacts in the same aspecific way as Ad_2-rhodamine did in the previous experiments. Since HEG-Ad does not contain a dye, these physisorbed molecules are not visible. With respect to supramolecular interactions, Ad_2-rhodamine binds much stronger than the monovalent HEG-Ad due to its multivalency. So Ad_2-rhodamine is a strong competitor compared to HEG-Ad, but only near the negative electrode where supramolecular interactions with CD are possible.

The fluorescence image and intensity profile after incubation with HEG-Ad and Ad_2-rhodamine (Figure 4.5) show a very clear gradient, but still in the wrong direction. While HEG-Ad should promote supramolecular interactions at the negative electrode, the gradient is much steeper than in Figure 4.4, thus indicating even less interactions between Ad_2-rhodamine and the CD gradient.

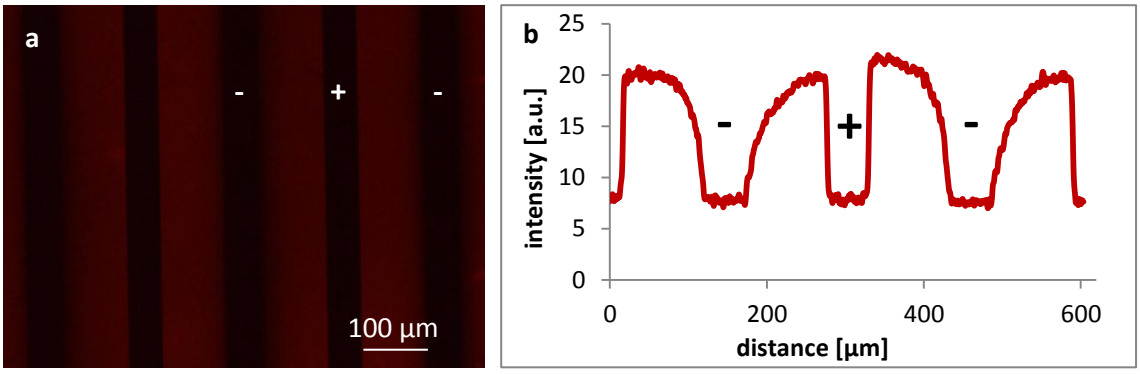

Figure 4.5. (a) Fluorescence image after incubation with HEG-Ad and Ad_2-rhodamine in step 4; exposure time 500 ms; (b) intensity profile of the fluorescence image

It is still unexplained why the guest gradient is formed in the wrong direction and the measured fluorescence of the guest molecules is so high near the positive electrode. An explanation might include the interaction of CD molecules with unreacted azide groups in step 2. Although this is very unlikely, it is worthwhile to switch step 2 and 3.

4.2 Host gradient on gold

Scheme 4.4 shows the proposed design for host gradient formation on gold. It was desired to desorb the CD heptathioether molecules by reduction, but thioether molecules cannot be reduced by gold [43]. However, thiol functionalized molecules are often used for reductive desorption [43, 44], so it would be useful to have CD molecules coupled to a long linker with thiol end groups. Since this

molecule was not available, the system was based on the indirect formation of a CD gradient. The substrate is firstly incubated with an alkanethiol, which can be desorbed by reduction. When an in-plane potential gradient is applied to the gold substrate, the thiol groups are reduced at one electrode and thus desorb, while they remain adsorbed near the oxidizing potential, thus creating a surface gradient [45]. The shown potentials are only indicative values, since the reduction potential strongly varies for different alkyl lengths [44]. The surface can be backfilled with CD heptathioether, which forms a surface gradient in the opposite direction. This gradient can be visualized by incubation with guest molecules, when gold does not quench the fluorescence of the guest molecules.

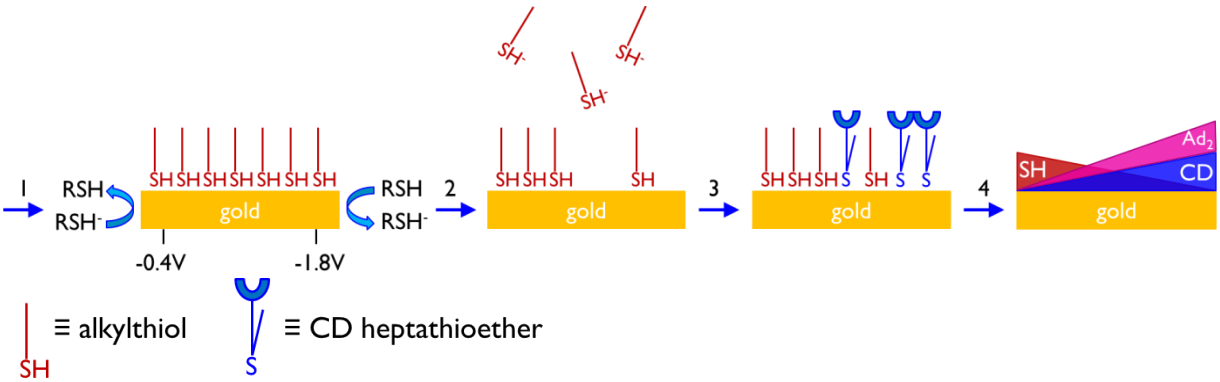

Scheme 4.4. CD gradient formation using 1) adsorption of an alkanethiol onto a gold substrate, 2) reductive desorption of thiol groups via an in-plane potential gradient, 3) backfilling with CD heptathioether and 4) fluorescent guest (Ad_2-rhodamine) incubation

The first steps have been tested already. At first, the desorption of a full monolayer of 1-hexadecanethiol was tested. This resulted in the cyclic voltammogram shown in Figure 4.6, where reductive desorption of the thiol groups can be observed around -0.85 V. The contact angle decreased from 111° to 44° during this step, which proves that the thiol molecules were desorbed. When the sample was backfilled with 16-mercaptohexadecanoic acid, the contact angle decreased even further to 21°, due its hydrophilic head group.

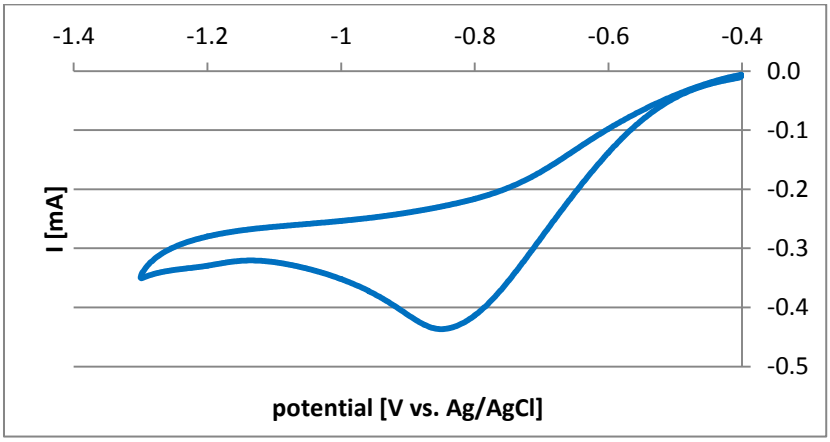

Figure 4.6. Cyclic voltammogram of a full monolayer of 1-hexadecanethiol on gold with 0.5 M KOH in methanol on top, measured at 100 mV/s

Therefore, the experiments were extended to the used of an in-plane potential gradient. A SAM of 1-hexadecanethiol was used, which was partly desorbed by applying a potential of -0.4 V and -1.8 V for 60 s on both sides of the gold substrate, respectively. The sample was backfilled with 16-mercaptohexadecanoic acid, which has a hydrophilic head group in contrary to 1-hexadecanethiol. Therefore, the higher the surface concentration of 1-hexadecanethiol, the higher

the hydrophobicity. This hydrophobicity gradient could be observed by contact angle measurements (Figure 4.7). The contact angle varied between 44° and 99° over approximately 1 cm, with further optimization possibilities. These results confirm the working principle of the alkanethiol gradient formation on the surface and are thus promising for step 3 and 4. However, these steps were not performed due to scarcity of CD heptathioether within MnF.

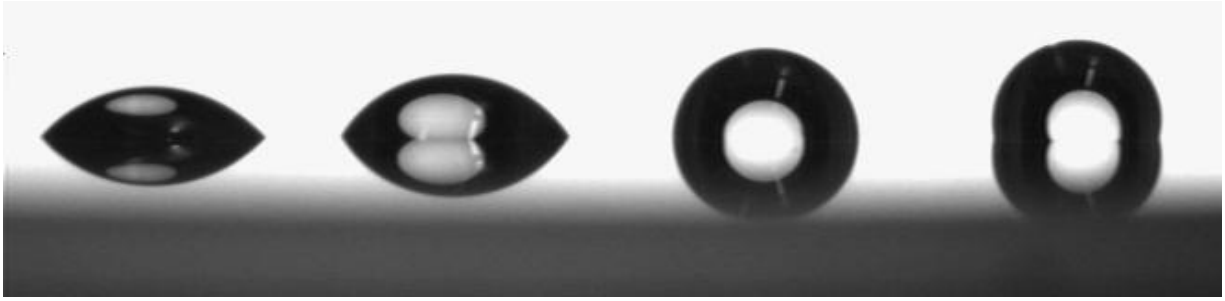

Figure 4.7. Hydrophobicity gradient after reductive thiol desorption visualized by contact angle measurements

4.3 Summary

A covalent host surface gradient on glass was fabricated via click chemistry, which could be visualized by fluorescence spectroscopy. However, incubation with guest molecules led to a gradient in the wrong direction, which has to be further investigated.

Reductive desorption was used to create a surface gradient of thiol functionalized molecules. Backfilling with CD heptathioether should lead to a host gradient, but this was not performed due to scarcity of the molecule. Backfilling with a hydrophilic thiol functionalized molecule resulted successfully in a hydrophobicity gradient that could be visualized by contact angle measurements.

5 Non-covalent guest gradient formation

In contrast to the previous chapter, non-covalent interactions are described in this chapter for the formation of a guest surface gradient, which provides more tunability since the direction of the gradient could be switched, for example. A surface gradient of guest molecules automatically includes an opposite gradient of free host molecules, which could direct the motion of molecules. Before motion could be tested, the working principle of gradient formation was tested by the production of static surface gradients in guest molecules. Electrochemically active ferrocene-functionalized guest molecules (section 5.1) and CD molecular printboards on glass (section 5.2) were firstly characterized. The guest molecules were used to design gradient formation systems on CD printboards on glass (section 5.3 through 5.5) and gold (section 5.6).

5.1 Ferrocene-functionalized guest molecules

5.1.1 Synthesis of Fc_4-rhodamine

Ferrocene-functionalized guest molecules are electrochemically active, since oxidation of this species ensures loss of its supramolecular interactions with a CD printboard [19]. In this way, the guest molecules desorb from the surface after oxidation. A new guest molecule was designed, as shown in Figure 5.1. The molecule Fc_4-rhodamine is based on a second-generation dendrimer, has four ferrocene groups at its periphery and a fluorescent rhodamine group in the focal point in order to make the guest molecule visible.

Since the guest molecules are meant to be desorbed by electrochemistry instead of competition or complexation, strong supramolecular interactions with the CD layer were necessary. Therefore, tetravalent interactions were chosen, which also increases the stability of the supramolecular system (Fc:CD = 1:1). Long tetraethylene glycol spacers were used to ensure enough flexibility to interact with four host molecules at once. Section 5.4 explains the desired application of Fc_4-rhodamine into a gradient formation process.

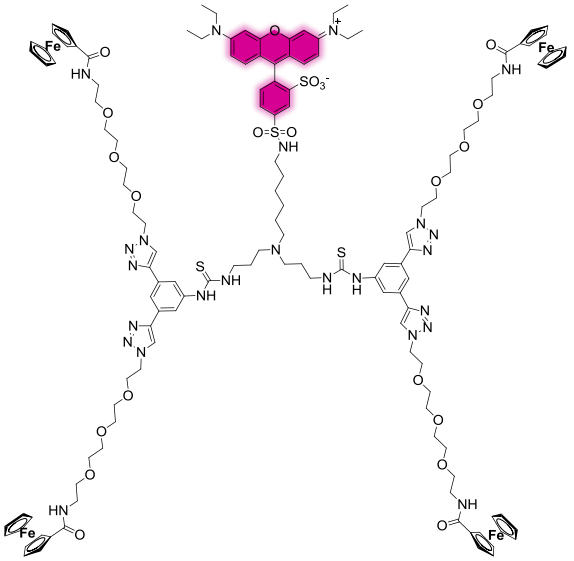

Figure 5.1. Fluorescent ferrocene-functionalized guest molecule Fc_4-rhodamine

The synthesis route for Fc_4-rhodamine **6** is shown in Scheme 5.1 below. The synthesis started with a click reaction between **1** and 3,5-diethynylaniline to form the divalent molecule **2** with ferrocene functionalities. The amine group was converted to an isothiocyanate group by using thiophosgene, resulting in molecule **3**. The number of functionalities was doubled to four by adding a carbamate,

which reacts in ratio 1:2 with molecule **3**. The protective *t*-Boc (*tert*-butyloxycarbonyl) group from the resulting molecule **4** was removed by using TFA, giving the free amine **5**. Finally, this amine was reacted with the fluorescent dye lissamine rhodamine B sulfonylchloride to result in the desired product **6**.

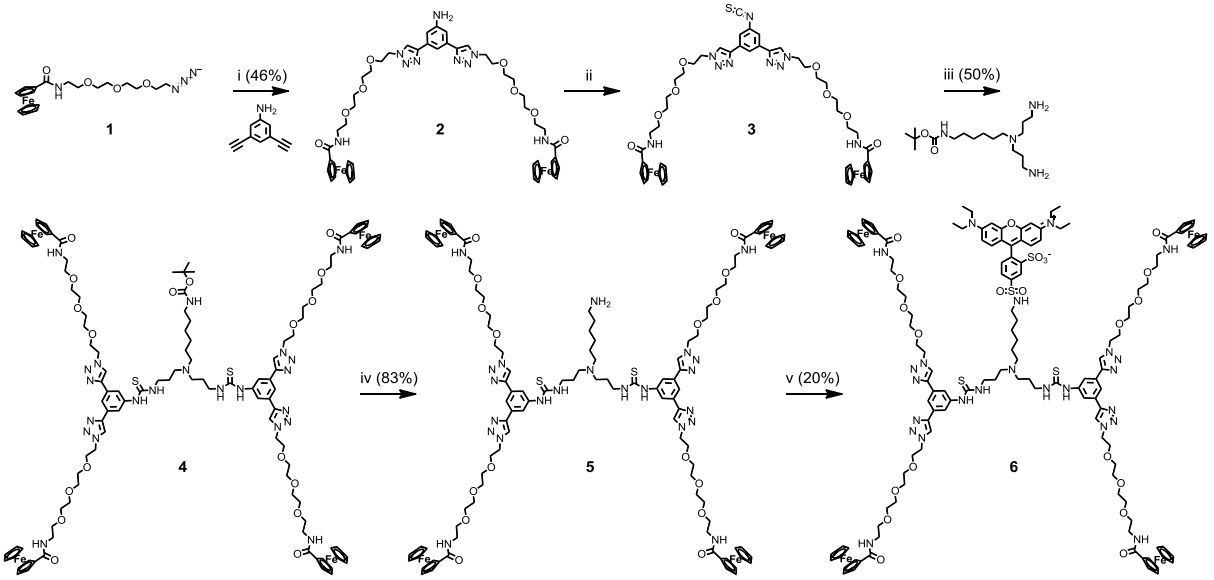

Scheme 5.1. Synthesis route towards the fluorescent ferrocene-functionalized guest molecule **6**: i. 3,5-diethynylaniline, $Cu(CH_3CN)_4PF_6$, TBTA, CH_2Cl_2/MeOH, r.t., 24 h; ii. a. saturated $NaHCO_3$, CH_2Cl_2, 0 °C, 5 min, b. $CSCl_2$, r.t., 45 min; iii. *tert*-butyl (6-(bis(3-aminopropyl)amino)hexyl)carbamate, CH_2Cl_2, r.t., o.n.; iv. TFA, CH_2Cl_2, 0 °C, 1 h; v. lissamine rhodamine B sulfonylchloride (mixture of isomers), DIPEA, CH_2Cl_2, r.t., o.n.

The yield of the different steps is shown in Scheme 5.1. The overall yield is about 4%, which is mainly due to the low yield of the last step, since it is quite difficult to couple the dye to **5** and purify the resulting product. The synthesis of Fc_4-rhodamine was confirmed by NMR spectroscopy and mass spectroscopy (Appendix A). UV/Vis spectroscopy (Appendix A) and fluorescence spectroscopy were performed to investigate the properties of the new compound.

The excitation and emission spectra of Fc_4-rhodamine, as shown in Figure 5.2, were measured by fluorescence spectroscopy. As a comparison, excitation and emission spectra were recorded of the pure dye (lissamine rhodamine B sulfonylchloride, also 1 µM) in water. The dye has maximal fluorescence excitation at 565 nm light and maximal fluorescence emission at 580 nm light. The emission and excitation profiles of the dye and Fc_4-rhodamine are comparable to each other and to spectra in literature [46].

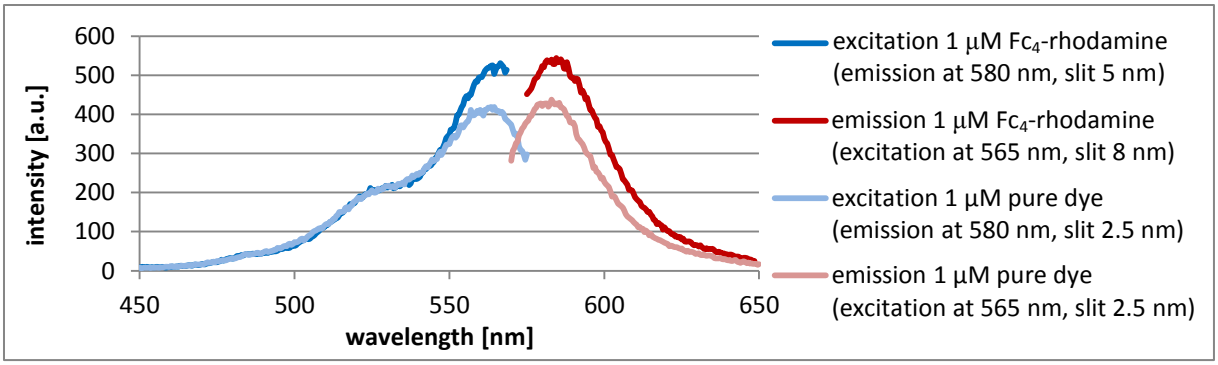

Figure 5.2. Excitation and emission spectra of Fc_4-rhodamine (1 µM in water, 0.5% MeOH, pH neutral) and of the pure dye (lissamine rhodamine B sulfonylchloride, 1 µM in water). The mentioned slit values equal to the emission slit.

When the same parameters were used in fluorescence spectroscopy, the measured maximum intensity of Fc_4-rhodamine was only 11% of the maximum fluorescence of the pure dye. This could be due to the poor solubility of Fc_4-rhodamine, but also quenching by the Fc groups of Fc_4-rhodamine could occur. This is confirmed by the observation that the maximum fluorescence of a solution with 0.5 µM pure dye and 5 µM Fc_4-rhodamine was 25% lower than that of a solution with only 0.5 µM pure dye, although the intensity should increase. The quenching effect was not further investigated, since the fluorescence was still high enough for visualization purposes.

To test the supramolecular interactions of Fc_4-rhodamine, CD monolayers were incubated with a 1 µM solution of Fc_4-rhodamine in water. The sample was rinsed with water and imaged with fluorescence microscopy, showing that the incubation was successful. The sample was consecutively rinsed with 10 mM CD in water, rinsed with 1% MeOH in water, and finally sonicated. The intensity did not change significantly after these steps, thus indicating a strong interaction between Fc_4-rhodamine and the substrate.

5.1.2 Electrochemistry

Next to the tetravalent guest molecule described in section 5.1.1, the already available Fc_2-rhodamine was used. The detection limit of cyclic voltammetry was too high (100 µM [47]) to measure the oxidation and reduction peaks of these guest molecules in water (5 µM). The guest concentration could not be increased due to poor solubility. Therefore, differential pulse voltammetry (DPV) was used, which has a detection limit of 10 nM under optimal conditions [47]. However, Fc_4-rhodamine (1 µM) was still not detectable with DPV. This might be due to the poor solubility of Fc_4-rhodamine, which induces precipitation of the guest molecules and thus a lower concentration than the desired 1 µM.

The differential pulse voltammogram of Fc_2-rhodamine is shown in Figure 5.3. A new peak arises at 0.43 V after adding the guest, which can thus be attributed to the oxidation and reduction of ferrocene. The peak position equals to E_{max} and can be used to calculate $E_{1/2}$: $E_{1/2} = E_{max} + \frac{\Delta E_p}{2}$ [47], so $E_{1/2}$ = 0.45 V (ΔE_p = amplitude = 40 mV). The Fc dendrimers used by Nijhuis are comparable in both structure and $E_{1/2}$ (0.50 V [25]). When an ideal peak separation of 57 mV is assumed, Fc_2-rhodamine is reduced at 0.42 V and oxidized at 0.48 V.

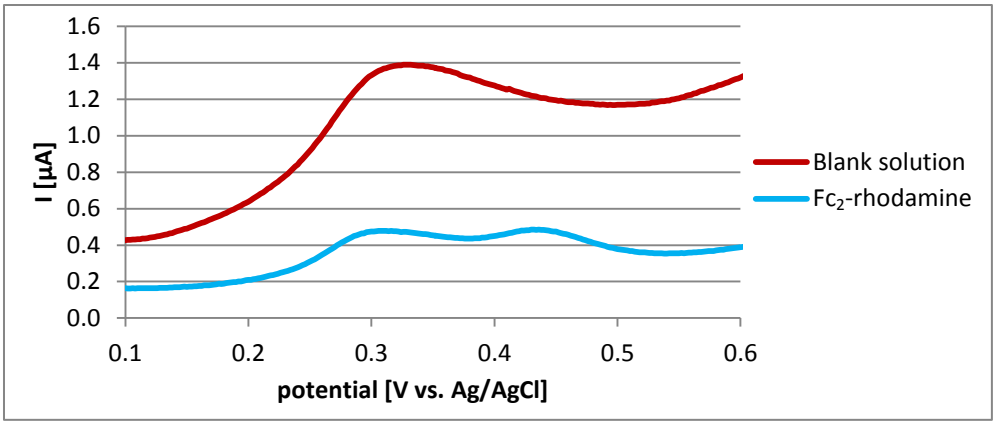

Figure 5.3. Differential pulse voltammogram of Fc_2-rhodamine (5 µM, 5% MeOH in water with 0.1 M K_2SO_4) and the same solution without guest as a blank; the amplitude was 40 mV.

5.2 Characterization of CD molecular printboard on glass

CD molecular printboards were synthesized on glass by a method developed by MnF [20]. Supramolecular interactions between the CD monolayer and guest molecules were tested by competition with CD in solution (10 mM in water, 4.5 h, four times refreshing). Extensive research has already been performed on competition with CD in solution for the adamantyl (Ad)-functionalized guests [16, 20]. The guest molecules used were Ad_2-rhodamine, Ad_3-rhodamine and Fc_4-rhodamine, whose results are shown in Figure 5.4. The shown intensity profiles consist of horizontal cross sections of pictures from the fluorescence microscope. The profiles are as expected, since the intensity is high in between the electrodes, and low on the electrodes where the guest molecules should not adsorb and the light is blocked by the Pt electrodes. The profiles were calculated by averaging three different places at the sample.

There are two trends for the different guest molecules. At first, the higher the multivalency, the higher the increase after the extra rinsing step with water. This observation cannot be explained, since it is unknown what happens after another extra rinsing step with water. These experiments were performed once, so no hard conclusions can be drawn.

The other trend is visible in the remaining intensity after incubation with CD in solution. If the remaining intensity is expressed as a percentage of the intensity after rinsing with water, the leftover is higher when the multivalency becomes higher. This is logical, since a higher multivalency induces stronger interactions in general, which can be applied directly to compare the divalent and trivalent guests to each other. However, the intrinsic binding constant of the adamantyl-CD interaction equals to $5.7 \cdot 10^4$ M^{-1}, which is stronger than the ferrocene-CD interaction with an intrinsic binding constant of $1.1 \cdot 10^3$ M^{-1} [33, 48]. Therefore, the trivalent and tetravalent guests cannot be compared directly.

These trends show that the CD monolayer reacts as expected and seems to work properly.

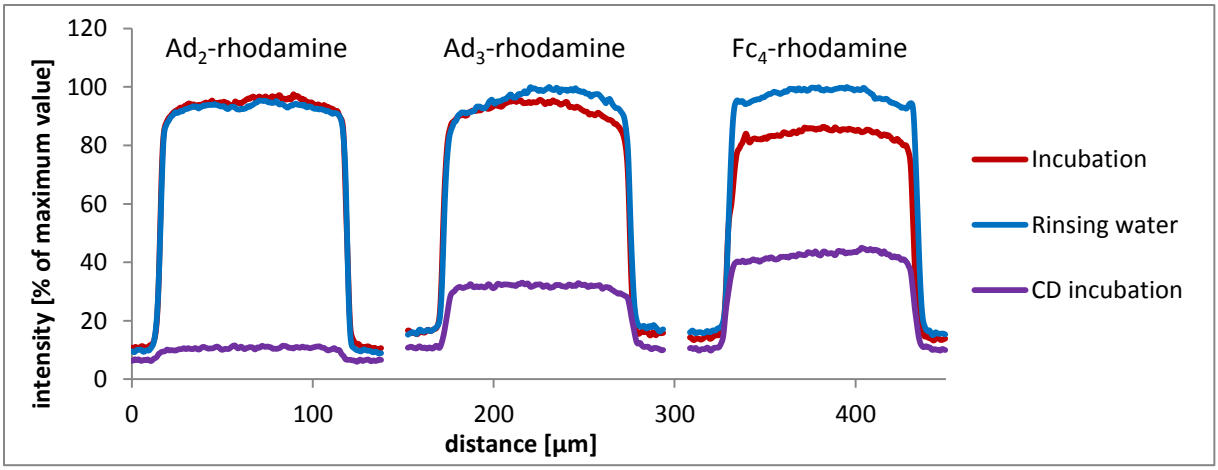

Figure 5.4. Intensity profiles of the different guests on a CD monolayer. The intensity is normalized to the highest measured value per guest. The different steps include incubation (10 min, 5 µM for Ad-guests and 1 µM for Fc_4-rhodamine), extra rinsing with water (1 min) and incubation with CD in water (4.5 h, 10 mM, refreshing 4 times).

5.3 Guest gradient on glass by a sink of divalent guest molecules

Guest molecules in solution were used to make a gradient of guest molecules on the surface (Scheme 5.2). The system is based on a CD molecular printboard in between electrodes on glass as host and divalent ferrocene-functionalized molecules as guest. The process starts with a full monolayer of Fc_2-rhodamine and 5 µM Fc_2-rhodamine in water on top with 5% MeOH to improve dissolution, and 0.1 M K_2SO_4 as electrolyte. When a potential is applied, Fc_2-rhodamine in solution is oxidized near the oxidizing electrode, thus creating a solution gradient of $(Fc^+)_2$-rhodamine. Because a sink of Fc_2-rhodamine is created near the oxidizing electrode, guest molecules desorb from the surface to restore the equilibrium and diffuse in solution from the reducing electrode to the oxidizing one because of concentration differences. In this way, a surface gradient of Fc_2-rhodamine is created and the supramolecular interactions can be monitored. $(Fc^+)_2$-rhodamine in solution and Fc_2-rhodamine on the surface could also react by exchanging an electron, but this does not happen frequently, because it is more difficult to oxidize Fc-CD than Fc [49]. The resulting surface gradient of guest molecules can be visualized by using fluorescence microscopy, since Fc_2-rhodamine contains a fluorescent dye.

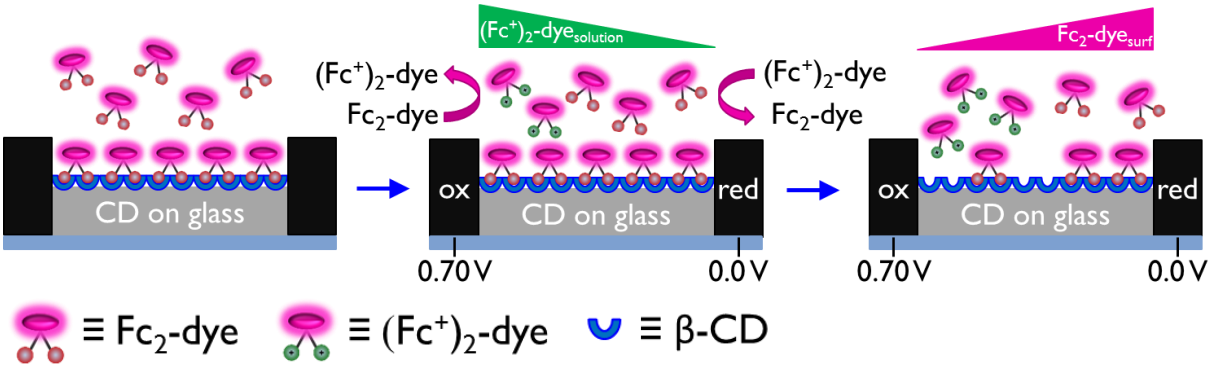

Scheme 5.2. Schematic overview of the electrochemically induced desorption process of Fc_2-rhodamine from the molecular printboard, resulting in guest gradient formation on the surface

The system was tested, although section 5.1.2 described that it was difficult to prove that Fc_2-rhodamine could be oxidized. A potential of 0.70 V was applied to one working electrode and 0.0 V to the other for 2 h. The sample was rinsed immediately after the experiment, since the gradient

disappears when no potential is applied. However, only a flat intensity profile was observed in between the electrodes, so the surface gradient formation did not work. The most remarkable point, however, was a tremendous increase in intensity. When the sample was measured in dry state, the maximum intensity was three times higher after applying the potential than after incubation. The intensity was barely lowered by sonication in water or a CD solution or incubation in 10 mM CD in water for 3.5 h.

Maybe the guest molecules in solution adsorb onto the surface, thus increasing the intensity. However, when the same experiment was performed without guest molecules in solution, the intensity still increased by 2 or 5 times while the potential was only applied for 10 s or 5 min, respectively. Therefore, it is assumed that guest molecules physisorb onto the electrodes during the incubation step, and adsorb onto the guest monolayer on the surface when the CD solution is placed on top. Physisorption during incubation could be avoided by starting with an empty monolayer.

Since guest gradient formation did not work, it was attempted to obtain the extreme situation of an empty monolayer without applying a potential. The sample was rinsed with water, incubated in water (45 min), incubated in 5% MeOH (4 h) and incubated in 10 mM CD in water (4 h), but the intensity was always higher than after incubation. Only a sample with microcontact printed lines of Fc_2-rhodamine showed a large decrease in intensity after incubation in 5% MeOH in water for 2.5 h. It is very remarkable that the intensity did not decrease by competition like the other guests did (section 5.2). Perl [33] has used the same guest molecule and observed desorption within 1 h when either water, 0.1 mM CD in water or 0.2 mM CD in water was placed on top, although only a small amount desorbed. This indicates that the Fc_2-rhodamine molecules do not work properly anymore, which might be due to the fact that the batch used was made in 2007. Consequently, experiments with the described system were not proceeded.

5.4 Guest gradient on glass with K_3IrCl_6 as mediator

Another option to desorb Fc guest molecules from the surface is by electron transfer by a mediator. Scheme 5.3 shows the gradient formation process, starting with a CD monolayer incubated with Fc_4-rhodamine. Fc_4-rhodamine was used because of its strong supramolecular interactions with the CD layer, so the molecules would only desorb by electrochemistry instead of competition or complexation. The two electrodes of the interdigitated electrode array are used as working (W) and counter (C) electrode, respectively. At first, a solution gradient of the mediator (K_3IrCl_6) is formed electrochemically, where $[IrCl_6]^{3-}$ is oxidized to $[IrCl_6]^{2-}$ at the working electrode and any $[IrCl_6]^{2-}$ that diffuses to the counter electrode is reduced back to $[IrCl_6]^{3-}$. Subsequently, this solution gradient is transferred to a surface gradient of guest molecules by spontaneous oxidation of ferrocene (Fc) to ferrocenium (Fc^+) by $[IrCl_6]^{2-}$. At the working electrode, the concentration of $[IrCl_6]^{2-}$ is the highest, so almost all Fc_4-rhodamine molecules are oxidized and desorb from the printboard. At the counter electrode, however, the concentration of $[IrCl_6]^{2-}$ is almost negligible, so the guest does not desorb.

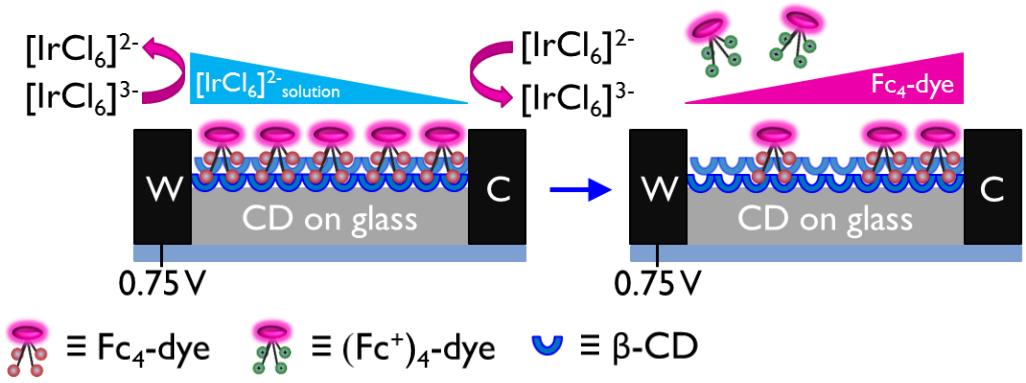

Scheme 5.3. Schematic overview of the electrochemically induced desorption process of Fc_4-rhodamine from the molecular printboard, inducing guest gradient formation

5.4.1 Cyclic voltammetry of mediator solution

The mediator solution, consisting of 2.0 mM $[IrCl_6]^{3-}$ as the mediator in its reduced form and 0.1 M K_2SO_4 as electrolyte, was characterized with cyclic voltammetry, as shown in Figure 5.5a. The anodic peak, lying at 0.85 V vs. Ag/AgCl, equals to the potential where $[IrCl_6]^{3-}$ is oxidized to $[IrCl_6]^{2-}$. In the reverse scan, $[IrCl_6]^{2-}$ is reduced to $[IrCl_6]^{3-}$ at about 0.71 V (cathodic peak).

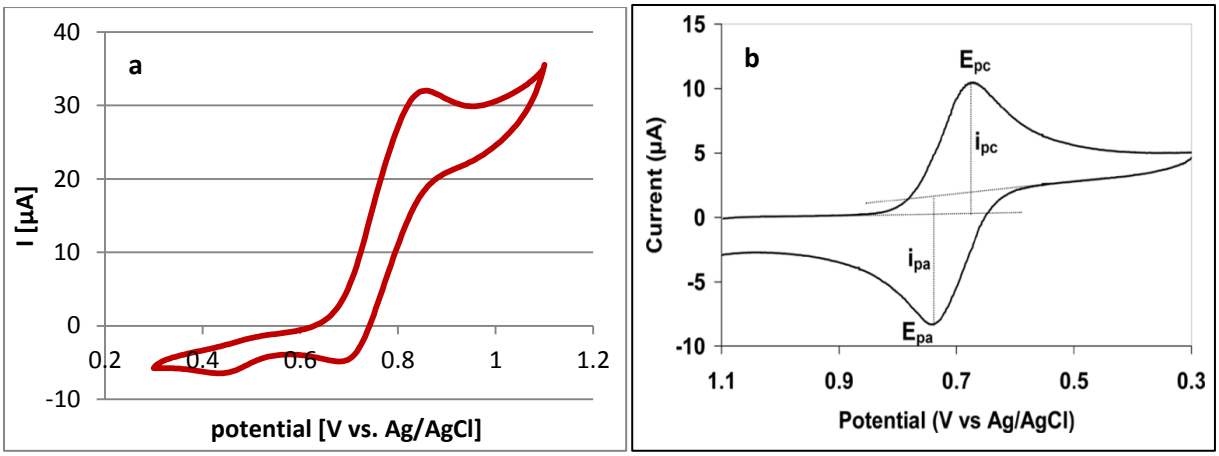

Figure 5.5. a) Cyclic voltammogram of the mediator solution used containing 2.0 mM $[IrCl_6]^{3-}$ and 0.1 M K_2SO_4, measured in the electrochemical cell at 40 mV/s with a step potential of 0.0044 V; b) Cyclic voltammogram from literature of 2.0 mM $[IrCl_6]^{2-}$ measured at 40 mV/s [50]

As a comparison, Figure 5.5b shows a cyclic voltammogram of a K_2IrCl_6 solution found in literature. The concentration is the same, but this graph starts with the mediator in its oxidized form. The graph is mirrored due to different conventions of positive and negative current values. The peaks of the literature graph are slightly shifted to higher potentials. Furthermore, Figure 5.5a shows a third peak at 0.44 V, which was not observed when only one electrode of the interdigitated electrode array and a separate counter electrode were used. The new peak might be due to the occurrence of another unknown reaction or the small distance between the working and counter electrode.

5.4.2 Desorption experiments

The potential was set at 0.75 V vs. Ag/AgCl for 100 s for the first desorption experiments, following the method of Nijhuis [25] and the results of Petrovic [50]. However, when looking at the cyclic voltammogram, it would have been better to use a potential around 0.8 V or slightly higher, in order

to decrease the portion of the cathodic reaction and increase the occurrence of the anodic reaction to produce $[IrCl_6]^{2-}$.

In the first experiments only one electrode of the interdigitated electrode array and a separate counter electrode were used, trying to prove that the desorption of Fc_4-rhodamine by oxidation is possible. The fluorescence intensity decreased dramatically after applying the potential and became almost equal to the profile of an empty monolayer, so it was assumed that the ferrocene functionalities were desorbed from the surface as expected.

Control experiments were performed by applying a potential at 0.3 V, where $[IrCl_6]^{2-}$ is converted to $[IrCl_6]^{3-}$ and the mediator is strongly reducing (see Figure 5.5). So when this potential is applied to a CD monolayer with Fc_4-rhodamine, the ferrocene functionalities should not be oxidized, thus Fc_4-rhodamine should not desorb and the fluorescence should not decrease. As can be seen in the intensity profiles in Figure 5.6, the resulting intensity is only half of the original value after applying a potential of 0.3 V, which does not agree with expectations. Subsequently, a potential of 0.75 V was applied and the fluorescence lowered to that of an empty monolayer, as expected.

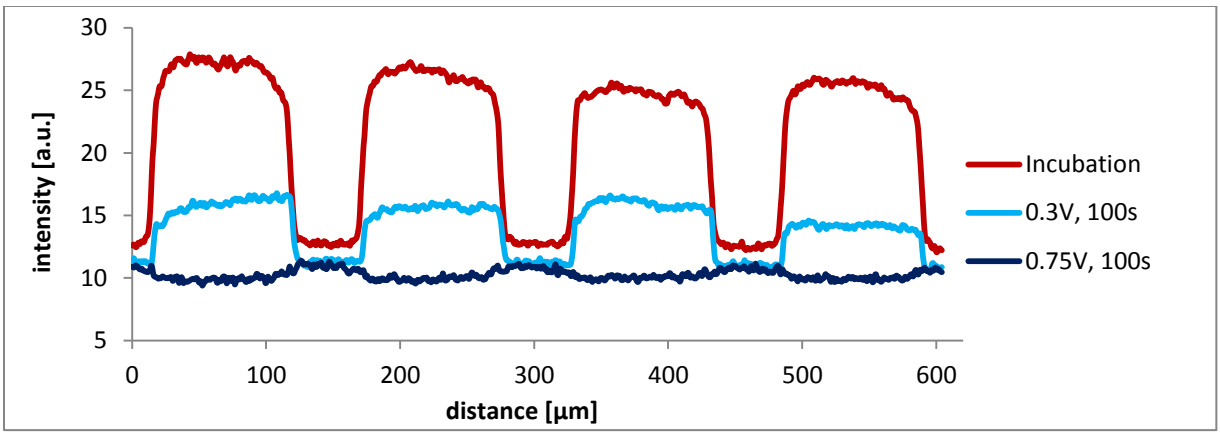

Figure 5.6. Intensity profiles of Fc_4-rhodamine on a CD monolayer (exposure time of the fluorescence images was 2000 ms). The different steps include incubation with Fc_4-rhodamine (10 min, 1 µM), applying a potential (0.3 V, 100 s) and applying another potential (0.75 V, 100 s).

Furthermore, control experiments were performed by using adamantyl-functionalized fluorescent guest molecules. Adamantyl moieties are not redox active, so they should not desorb when applying a potential. Figure 5.7 shows the intensity profiles of the control experiments with Ad_2-fluorescein. After incubation, the intensity is lowered a bit by rinsing with water, which could be due to the removal of physisorbed molecules, for example. After applying a potential of 0.75 V, the intensity became equal to that of an empty monolayer, although the adamantyl groups should not desorb.

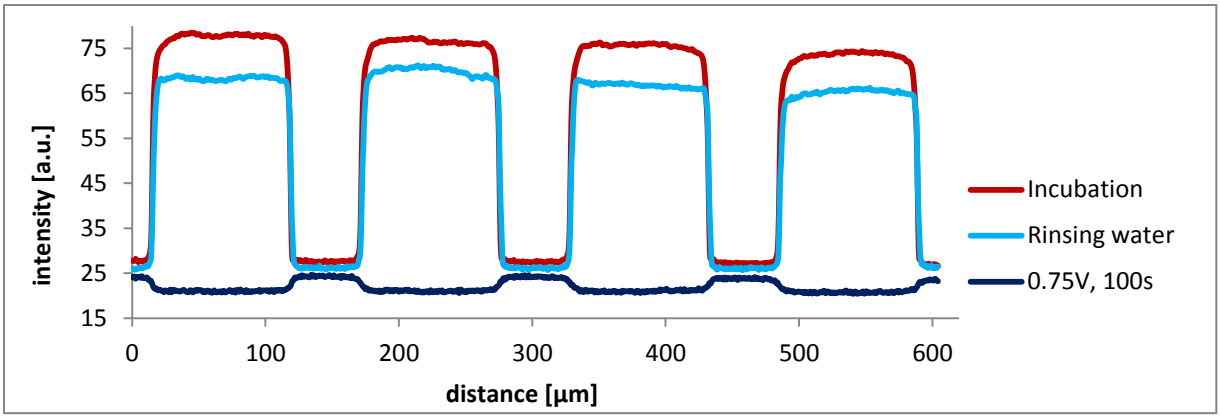

Figure 5.7. Intensity profiles of Ad_2-fluorescein on a CD monolayer (exposure time of the fluorescence images was 2000 ms). The different steps include incubation with Ad_2-fluorescein (10 min, 50 µM), extra rinsing with water (1 min) and applying a potential (0.75 V, 100 s).

In conclusion, the fluorescence of Fc_4-rhodamine decreased when applying a potential of 0.3 V, although Fc_4-rhodamine could not be oxidized at that potential, and the measured intensity of Ad_2-fluorescein decreased after applying a potential of 0.75 V, while Ad_2-fluorescein should not desorb since the adamantyl groups cannot be oxidized. Therefore, the influence of the electrochemistry was investigated.

During electrochemistry, the redox couple in solution can be monitored when the current at constant potential is measured in time. The I,t-curves (chronoamperograms) of the control experiments are shown in Figure 5.8. The figure shows results as expected. For the graphs at 0.75 V, the current starts at a relatively high value (about 100 µA) and decays to a stable plateau, meaning that an electrochemical reaction occurs. The experiments at 0.75 V show approximately the same graph. When applying 0.3 V, the high starting current can be explained by a capacitance effect due to charging of the electrodes. The plateau value is only a few nA, which means that almost no electrochemical reaction occurs. It can be concluded that the decrease in intensity in this case cannot be due to an electrochemical reaction.

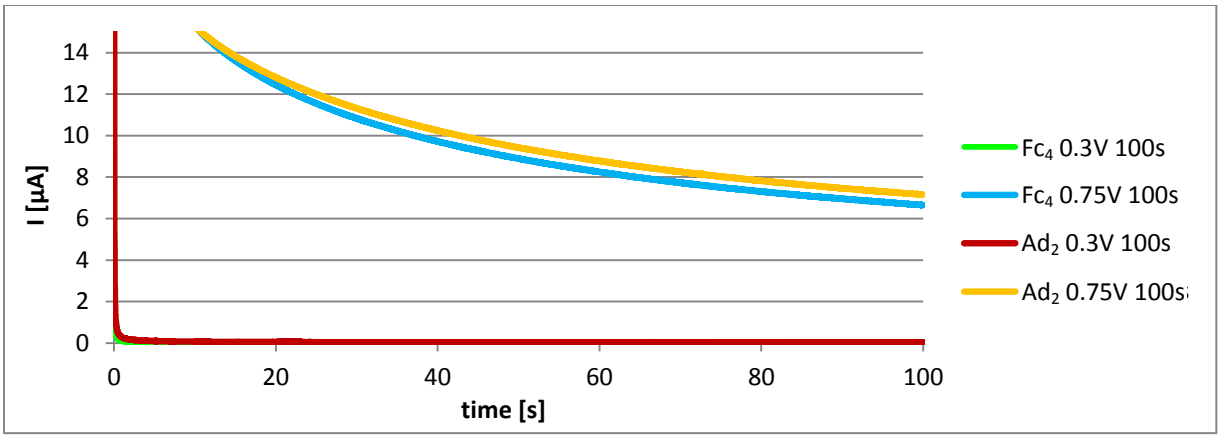

Figure 5.8. Chronoamperograms obtained by applying a potential for 100 s at 0.3 V or 0. 75 V (vs. Ag/AgCl) on a CD monolayer with Fc_4-rhodamine or Ad_2-fluorescein

5.4.3 Influence of mediator solution

Based on the results shown in the previous section, it can be inferred that the fluorescence intensity also lowers when there are almost no electrochemical reactions. This leads to the assumption that the mediator solution influences the system. This was tested by rinsing or incubation with the

mediator solution. Figure 5.9 shows the intensity profiles of the experiments with Fc_4-rhodamine. The extra rinsing step with water influences the intensity a bit, but the most important conclusion is that incubation with the mediator solution leads to a significant decrease in the intensity.

It was hypothesized that the fluorescence was quenched by the mediator solution, comparable to the results of Basabe-Desmonts who used the quenching of fluorophores as ion sensing method [51]. Therefore, the sample was incubated with an EDTA solution (10 mM), since EDTA is a good chelating agent that removes cations. This appears to increase the intensity, but the sample was very inhomogeneous, so no hard conclusions could be drawn. This test was also performed for other experiments, but the intensity profiles increased only a bit or did not change after rinsing or incubation with EDTA. The original intensity was never reached again.

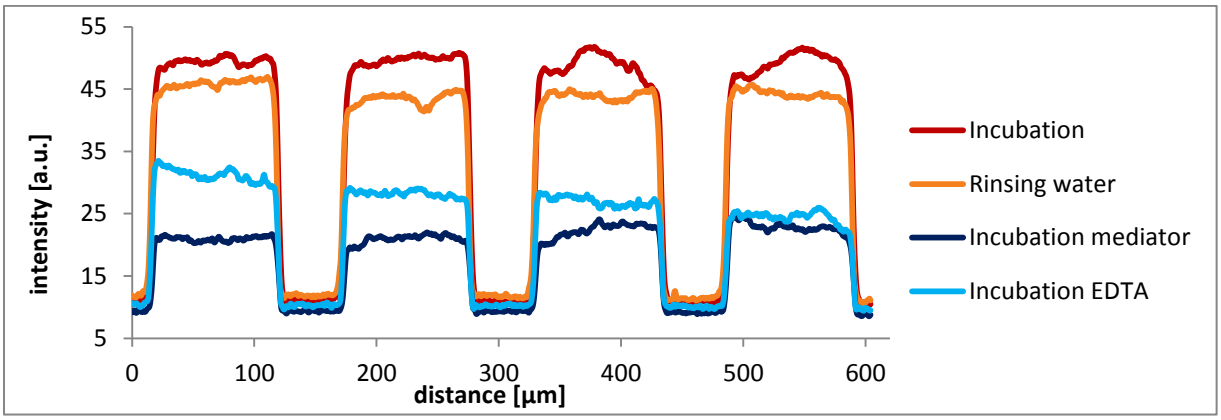

Figure 5.9. Intensity profiles of Fc_4-rhodamine on a CD monolayer (exposure time of the fluorescence images was 2000 ms). The different steps include incubation with Fc_4-rhodamine (10 min, 1 µM), extra rinsing with water (1 min), incubation with mediator solution (10 min) and incubation with EDTA solution (10 mM, 10 min).

In the same way, the influence of the mediator solution on the fluorescence of Ad_2-fluorescein was tested, as shown in Figure 5.10. After rinsing the sample with mediator solution for a short time, the intensity drops significantly, so it can be concluded that the mediator solution influences the fluorescence of fluorescein too. When a potential of 0.3 V was applied, the intensity did not change, while the intensity became equal to that of an empty monolayer after applying a potential of 0.75 V.

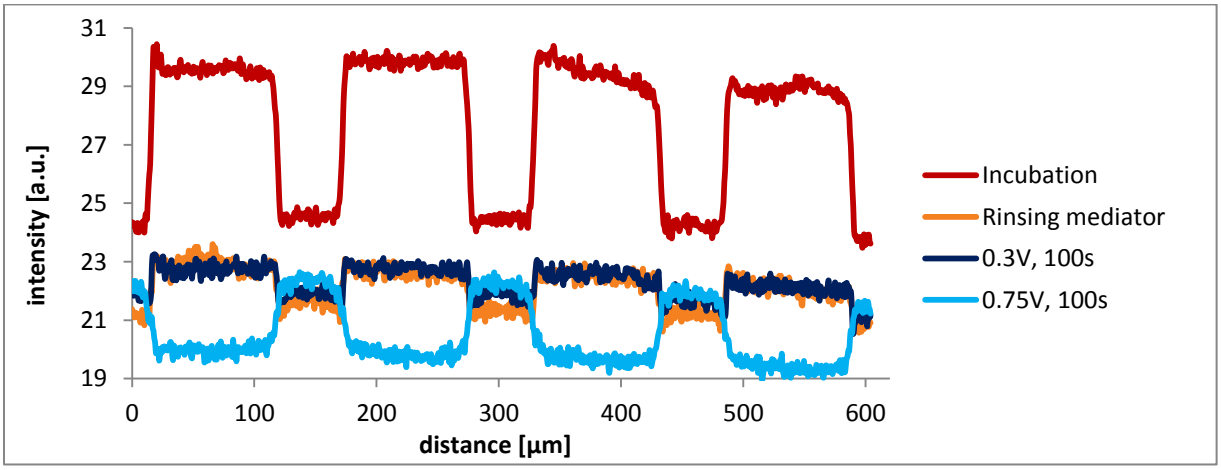

Figure 5.10. Intensity profiles of Ad_2-fluorescein on a CD monolayer (exposure time of the fluorescence images was 2000 ms). The different steps include new incubation with Ad_2-fluorescein (10 min, 50 µM), rinsing with mediator solution (1 min), applying a potential (0.3 V, 100 s) and applying another potential (0.75 V, 100 s).

In short, the mediator solution affects the fluorescence intensity of both the rhodamine and the fluorescein dye without applying a potential. It is unlikely that the mediator solution destructs the CD layer, since the same combination was successfully used by Nijhuis [25]. However, Nijhuis did not use fluorescence as visualization method, so maybe the mediator solution affects both the rhodamine and the fluorescein dye. Therefore, the influence of the different components of the mediator solution, including K^+, SO_4^{2-} and $[IrCl_6]^{3-}$, on the fluorescence of Fc_4-rhodamine was investigated. The emission spectra in Figure 5.11 show that K^+ and SO_4^{2-} do not significantly influence the fluorescence intensity of Fc_4-rhodamine, while the mediator solution in total has a large influence.

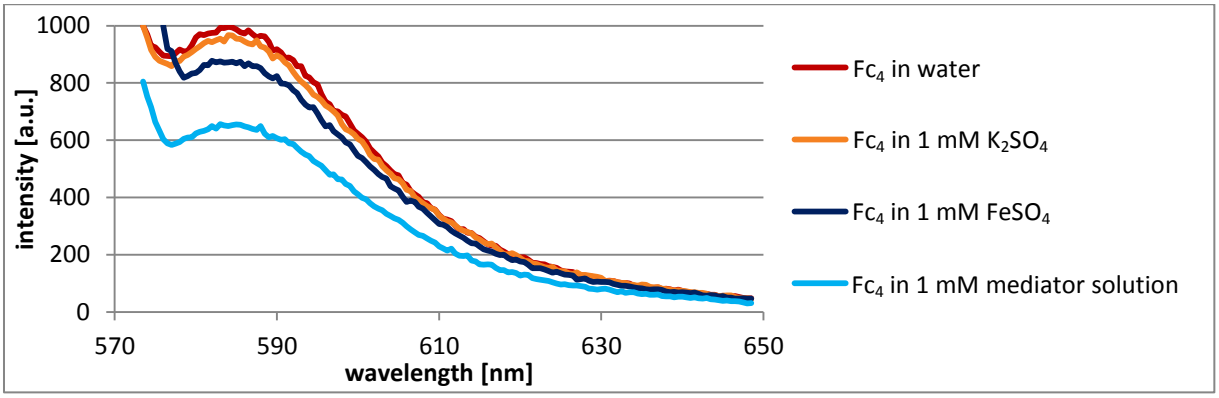

Figure 5.11. Emission spectra of Fc_4-rhodamine (0.5 µM in different solutions, 0.25% MeOH) with the excitation wavelength fixed at 565 nm, measured with an emission slit of 10 nm

The same results were observed for Ad_3-rhodamine. The decrease in intensity is for both guest molecules not as significant as observed for the intensity profiles. This is probably due to the used ratio of guest to mediator in solution (1:2000) which is much lower than when the guest molecules are adsorbed on the surface and the mediator solution is available in bulk amounts.

Besides the previous described experiments, refilling of the CD layer was tested by a second incubation step after desorption. It was expected that if there is nothing inside the CD molecules after desorption, new incubation should lead to an intensity that is comparable to the value after the first incubation step. While this refilling experiment was performed several times with different guest molecules, none of them reached the original intensity.

Therefore, it could be possible that the mediator solution destroys the guest molecules irreversibly. This could induce a loss in fluorescence by destroying the dye or even disconnecting the dye from the rest of the guest molecules. If the remaining part keeps adsorbed on the CD layer, a large part of the CD layer is still occupied, which would explain why it is not possible to refill the monolayer. However, this irreversible influence would be surprisingly high for a solution that only contains salt ions.

In conclusion, the mediator has a detrimental influence on the fluorescence of the guest molecules. Consequently, it was not possible to draw conclusions from the fluorescence intensity profiles and the experiments with this system were not proceeded.

5.5 Guest gradient on glass with FcMeOH as competitor

A new system was designed without Fc_2-rhodamine molecules in solution or K_3IrCl_6 as mediator. However, still an electrochemically active species is needed to make a solution gradient. Therefore, ferrocenemethanol (FcMeOH) is added in the solution as a monovalent competitor. Its cyclic voltammogram (Figure 5.12) shows an oxidation peak at 0.275 V and a reduction peak at 0.195 V.

With an overpotential of about 0.2 V, the two working electrodes were set at 0.47 V and 0.0 V with the bipotentiostat to make a solution gradient of $FcMeOH^+$ in between the electrodes.

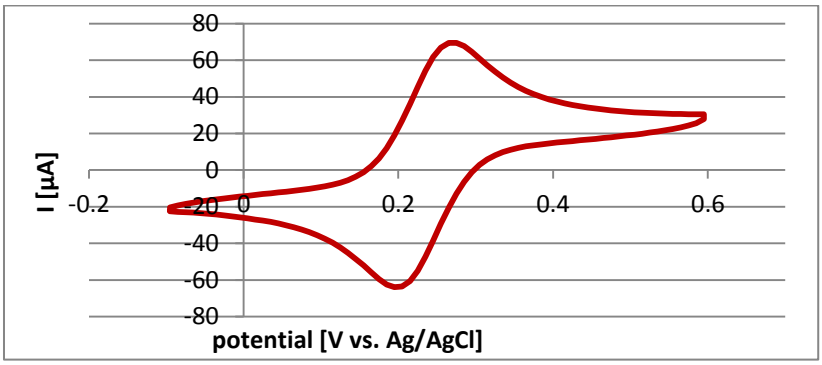

Figure 5.12. Cyclic voltammogram of 1 mM FcMeOH in water with 0.1 M K_2SO_4, measured at 100 mV/s

Scheme 5.4 shows that the process starts with a full monolayer of Ad_2-rhodamine on a CD monolayer on glass. After applying the described potentials, it should be straightforward to create a $FcMeOH^+$ gradient in solution. However, in fact the inverse gradient of FcMeOH is needed to create the surface gradient of guest molecules. The idea is that FcMeOH is present in large excess near the reducing electrode (the starting solution contains 1 mM FcMeOH), where it should compete with Ad_2-rhodamine, even though FcMeOH is only a monovalent guest. The competition results in loss of the fluorescence guest molecules and thus darkening occurs near the reducing electrode. On the other hand, a part of FcMeOH near the oxidizing electrode is reacted into $FcMeOH^+$, thus less competitor is available and less Ad_2-rhodamine molecules desorb. It should be noted that the FcMeOH concentration in solution should not be too high, because in that case FcMeOH would still be present in large excess near the oxidizing electrode and the effective concentration difference near the two electrodes is too low to establish a surface gradient of guest molecules. On the other hand, the concentration of FcMeOH should be high enough to obtain enough competition with the divalent guest on the surface.

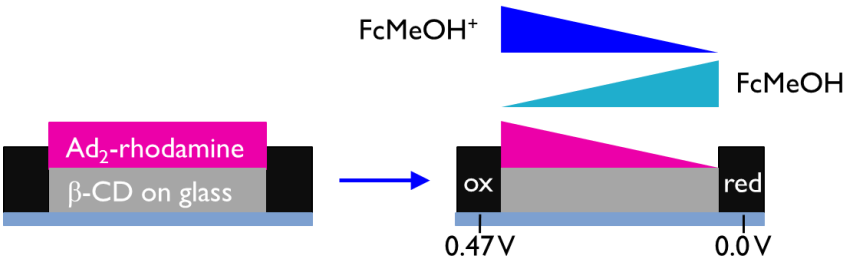

Scheme 5.4. Guest gradient formation on a CD molecular printboard on glass by using a FcMeOH solution gradient

The intensity profiles after applying a potential are shown in Figure 5.13 for two different samples. Gradients of Ad_2-rhodamine were formed in the right direction. Backfilling with Ad_2-fluorescein resulted in gradients in the opposite direction, thus the system worked as expected. This is the first time, to our knowledge, a surface gradient of guest molecules was created.

The maximum intensity of the gradient was a factor of 3-4 lower than after incubation, and the observed intensity differences within the gradient were relatively low. The steepest gradient would arise when the intensity close to the oxidizing electrode is equal to the intensity after incubation, while the intensity close to the reducing electrode equals that of an empty monolayer. Therefore, further optimization is possible by varying parameters, e.g. time of applying a potential, applied

potential, FcMeOH concentration in solution, and CD concentration in solution, but this was not performed due to lack of time.

Figure 5.13a shows smooth gradients, while Figure 5.13b shows inhomogeneity within the gradient (gradient 1 and gradient 2 include different places on the sample). This was due to black spots randomly spread over the surface after applying a potential, which were larger on the sample of Figure 5.13b. Further research is necessary to explain the occurring black spots, but it can be ruled out that the gradient arises because of a gradient in black spots, since the spots were observed randomly on the surface.

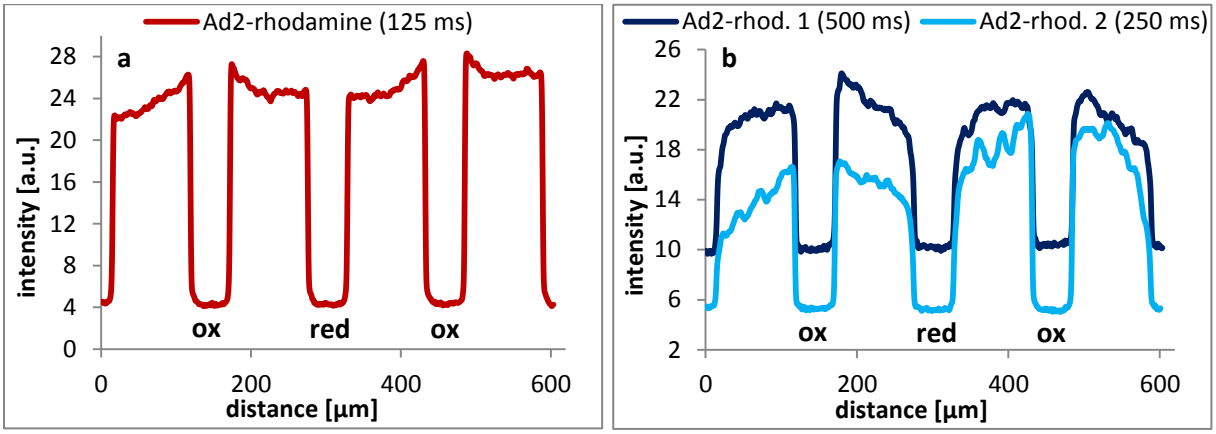

Figure 5.13. Intensity profiles of Ad_2-rhodamine gradients on a CD monolayer for two different samples, after applying a potential (0.47 V & 0.0 V, 3 h) with a solution of 1 mM FcMeOH and 0.1 M K_2SO_4 in water on top

Since the designed system of Scheme 5.4 worked as expected, the system was extended by adding CD in solution. It was expected that this would switch the direction of the gradient, as shown in Scheme 5.5. Since FcMeOH (1 mM) could also interact with CD (0.6 mM) in solution, a large amount of CD will be bound to FcMeOH, especially near the reducing electrode. Near the oxidizing electrode, a lot of $FcMeOH^+$ is present that does not interact with CD, thus a lot of free CD molecules are available. A solution gradient of free CD molecules is formed, that increases the desorption rate near the oxidizing electrode, and results in a lower fluorescence intensity.

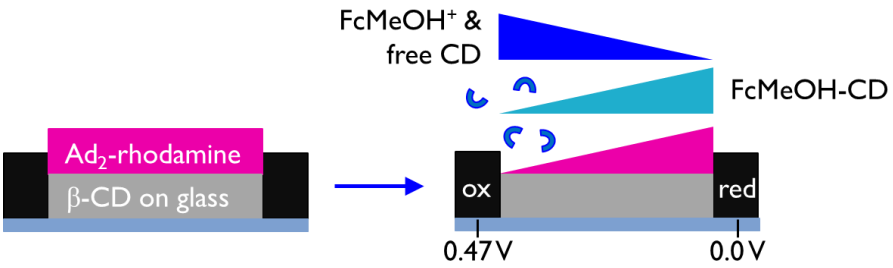

Scheme 5.5. Guest gradient formation on a CD molecular printboard on glass by using a solution gradient of free CD molecules

Figure 5.14 shows very clear gradients after 3 h. The exposure time of the incubation step was four times lower than for the other images, so the fluorescence intensity actually decreased a lot after gradient formation. The gradients were observed over the whole reaction area, although gradients with different intensities were found (“gradient 1” and “gradient 2”). The direction of the gradient was reversed as expected, since the highest intensity was observed at the reducing electrode instead of the oxidizing electrode.

Not all FcMeOH (1 mM) could be bound to CD (0.6 mM), so there is probably still a small FcMeOH gradient present in solution that induces a gradient in the original direction (Figure 5.13). Therefore, further optimization is possible by lowering the FcMeOH gradient.

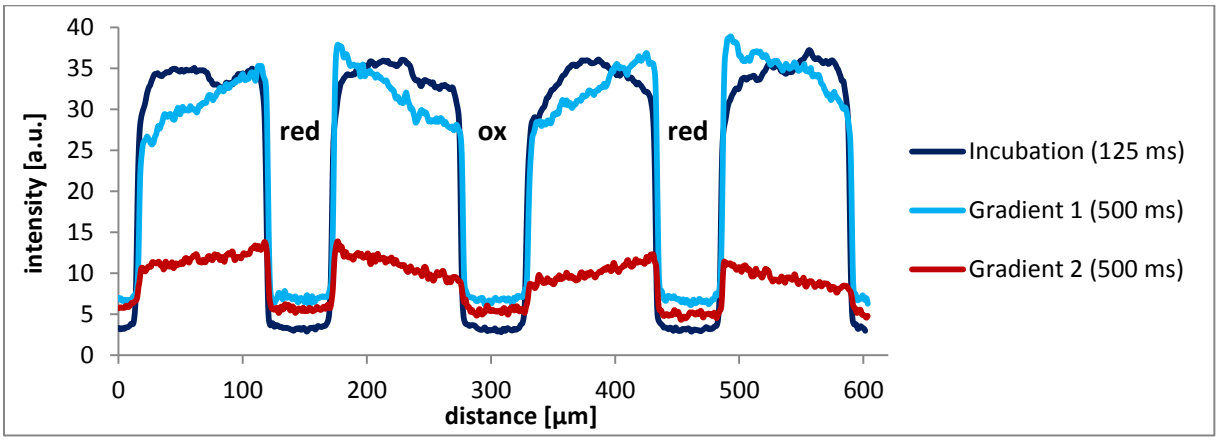

Figure 5.14. Intensity profiles of Ad_2-rhodamine on a CD monolayer with on top a solution of 1 mM FcMeOH, 0.1 M K_2SO_4 and 0.6 mM CD in water (exposure time of the fluorescence images of the incubation step was 125 ms, while 500 ms was used after gradient formation). The different steps include incubation with Ad_2-rhodamine (10 min, 5 µM) and applying a potential (0.47 V & 0.0 V, 3 h).

5.6 Guest gradient on gold

In this section, the substrate is changed from glass to gold. Gold is advantageous because of its conductivity, so electrons can be transported via the substrate and no mediator or electrochemical solution gradient is needed. The system is based on a molecular printboard of CD on gold, already used within MnF [41], and guests with Fc groups and a dye (Fc_2-rhodamine or Fc_4-rhodamine). The Fc groups can be oxidized to Fc^+ when an oxidizing potential is applied to gold, which leads to electron uptake by the gold working electrode and desorption of the guest molecules. By applying an in-plane potential gradient on gold, a surface gradient of guest molecules can be established (Scheme 5.6). A bipotentiostat can be used to apply an in-plane potential gradient at the gold working electrodes, as described by Wang et al. [52]. In this way, the Fc groups are oxidized, and thus desorbed, at the side with the oxidizing potential (i.e. 0.70 V) and keep interacted with CD at the side with the reducing potential (i.e. 0.0 V). A relatively large overpotential is used, since there is a potential decay between the place where the potential is applied and the reaction area with the solution on top.

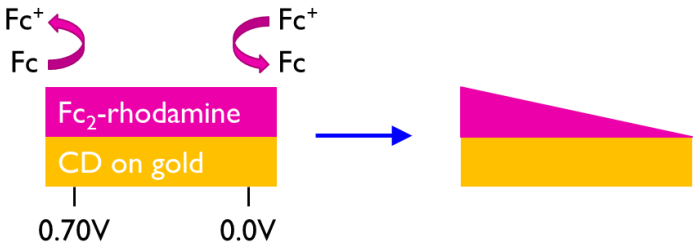

Scheme 5.6. Guest gradient formation on a CD molecular printboard on gold by using an in-plane potential gradient

At first, oxidation of a full monolayer of ferrocene guests from a CD monolayer on gold was tested by cyclic voltammetry. Nijhuis [25] has performed the same experiments with Fc dendrimers. Only desorbed molecules that stay close to the surface could be reduced and bind back to the CD layer. Consequently, the intensity should decrease when the number of scans increases and the oxidation and desorption of Fc guest molecules can be visualized. However, during cyclic voltammetry the

oxidation and reduction peaks of Fc_2-rhodamine were hardly visible (Figure 5.15 shows the best graph), and the cyclic voltammograms of Fc_4-rhodamine did not show any peak. Therefore, the desorption of Fc_2-rhodamine and Fc_4-rhodamine could not be proven. Maybe the Fc dendrimers of Nijhuis were better detectable due to the higher concentration of Fc groups. The signal might improve when using a better CD monolayer, since the CD molecules on the current substrate were poorly packed (section 3.2.2). As an alternative, surface plasmon resonance might be used to visualize the adsorption and desorption of the guest molecules.

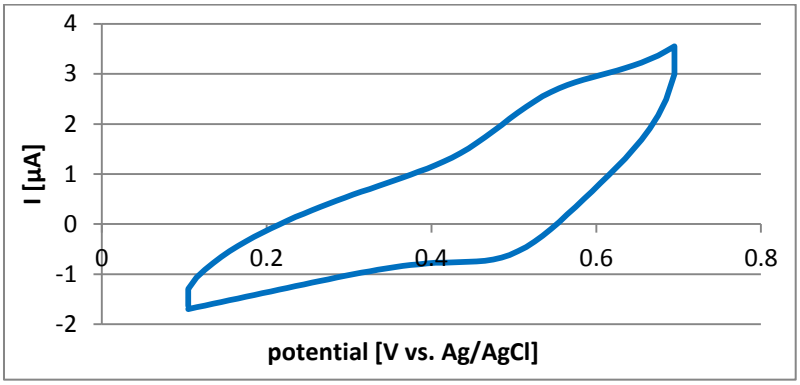

Figure 5.15. Cyclic voltammogram of Fc_2-rhodamine on a CD layer on gold with 0.1 M K_2SO_4 in water on top, measured at 100 mV/s

Since it is assumed that the ferrocene guests can be oxidized by gold, but only the measurement by cyclic voltammetry was unsuccessful, the system could be extended to guest gradient formation. However, still a method is needed to visualize the guest gradient. Fluorescence would be an effective method, but gold quenches fluorescence in general [53]. Therefore, at first the fluorescence was measured of Fc guests on a CD monolayer on 20 nm thick gold layer. The fluorescence of microcontact printed lines of Fc_2-rhodamine was only barely visible after a long exposure time (2 s). After rinsing, the fluorescence of the same sample was not visible anymore. When Fc_4-rhodamine was microcontact printed, no fluorescence was observed.

Before the system as described in Scheme 5.6 can be tested, at first a good visualization method had to be found. To avoid the problem with fluorescence on gold, the substrate was changed to indium tin oxide (ITO). This substrate is conductive, so an in-plane potential gradient can be applied, and does not quench fluorescence [54]. However, there is no procedure available to make a CD monolayer on ITO. Since both glass and ITO are oxide materials, the procedure for CD on glass was applied to ITO. Changes in contact angle were measured in another trend than on glass (Table 5.1) and no fluorescence of microcontact printed lines of Fc_2-rhodamine was observed. Therefore, probably no CD monolayer was formed on ITO, which is a requirement to proceed with surface gradients on ITO.

Table 5.1. Static contact angle measurements for CD on ITO compared to glass

Reaction step	Static value on glass [°]	Static value on ITO [°]
OH (oxygen plasma)	< 20	< 20
NH_2	44	32 ± 2.7
SCN	54	41 ± 3.6
β-CD	47	52 ± 1.9

5.7 Summary

Different systems were designed based on the oxidation of ferrocene groups, which do not interact with CD on the surface and thus desorb. However, the use of Fc_2-rhodamine in solution led to unexplained intensity increases, and the use of K_3IrCl_6 as mediator resulted in a detrimental influence on the fluorescence of the guest molecules. Therefore, the experiments with these systems were not proceeded.

The designed system for a non-covalent guest gradient on gold could not be tested due to quenching of fluorescence on gold.

To our knowledge, the first non-covalent surface gradient of guest molecules was created. Electrochemistry was used to produce a solution gradient of FcMeOH, which acted as a competitor for Ad_2-rhodamine on the CD printboard. The direction of the gradient could be reversed by adding CD in solution. Further research is necessary to optimize the steepness of the gradients.

6 Steering molecular motion by surface gradients

Directed motion was desired in two ways, namely via a host gradient on the surface or a solution gradient of a host or competitor. The host gradient could be made directly (irreversible) or via guest gradient formation with an opposite gradient of free host molecules (reversible). However, since the observed host gradient was not completely understood yet, motion was not tested on this system. Motion on the guest gradient system was not tested due to lack of time. Therefore, this chapter only describes an experiment with the second option, namely directed motion of microcontact printed (μCP) lines via a host gradient in solution. At first, spreading experiments of Perl were repeated (section 6.1) to obtain symmetric spreading of molecules. Subsequently, an attempt was made to direct the spreading profiles differently for different places at the surface (section 6.2).

6.1 Symmetric spreading of microcontact printed lines

Within MnF, Perl [16, 33] has studied the spreading of multivalent guests on a CD molecular printboard on glass. When guest molecules were microcontact printed in lines, a stable system is made where no motion is observed under dry conditions. However, when CD in solution is placed on top of the substrate, competition is induced for the guest moieties to interact with host sites at the surface or in solution (Scheme 6.1). Consequently, the guest molecules start to move and spreading of the lines can be observed by fluorescence microscopy. Depending on the multivalency of the guests and the CD concentration in solution, different spreading mechanisms were observed.

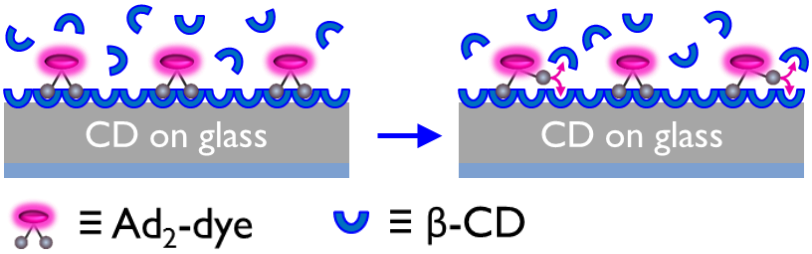

Scheme 6.1. Microcontact printed lines of Ad_2-rhodamine on a CD molecular printboard on glass. CD in solution induces competition and thus spreading of the guest molecules on the surface.

The experiments of Perl were repeated for a divalent guest (Ad_2-rhodamine) with 0.6 mM CD in solution (Scheme 6.1). Figure 6.1 shows the fluorescence images in time together with the intensity profiles. Every image is taken in situ, and at the same place of the sample. As can be seen in Figure 6.1b, the background increases in time, which was also observed by Perl. This increase is due to spread molecules on the surface and measured fluorescence of desorbed molecules in solution. To make a better comparison, the difference between the background from each image and the background at 0 min was subtracted (Figure 6.1c). This does not change the fitting of the graphs, so the width of the peaks remains equal. A decrease in intensity can be observed.

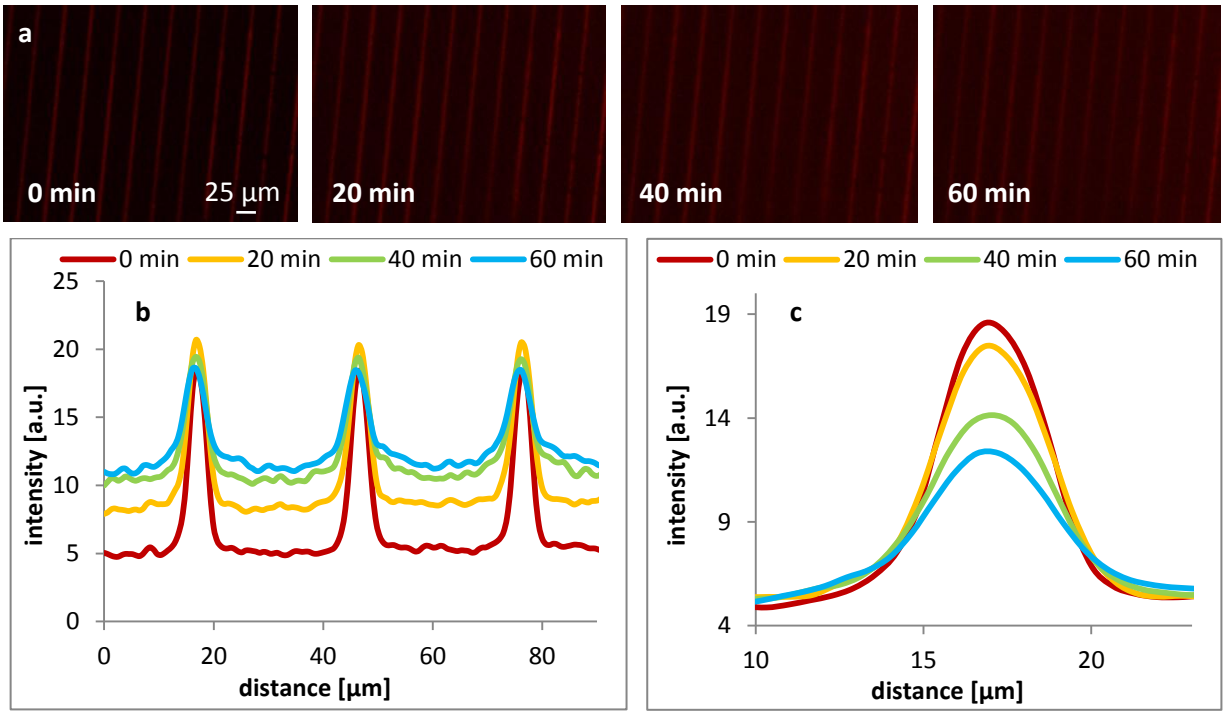

Figure 6.1. Spreading of Ad_2-rhodamine on a molecular printboard when 0.6 mM CD was placed on top: (a) fluorescence images (exposure time 500 ms); (b) intensity profiles; (c) intensity profiles after subtracting background

The changes of the supramolecular patterns in time were described by the peak width at half maximum, which was determined by fitting a Gaussian curve. Figure 6.2 shows that the spreading of Ad_2-rhodamine increased linearly in time. The spreading rate is represented by the slope of this graph, which equals to 0.25 ± 0.026 nm/s. This value corresponds reasonably well with the value found by Perl (0.56 ± 0.072 nm/s), especially when differences in experimental conditions are taken into account, i.e. another lamp in the fluorescence microscope was used and the batch of Ad_2-rhodamine molecules was from 2007. Furthermore, differences in the background subtraction could explain the different spreading rates measured. No distinction could be made between the background signal of spread molecules on the surface or desorbed molecules in solution. The whole background was thus subtracted, while actually only the latter background signal should be removed to measure the spreading. Consequently, the width should be higher than measured, thus resulting in the same trend, but with a higher slope and a higher spreading rate.

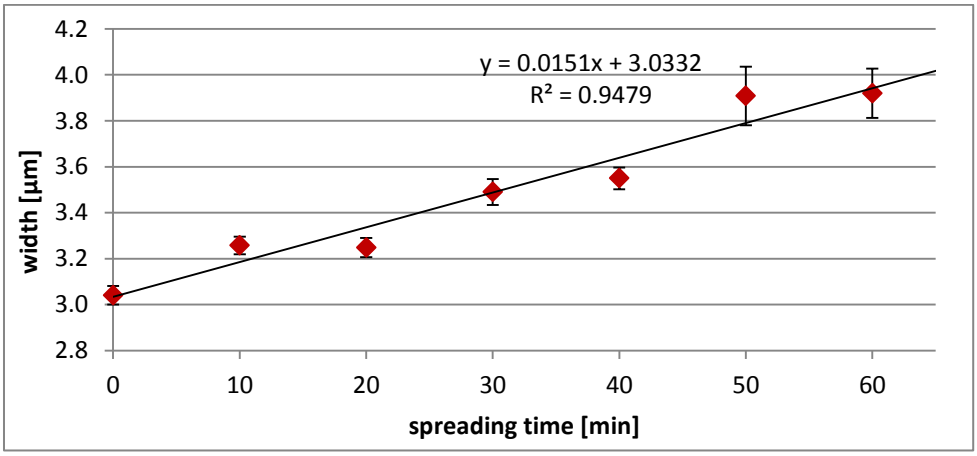

Figure 6.2. Spreading of Ad_2-rhodamine on a molecular printboard: the plot and linear fit of the peak width at half maximum as a function of time

6.2 Directed spreading of microcontact printed lines

The main aim of this report was to induce the directed motion of molecules by gradients. Therefore, it was attempted to create unequal spreading profiles for different places at the surface. The experiments of Perl were extended by adding a solution of FcMeOH and CD (Scheme 6.2). In the same way as described in section 5.5, a solution gradient of free CD molecules is formed. Therefore, it is expected that the spreading of lines close to the oxidizing electrode is similar to the experiments without FcMeOH, since the same CD concentration in solution was used. On the other hand, almost no free CD molecules will be present near the reducing electrode, so the spreading rate of guest molecules is lower. In this way, unequal spreading of the profiles should be observed for different places at the surface and the motion of molecules can be directed locally.

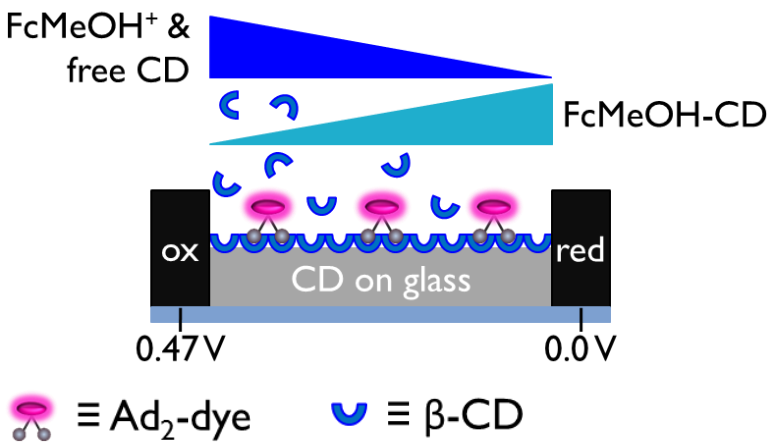

Scheme 6.2. Microcontact printed lines of Ad_2-rhodamine on a CD molecular printboard on glass with unequal spreading induced by a solution gradient of free CD molecules

Figure 6.3a shows the intensity profiles of the fluorescence images in time. The images were taken in situ and all on the same spot. Compared to Figure 6.1a, the background increased much faster, since the lines could not be observed anymore after 20 min. This large increase in background was always observed when a substrate with electrodes was used and started at the moment that the solution was placed on top of the substrate. When the spreading experiment of Perl was repeated on an interdigitated electrode array, but without any electrochemistry, the background increased much faster than for the experiment on a glass slide. This indicates that guest molecules are physisorbed on the electrodes during microcontact printing, and diffuse into the solution at the moment the CD solution is added, which increases the background fluorescence.

The graph was edited by subtracting the difference between the background of each graph and the background at 0 min (Figure 6.3b). The maximum peak intensity decreased again, but no differences in spreading rate could be observed immediately.

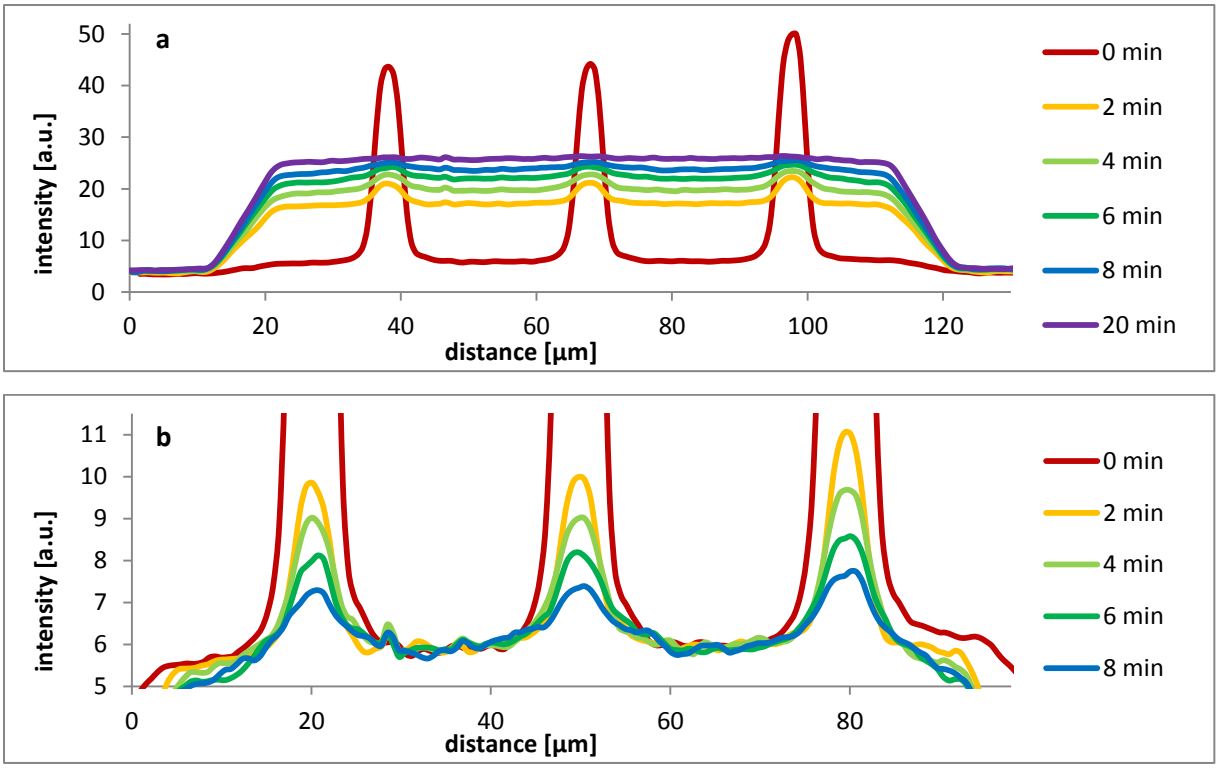

Figure 6.3. Spreading of Ad_2-rhodamine on a molecular printboard with a solution gradient of free CD molecules on top: (a) intensity profiles; (b) intensity profiles after subtracting background

The spreading rate was again determined by fitting a Gaussian curve, and plotting the width values in time. In this case, data from three peaks in between two electrodes were edited (Figure 6.4). Due to the fast increase in background, the Gaussian fits were worse than in the experiments described before. The base line often differed at the left and the right side, and the background was not flat. The data upward of 6 minutes could not be edited in a proper way.

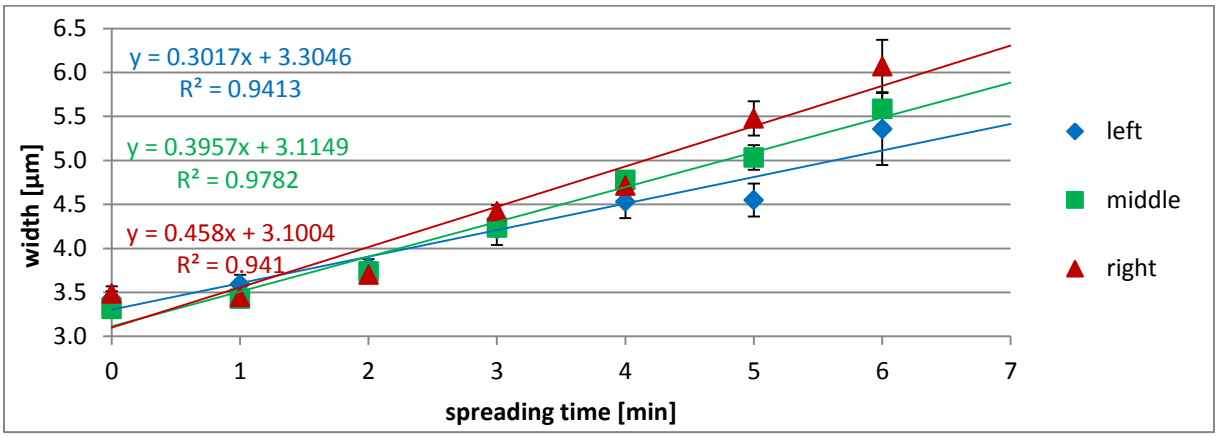

Figure 6.4. Spreading of Ad_2-rhodamine on a molecular printboard with a solution gradient of free CD molecules on top: the plot and linear fit of the peak width at half maximum as a function of time, for three peaks in between two electrodes

Since the Gaussian peaks resulted in large errors and the amount of data points in time is limited, the spreading rate was determined for different data sets to increase the credibility (Figure 6.5). The horizontal axis shows which data are taken into account for the slope calculation. The diffusion time for $FcMeOH^+$, created at the oxidizing electrode and diffused to the reducing electrode (100 µm), is estimated to be 3.2 s (diffusion length = $2\sqrt{Dt}$, with $7.8 \cdot 10^{-10}$ m^2/s [55] as diffusion constant D for

FcMeOH in water). This means that the time for the formation of a gradient is negligible with respect to the used data sets.

Figure 6.5 shows that the different design of this experiment influences the spreading rate significantly, because all rates (4-8 nm/s) are much higher than 0.25 nm/s obtained in the previous experiment without FcMeOH. Moreover, a trend in the spreading rates is visible, where the left peak has the lowest spreading rate and the right one the highest, except for the data set 0-4 min.

Although these results seem to be promising, the data are not understood. If the spreading rates are induced by the electrochemically produced solution gradient of free CD molecules, the trend should be mirrored for the three peaks at the other side of an electrode. However, editing of this peak series resulted in the same trend as seen in Figure 6.5. Furthermore, not all peak series showed a trend in spreading rate, since the spreading rate was sometimes the highest for the peak in the middle, for example. This indicates that the differences in spreading rate were not induced by the CD solution gradient. New measurements, especially without CD in solution, are needed to draw hard conclusions. However, differences in the spreading rate were observed, which is promising.

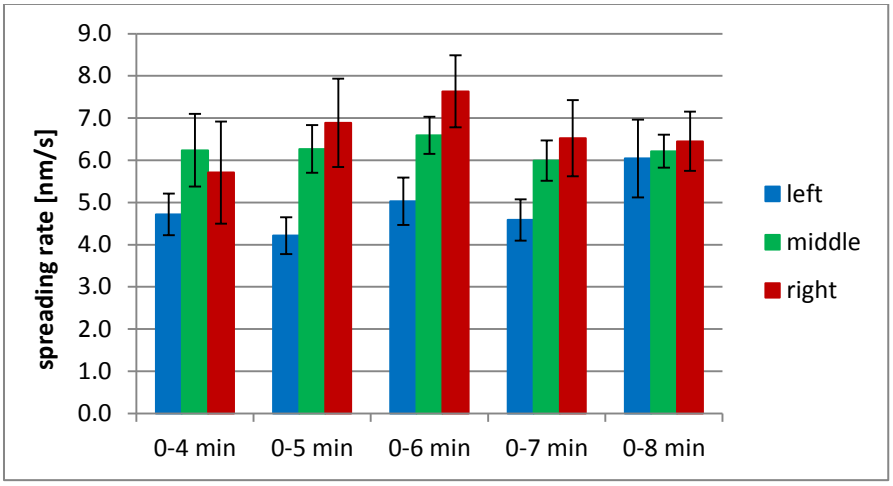

Figure 6.5. Determined spreading rates for different data sets of three peaks in between two electrodes

6.3 Summary

The experiments of Perl were successfully repeated to obtain spreading of microcontact printed lines of Ad_2-rhodamine on a CD molecular printboard. A spreading rate of 0.25 ± 0.026 nm/s was observed when placing a 0.6 mM CD solution in water on top of the substrate.

The system was extended by adding a solution of FcMeOH and CD to make a solution gradient of free CD molecules on top of the microcontact printed lines. While different spreading rates were observed for different lines, no directionality was observed.

7 Conclusions

A covalent host surface gradient on glass was fabricated at the µm scale. Click chemistry was used to synthesize the gradient, which could be visualized by fluorescence spectroscopy. Incubation with guest molecules led to a gradient in the wrong direction, which has to be further investigated.

For the first time, to our knowledge, a non-covalent surface gradient of guest molecules was created. A solution gradient of FcMeOH was produced electrochemically, that acted as a competitor for Ad_2-rhodamine on the CD printboard and resulted in a surface gradient of guest molecules at the µm scale. The direction of the gradient could be reversed by adding CD in solution. Further research is necessary to optimize the gradients, e.g. in steepness.

The experiments of Perl were successfully repeated to obtain spreading of microcontact printed lines of Ad_2-rhodamine on a CD molecular printboard. The system was extended by adding a host solution gradient on top in order to achieve directed spreading of the lines. While different spreading rates were observed for different lines, no directionality was observed.

The main aim of this research was to induce the directed motion of molecules by using electrochemically controlled gradients. In conclusion, the first two minor objectives were achieved by electrochemically producing a covalent host gradient and a non-covalent guest gradient. However, further research is needed to understand the systems completely and direct the motion of molecules by the produced gradients. The two successfully synthesized gradients are the most promising to achieve the third minor objective, namely the directed motion of molecules.

8 Recommendations

The tested systems resulted in a lot of new knowledge about gradient formation by combining host-guest chemistry and electrochemistry. Although no directed motion was observed yet, some systems are promising to proceed with and achieve the main aim.

8.1 Avoid the divalent and tetravalent ferrocene guests

In general, it is recommended to focus on systems without the divalent or tetravalent ferrocene guests. In theory, the designed systems with these guests were based on both their supramolecular and electrochemical properties. With respect to supramolecular properties, Fc_4-rhodamine worked properly in competition tests with CD in solution, but Fc_2-rhodamine could not be desorbed by competition or incubation with other solutions. On the other hand, Fc_2-rhodamine showed a small peak in cyclic voltammetry on gold and in differential pulse voltammetry, but no electrochemical oxidation and reduction of Fc_4-rhodamine was observed. In conclusion, both guests were not reliable enough to proceed with.

The ferrocene guests might be replaced by Fc dendrimers, for example in the guest gradient formation on glass with dendrimers in solution or in the guest gradient formation on gold. Nijhuis [25] has already proven that the desorption of Fc dendrimers from a CD printboard on gold is possible by oxidation. This indicates that the supramolecular and electrochemical properties of these guests are reliable. However, visualization is less straightforward than for the fluorescent guest molecules.

The dendrimers could be visualized by incubation with a dye after gradient formation, since negatively charged dyes can be bound to the positively charged core of the dendrimers. Furthermore, it could also be possible to use fluorescent polystyrene nanoparticles coupled to CD (CD-NPs [56]) as visualization method. When the dendrimers are bound on the surface, only a part of the ferrocene moieties is connected to the surface. After formation of a gradient in dendrimer molecules, the remaining ferrocene functionalities that stick upwards can be bound to the CD-NPs and thus visualized by fluorescence microscopy. However, the disadvantage of this system is that the gradient formation cannot be measured in situ, which is necessary to study the directed motion of molecules.

Another general remark about ferrocene is that the ferrocenium cation (Fc^+) is not stable towards nucleophiles, such as hydroxide and chloride [57, 58]. Fc^+ is stable in (acid) aqueous solutions, but could decompose in alkaline aqueous solutions or DMSO [59]. It is important to take this into account when new gradient formation systems are designed.

8.2 Problems with increasing background

The background of the fluorescence intensity profiles increased significantly faster when glass slides with electrodes were used compared to glass slides only. It is assumed that this increase is due to molecules that physisorb onto the electrodes during the incubation or microcontact printing step. Therefore, it is recommended to use a so-called transfer gradient, which was used successfully within MnF in click chemistry experiments. Scheme 8.1 shows how a transfer gradient can be applied to the unequal spreading of Ad_2-rhodamine lines by a solution gradient of free CD molecules. The microcontact or incubation step is carried out on a glass substrate without electrodes and physisorption on electrodes is avoided during this step. Afterwards, this substrate is placed on top of an interdigitated electrode array with in between the solution with FcMeOH, CD and electrolyte. The rest of the process is the same.

There is no space for the reference and counter electrode in between the two glass substrates, so transfer gradients were produced by a power supply within MnF. However, it is desired to use the bipotentiostat for the system shown in Scheme 8.1 to control the applied potential. This problem has to be solved before transfer gradients can be tested. Furthermore, it might be challenging to find the right focus at the fluorescence microscope, and mark the places where the electrodes have been working on the upper substrate.

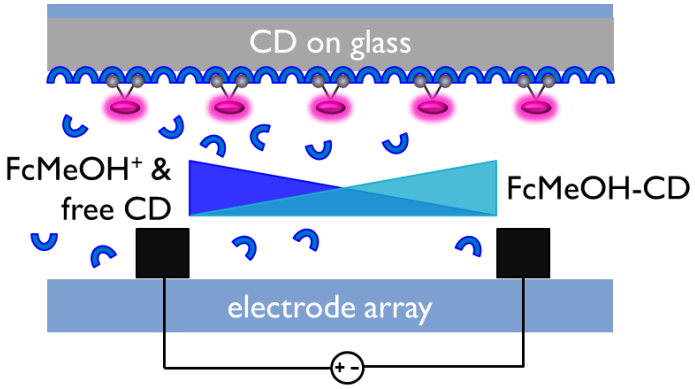

Scheme 8.1. Principle of transfer gradient applied to the unequal spreading of guest molecules by a gradient of free CD molecules in solution

8.3 Visualization method on gold

Before the gradient formation on gold can be tested, a suitable visualization method has to be found. It is recommended to measure the fluorescence on substrates with a thinner gold layer, for example 5 or 10 nm, since the amount of quenching will decrease on a thinner gold layer. Furthermore, the fluorescence of Fc-NPs, which were synthesized within MnF, might be measurable due to their larger distance from the gold substrate. The particles consist of fluorescent green silica particles with a diameter of 50 nm as a core, functionalized with long PEG chains (MW = 10,000) and ferrocene groups.

Different alternative visualization methods might be used to check the gradient formation, including contact angle measurements [60], Scanning Electrochemical Microscopy (SECM) and Atomic Force Microscopy (AFM). However, contact angles can only be measured on a mm scale and none of the systems allows in situ measurements needed for the visualization of directed motion.

8.4 Host gradient on glass

It is recommended to switch step 2 and 3, since that might switch the guest gradient to the right direction. If that does not work, it is recommended to functionalize CD directly with alkyne groups, so the coumarin molecule is not necessary anymore and a CD gradient can be synthesized directly via click chemistry. Although the coumarin molecule is useful for the visualization of the connection with CD, the CD molecules could be stacked vertically, so it does not proof that the CD molecules are available for host-guest chemistry. Direct functionalization might clarify the system, although it does not explain the results of the current process.

8.5 Guest gradient on glass with FcMeOH as competitor

Another control experiment to test the system includes the immersion in a CD solution after gradient formation. It is expected that the gradient is transferred back into a homogeneous monolayer.

The observed gradients can be optimized by varying parameters, including time of applying a potential, applied potential, FcMeOH concentration in solution, and CD concentration in solution. It is recommended to start with lowering the FcMeOH concentration, since this probably results in a steeper gradient in either FcMeOH molecules for the system without CD or in free CD molecules for the reverse system. Also, research is necessary to explain the randomly arising black spots on the surface.

8.6 Motion

With respect to the CD solution gradient on top of microcontact printed lines of Ad_2-rhodamine, better results could be obtained when the background would not increase so quickly. Next to the mentioned alternative of a transfer gradient, differences in spreading might be measurable when the gradient is applied for less than 10 min and the dry sample is measured afterwards. A disadvantage of this method is that sample cannot be measured in situ anymore.

Furthermore, it is recommended to test the system without CD in solution, since a FcMeOH solution gradient could influence the spreading rate by competition, comparable to the influence on a full monolayer (section 5.5). It is also possible to print a broader line, 25 µm for example, and test the asymmetric spreading of these molecules with a CD solution gradient on top. Also Fc-NPs could be microcontact printed and feel a larger influence of the gradient, since they are larger than Ad_2-rhodamine molecules.

Acknowledgements

I would like to thank the people from my graduation committee. First of all, I would like to thank Sven Krabbenborg, my daily supervisor, for guiding me in the research, for all the advice and helpful discussions, and for reviewing this report. Secondly, I would like to thank Carlo Nicosia, my daily supervisor for the synthesis part in the beginning of the project, for the help with all syntheses and his knowledge of organic chemistry. Furthermore, I would like to thank Jurriaan Huskens, professor of the MnF group, for providing me with this master's assignment and all new ideas to proceed with the project. Thanks for giving me what I was looking for: a challenging project! Finally, Serge Lemay is thanked for the useful input as the external member of my graduation committee.

I would like to thank all people within the Molecular NanoFabrication and Biomolecular Nanotechnology group, because I had a great time during my master's assignment. I am happy to have such nice colleagues for the next four years!

References

1. Hess, H., et al., *Light-controlled molecular shuttles made from motor proteins carrying cargo on engineered surfaces.* Nano Letters, 2001. **1**(5): p. 235-239.
2. von Delius, M., E.M. Geertsema, and D.A. Leigh, *A synthetic small molecule that can walk down a track.* Nature Chemistry, 2010. **2**(2): p. 96-101.
3. Kelly, T.R., *Molecular motors: Synthetic DNA-based walkers inspired by kinesin.* Angewandte Chemie-International Edition, 2005. **44**(27): p. 4124-4127.
4. Berna, J., et al., *Macroscopic transport by synthetic molecular machines.* Nature Materials, 2005. **4**(9): p. 704-710.
5. Cohen, A.E. and W.E. Moerner, *Method for trapping and manipulating nanoscale objects in solution.* Applied Physics Letters, 2005. **86**(9).
6. Edwards, B., N. Engheta, and S. Evoy, *Electric tweezers: Experimental study of positive dielectrophoresis-based positioning and orientation of a nanorod.* Journal of Applied Physics, 2007. **102**(2).
7. Wu, L.Q., et al., *Magnetic nanoparticle migration in microfluidic two-phase flow.* Journal of Applied Physics, 2009. **105**(12).
8. Grier, D.G., *A revolution in optical manipulation.* Nature, 2003. **424**(6950): p. 810-816.
9. Chaudhury, M.K. and G.M. Whitesides, *How to Make Water Run Uphill.* Science, 1992. **256**(5063): p. 1539-1541.
10. Walder, R., A. Honciuc, and D.K. Schwartz, *Directed Nanoparticle Motion on an Interfacial Free Energy Gradient.* Langmuir, 2010. **26**(3): p. 1501-1503.
11. Sarvestani, A.S. and E. Jabbari, *Analysis of Cell Locomotion on Ligand Gradient Substrates.* Biotechnology and Bioengineering, 2009. **103**(2): p. 424-429.
12. Morgenthaler, S., C. Zink, and N.D. Spencer, *Surface-chemical and -morphological gradients.* Soft Matter, 2008. **4**(3): p. 419-434.
13. Genzer, J. and R.R. Bhat, *Surface-bound soft matter gradients.* Langmuir, 2008. **24**(6): p. 2294-2317.
14. Chang, T., et al., *Directional movement of dendritic macromolecules on gradient surfaces.* Nano Letters, 2007. **7**(4): p. 978-980.
15. Burgos, P., et al., *Directed Single Molecule Diffusion Triggered by Surface Energy Gradients.* ACS Nano, 2009. **3**(10): p. 3235-3243.
16. Perl, A., et al., *Gradient-driven motion of multivalent ligand molecules along a surface functionalized with multiple receptors.* Nature Chemistry, 2011. **3**(4): p. 317-322.
17. Huskens, J., M.A. Deij, and D.N. Reinhoudt, *Attachment of molecules at a molecular printboard by multiple host-guest interactions.* Angewandte Chemie-International Edition, 2002. **41**(23): p. 4467-4471.
18. Cooke, G., *Electrochemical and photochemical control of host-guest complexation at surfaces.* Angewandte Chemie-International Edition, 2003. **42**(40): p. 4860-4870.
19. Nijhuis, C.A., et al., *Multivalent dendrimers at molecular printboards: Influence of dendrimer structure on binding strength and stoichiometry and their electrochemically induced desorption.* Langmuir, 2005. **21**(17): p. 7866-7876.
20. Onclin, S., et al., *Molecular printboards: Monolayers of beta-cyclodextrins on silicon oxide surfaces.* Langmuir, 2004. **20**(13): p. 5460-5466.
21. Hiratsuka, Y., et al., *Controlling the direction of kinesin-driven microtubule movements along microlithographic tracks.* Biophysical Journal, 2001. **81**(3): p. 1555-1561.
22. Xia, Y.N. and G.M. Whitesides, *Soft lithography.* Angewandte Chemie-International Edition, 1998. **37**(5): p. 551-575.
23. Steed, J.W. and J.L. Atwood, *Supramolecular Chemistry*. 2nd ed. 2009, West Sussex: Wiley.
24. Mulder, A., *Multivalent cyclodextrin receptors in solution and at surfaces*. 2004, University of Twente: Enschede.

25. Nijhuis, C.A., *Redox-active dendrimers at molecular printboards*. 2006, University of Twente: Enschede.
26. Dubacheva, G.V., et al., *Electrochemically Controlled Adsorption of Fc-Functionalized Polymers on beta-CD-Modified Self-Assembled Monolayers.* Langmuir, 2010. **26**(17): p. 13976-13986.
27. Chen, Y.F., et al., *Attachment of ferrocene nanotubes on beta-cyclodextrin self-assembled monolayers with molecular recognitions.* Langmuir, 2004. **20**(20): p. 8409-8413.
28. Ling, X.Y., D.N. Reinhoudt, and J. Huskens, *Reversible attachment of nanostructures at molecular printboards through supramolecular glue.* Chemistry of Materials, 2008. **20**(11): p. 3574-3578.
29. Schwabacher, A.W., et al., *Desymmetrization reactions: Efficient preparation of unsymmetrically substituted linker molecules.* Journal of Organic Chemistry, 1998. **63**(5): p. 1727-1729.
30. Bérubé, M. and D. Poirier, *Synthesis of Simplified Hybrid Inhibitors of Type 1 17β-Hydroxysteroid Dehydrogenase via Cross-Metathesis and Sonogashira Coupling Reactions.* Organic Letters, 2004. **6**(18): p. 3127-3130.
31. Guo, R.Y., et al., *Synthesis and Optical Properties of 6-Substituted-beta-cyclodextrin Derivatives.* Letters in Organic Chemistry, 2009. **6**(8): p. 604-612.
32. Chan, T.R., et al., *Polytriazoles as Copper(I)-Stabilizing Ligands in Catalysis.* Organic Letters, 2004. **6**(17): p. 2853-2855.
33. Perl, A., *Multivalent self-assembly at interfaces: from fundamental kinetic aspects to applications in nanofabrication*. 2009, University of Twente: Enschede.
34. Tidwell, T.T., et al., *Ferrocenylketene and ferrocenyl-1,2-bisketenes: Direct observation and reactivity measurements.* Journal of Organic Chemistry, 2005. **70**(23): p. 9556-9561.
35. Nicosia, C., et al., *A Fluorogenic Reactive Monolayer Platform for the Signaled Immobilization of Thiols.* Chembiochem, 2012. **13**(6): p. 778-782.
36. Mulder, A., et al., *Molecular printboards on silicon oxide: Lithographic patterning of cyclodextrin monolayers with multivalent, fluorescent guest molecules.* Small, 2005. **1**(2): p. 242-253.
37. Rojas, M.T., et al., *Supported monolayers containing preformed binding sites. Synthesis and interfacial binding properties of a thiolated β-cyclodextrin derivative.* Journal of the American Chemical Society, 1995. **117**(1): p. 336-343.
38. Ludden, M.J.W., et al., *Molecular Printboards as a General Platform for Protein Immobilization: A Supramolecular Solution to Nonspecific Adsorption.* Angewandte Chemie, 2007. **119**(22): p. 4182-4185.
39. Gill, H.S., et al., *A Modular Platform for the Rapid Site-Specific Radiolabeling of Proteins with 18F Exemplified by Quantitative Positron Emission Tomography of Human Epidermal Growth Factor Receptor 2.* Journal of Medicinal Chemistry, 2009. **52**(19): p. 5816-5825.
40. Ashton, P.R., et al., *Amino acid derivatives of beta-cyclodextrin.* Journal of Organic Chemistry, 1996. **61**(3): p. 903-908.
41. de Jong, M.R., J. Huskens, and D.N. Reinhoudt, *Influencing the binding selectivity of self-assembled cyclodextrin monolayers on gold through their architecture.* Chemistry-a European Journal, 2001. **7**(19): p. 4164-4170.
42. Hakkinen, H., *The gold-sulfur interface at the nanoscale.* Nature Chemistry, 2012. **4**(6): p. 443-455.
43. Zhong, C.J., et al., *Organosulfur monolayers at gold surfaces: Reexamination of the case for sulfide adsorption and implications to the formation of monolayers from thiols and disulfides.* Langmuir, 1999. **15**(2): p. 518-525.
44. Williams, J.A. and C.B. Gorman, *Alkanethiol reductive desorption from self-assembled monolayers on gold, platinum, and palladium substrates.* Journal of Physical Chemistry C, 2007. **111**(34): p. 12804-12810.

45. Wang, X.J., et al., *Length scale heterogeneity in lateral gradients of poly(N-isopropylacrylamide) polymer brushes prepared by surface-initiated atom transfer radical polymerization coupled with in-plane electrochemical potential gradients.* Langmuir, 2006. **22**(2): p. 817-823.
46. Coppeta, J. and C. Rogers, *Dual emission laser induced fluorescence for direct planar scalar behavior measurements.* Experiments in Fluids, 1998. **25**(1): p. 1-15.
47. Kaifer, A.E. and M. Gómez-Kaifer, *Supramolecular Electrochemistry*. 1999, Weinheim: Wiley.
48. Rekharsky, M.V. and Y. Inoue, *Complexation thermodynamics of cyclodextrins.* Chemical Reviews, 1998. **98**(5): p. 1875-1917.
49. Strelets, V.V., et al., *Electrochemistry of Inclusion Complexes of Organometallics - Complexation of Ferrocene and Azaferrocene by Cyclodextrins.* Journal of Electroanalytical Chemistry, 1991. **310**(1-2): p. 179-186.
50. Petrovic, S., *Cyclic Voltammetry of Hexachloroiridate(IV): An Alternative to the Electrochemical Study of the Ferricyanide Ion.* Chemical Educator, 2000. **5**(5): p. 231-235.
51. Basabe-Desmonts, L., et al., *A simple approach to sensor discovery and fabrication on self-assembled monolayers on glass.* Journal of the American Chemical Society, 2004. **126**(23): p. 7293-7299.
52. Wang, X.J. and P.W. Bohn, *Anisotropic in-plane gradients of poly(acrylic acid) formed by electropolymerization with spatiotemporal control of the electrochemical potential.* Journal of the American Chemical Society, 2004. **126**(21): p. 6825-6832.
53. Schneider, G., et al., *Distance-dependent fluorescence quenching on gold nanoparticles ensheathed with layer-by-layer assembled polyelectrolytes.* Nano Letters, 2006. **6**(3): p. 530-536.
54. Würthner, F. and A. Ajayaghosh, *Supramolecular dye chemistry*. Topics in Current Chemistry, ed. F. Würthner. 2005, Berlin: Springer.
55. Miao, W., Z. Ding, and A.J. Bard, *Solution Viscosity Effects on the Heterogeneous Electron Transfer Kinetics of Ferrocenemethanol in Dimethyl Sulfoxide−Water Mixtures.* The Journal of Physical Chemistry B, 2002. **106**(6): p. 1392-1398.
56. Crespo-Biel, O., et al., *Supramolecular Layer-by-Layer Assembly: Alternating Adsorptions of Guest- and Host-Functionalized Molecules and Particles Using Multivalent Supramolecular Interactions.* Journal of the American Chemical Society, 2005. **127**(20): p. 7594-7600.
57. Breuer, R. and M. Schmittel. *Forget Ferrocene for Applications in Aqueous Media!* in *59th Annual Meeting of the International Society of Electrochemistry*. 2008. Seville, Spain.
58. Prins, R., A.R. Korswagen, and A.G.T.G. Kortbeek, *Decomposition of the ferricenium cation by nucleophilic reagents.* Journal of Organometallic Chemistry, 1972. **39**(2): p. 335-344.
59. McDowell, M.S., J.H. Espenson, and A. Bakac, *Kinetics of aqueous outer-sphere electron-transfer reactions of superoxide ion. Implications concerning the dioxygen/superoxide (O_2/O_2^-) self-exchange rate constant.* Inorganic Chemistry, 1984. **23**(15): p. 2232-2236.
60. Yamada, R. and H. Tada, *Manipulation of droplets by dynamically controlled wetting gradients.* Langmuir, 2005. **21**(10): p. 4254-4256.
61. Tanner, P.S., et al., *The Synthesis and Characterization of Ferrocene*, in *210th National Meeting of the American Chemical Society*. 1995: Chicago.
62. Jolly, W.L., *The Synthesis and Characterization of Inorganic Compounds*. 1970, New Jersey: Prentice-Hall.

Appendix A. Characterization of Fc_4-rhodamine

The synthesized Fc_4-rhodamine (section 5.1.1) was characterized by NMR spectroscopy, mass spectrometry and UV/Vis spectroscopy.

A.1 NMR spectroscopy

NMR spectroscopy was performed to investigate the purity of the products and to confirm the synthesis of the desired molecules. The ^{1}H NMR spectrum of **1** corresponded with literature data [33]. The other steps have not been described in literature, so the spectra of these steps cannot be compared with reference spectra. However, the differences between the spectra before and after each reaction were explainable and could be logically attributed to the appearing or disappearing groups. Only the spectra of the last two products are described below.

The ^{1}H NMR spectrum of product **5** of the one-to-last step is shown in Figure A.1. The peaks are assigned to the protons of the amine, where Fc means ferrocene and TEG means triethyleneglycol (the long spacer chains), excluding the solvent peaks of $CHCl_3$ and CH_2Cl_2 at 7.2 and 5.3 ppm, respectively. The peak of the tBOC protecting group, observed at 1.36 ppm in the ^{1}H NMR spectrum of the previous step **4**, is not present in the spectrum of **5**, indicating that this group is converted into the amine group.

Figure A.2 shows the ^{1}H NMR spectrum of the end product **6**, including the differences with the spectrum of Figure A.1. These differences can all be attributed to the coupling with the dye, since new peaks arise in the aromatic region and the ethyl groups of the dye are present in the aliphatic region.

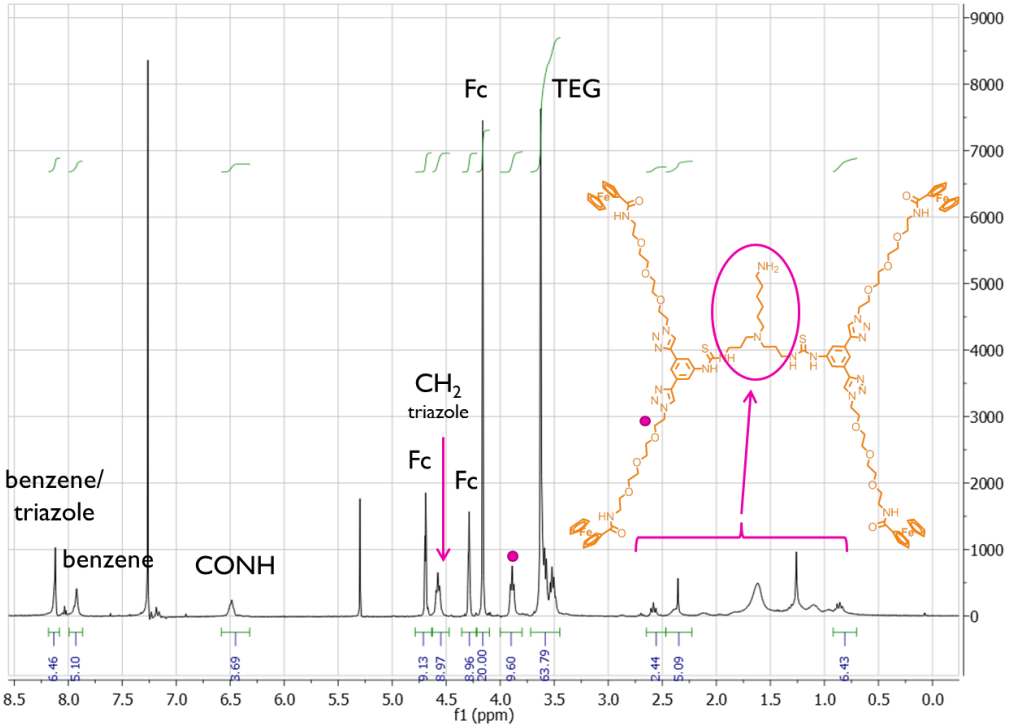

Figure A.1. ^{1}H NMR spectrum of the amine **5** including the assignment of the peaks

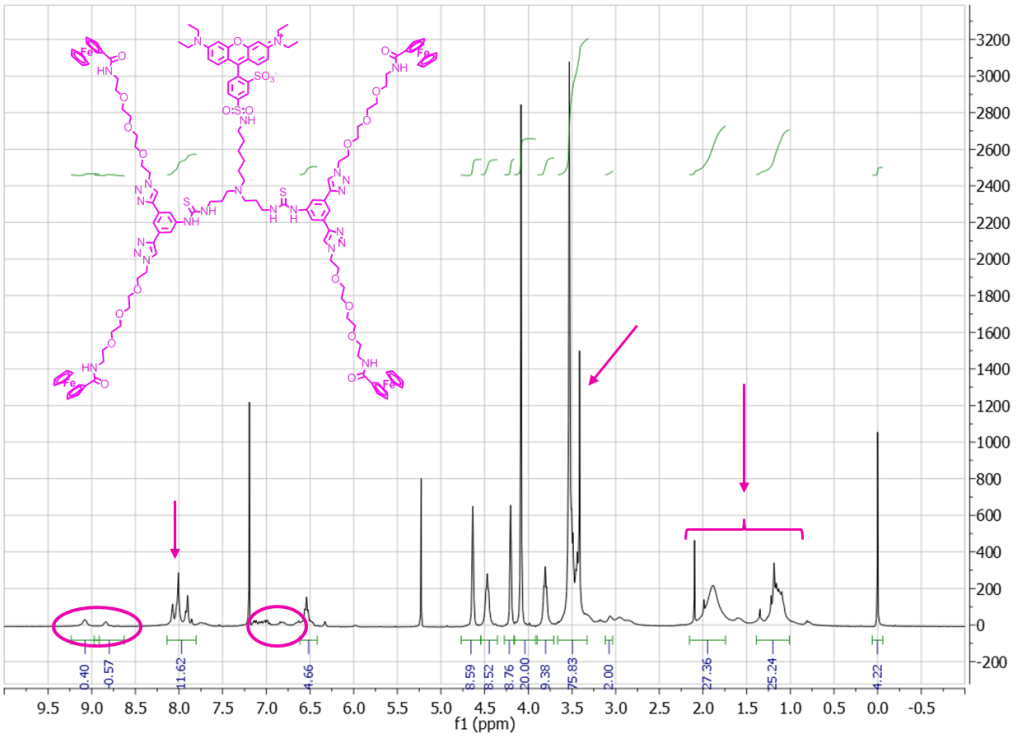

Figure A.2. ^{1}H NMR spectrum of Fc_4-rhodamine **6** including the assignment of the differences with the spectrum of **5**

A.2 Mass spectrometry

Mass spectrometry was performed to verify the synthesis of the desired molecules in the last two steps. The MALDI-TOF spectra of **5** and **6** are shown in Figure A.3 and Figure A.4, respectively. The observed mass of the $[M+H]^+$ peak of **5** (2,320 m/z) corresponds quite well with the calculated value (2,319 m/z). For compound **6**, the match is a bit worse (2,867 m/z of the $[M+H]^+$ peak versus the theoretical value of 2,860 m/z), which could be due to the resolution of the mass spectrometer.

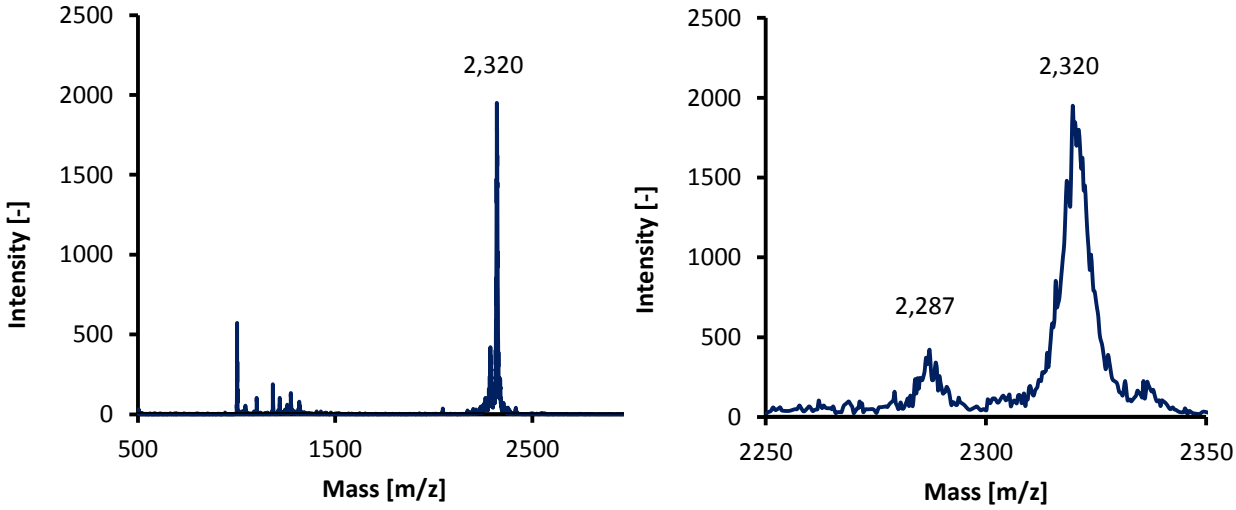

Figure A.3. MALDI-TOF spectra of free amine **5** (calculated: 2,319 m/z) from 500 till 3000 m/z (left) and from 2250 till 2350 m/z (right)

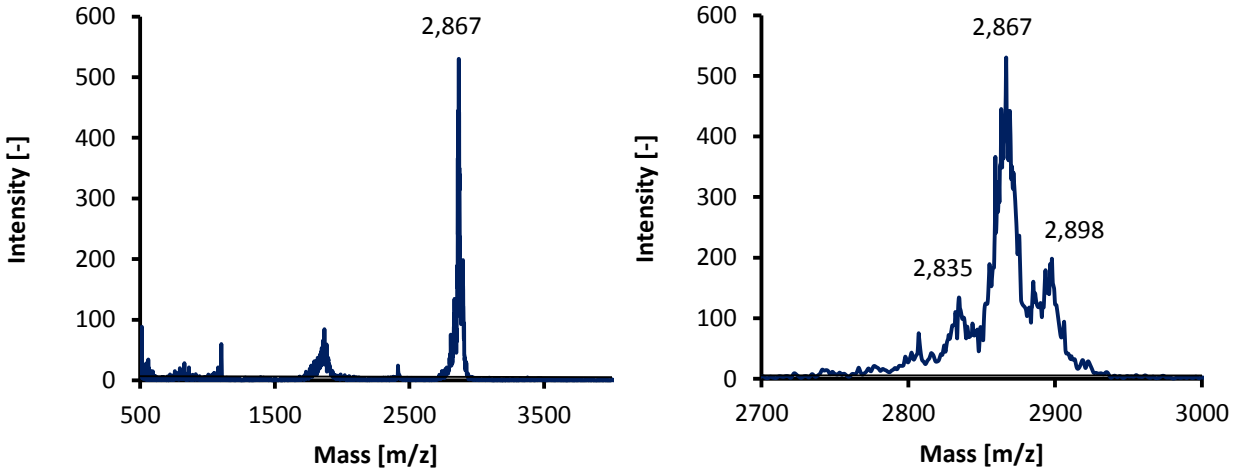

Figure A.4. MALDI-TOF spectra of Fc_4-rhodamine **6** (calculated: 2,860 m/z) from 500 till 4000 m/z (left) and from 2700 till 3000 m/z (right)

Mass spectrometry of **6** was also performed using ESI (Electrospray Ionization), since this technique has a higher resolution than MALDI-TOF. The highest peaks were observed at 969, 1066, 1219 and 1444 m/z. The mass of the triple charged molecules $[M+3Li]^{3+}$ and $[M+3K]^{3+}$ and the double charged molecule $[M+2Li]^{2+}$ equal to 968, 1070 and 1444 m/z, closely to the first, second and last mentioned peaks. It can be concluded that the desired molecule has been synthesized.

The peak at 1219 m/z is probably coming from the amine molecule **5**, since $[\mathbf{5}+Na+K]^{2+}$ equals to 1219 m/z. Since compound **5** was not visible in the NMR spectrum of Fc_4-rhodamine, probably only traces of the compound are present.

A.3 UV/Vis spectroscopy

Figure A.5 shows the UV/Vis absorption spectrum of the tetravalent guest molecule in water. The observed peaks are very broad with a broad maximum between 590 and 615 nm. As reported in literature, the maximum absorbance of lissamine rhodamine B sulfonylchloride in water lies around 565 nm [46]. The measured graph does not correspond with this literature value, which could be due to influences of the medium or the other part of the Fc_4-rhodamine molecule.

In the measured graph of the tetravalent guest, no maxima can be assigned below 500 nm, since only a very broad peak is observed. According to a literature report, the UV/Vis spectrum of ferrocene in acetonitrile [61] shows maxima at 330 nm and 440 nm, and a rising short-wavelength absorption at 225 nm, which is comparable to a reported spectrum in ethanol [62] according to the authors of the first mentioned report. Although the media of the mentioned literature spectra are different than the solution used for Fc_4-rhodamine, it can be assumed that the observed broad peak below 500 nm includes absorption bands of the ferrocene functionalities.

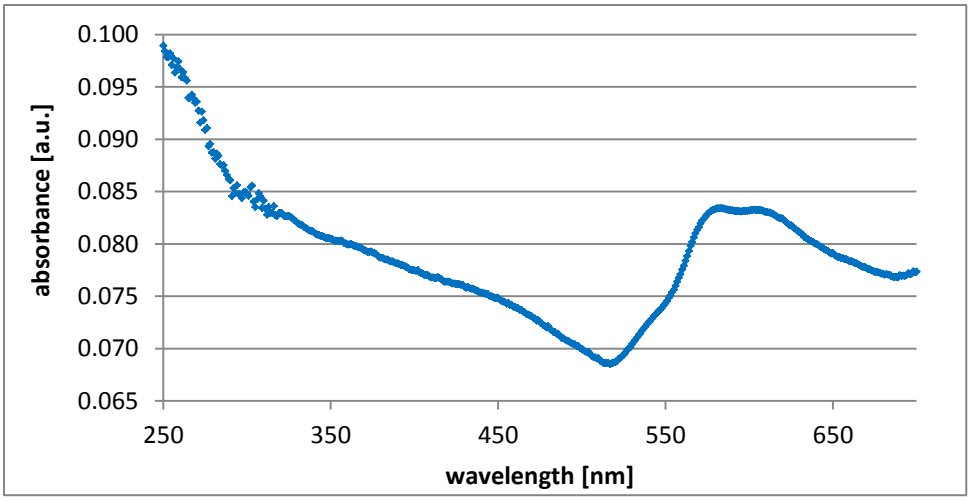

Figure A.5. UV/Vis absorption spectrum for the tetravalent guest molecule (10 µM in water, 1% MeOH, pH 2)